Master's thesis

NTNU
Norwegian University of Science and Technology
Faculty of Medicine and Health Sciences
Department of Clinical and Molecular Medicine

Daniel Edvin Pedersen Schjerpen

Multiple myeloma bioenergetics: Mitochondrial uncoupling in malignant plasma cells & its effects on PRL-3 in acidic and hypoxic tumor microenvironment

Master's thesis in Molecular Medicine
Supervisor: Magne Børset
Co-supervisor: Sara Beate Stjern Årbogen
May 2024

NTNU
Norwegian University of Science and Technology

Daniel Edvin Pedersen Schjerpen

Multiple myeloma bioenergetics: Mitochondrial uncoupling in malignant plasma cells & its effects on PRL-3 in acidic and hypoxic tumor microenvironment

Master's thesis in Molecular Medicine
Supervisor: Magne Børset
Co-supervisor: Sara Beate Stjern Årbogen
May 2024

Norwegian University of Science and Technology
Faculty of Medicine and Health Sciences
Department of Clinical and Molecular Medicine

NTNU
Norwegian University of
Science and Technology

Abstract

Multiple myeloma is a type of hematologic cancer that affects B lymphocytes in the bone marrow BM, originating from the antibody-producing plasma cells of the body. A hallmark of cancer cells is the rewiring of metabolism toward aerobic glycolysis, a phenomenon in which cancer cells favor glycolysis over oxidative phosphorylation to produce ATP, even in the presence of sufficient oxygen. The tumor microenvironment is complex, characterized by acidic pH and low oxygen levels, which are crucial in shaping cancer cell metabolism and promoting tumor progression.

Phosphatase of regenerating liver-3 (PRL-3), a metastasis-associated phosphatase, has emerged as a key regulator of cancer cell metabolism, orchestrating metabolic adaptations to support tumor growth and survival amid these harsh conditions. In this study, we investigated the impact of the uncoupling agents BAM15 and CCCP, and the glycolysis inhibitor 2-Deoxy-D-Glucose (2-DG) on energy production in INA-6 multiple myeloma (MM) cells. Mitochondrial uncouplers disrupt the electron transport chain and ATP synthesis by transporting H^+ ions from the intermembrane space to the mitochondrial matrix, thereby collapsing the electrochemical gradient necessary for powering ATP synthase. 2-DG, a glucose analog lacking a critical hydroxyl group, accumulates during the initial phase of glycolysis, competitively blocking glucose metabolism and thus diminishing glycolytic energy output.

Our objective was to elucidate the efficacy of these compounds in disrupting metabolic pathways crucial for cancer cell survival, with a focus on the role of PRL-3 and the effects of metabolic acidosis and hypoxia. Previous studies have demonstrated that PRL-3-expressing cancer cells exhibit increased ATP production, upregulating both OXPHOS and glycolysis compared to control cells, suggesting a potential vulnerability in targeting energy production.

Our findings indicate that PRL-3-expressing cancer cells display enhanced respiratory and glycolytic activities, as evidenced by increased oxygen consumption and extracellular acidification rates. Given that hypoxia typically promotes glycolysis while metabolic acidosis inhibits it, we investigated the interplay of these factors. Interestingly, PRL-3 cells maintained similar or higher levels of proliferation and viability under hypoxia and low pH when exposed solely to uncoupling agents. However, the introduction of a glycolysis inhibitor reversed this trend, substantially altering the viability of PRL-3-expressing cells, highlighting glucose addiction as a potential weakness.

We assessed the expression of key proteins involved in metabolism and adaptation to hypoxia and low pH. Our results showed that p-AMPK in PRL-3 cells exhibited paradoxical downregulation under conditions of energy stress induced by shutting down ATP production, and that the expression of GLUT1 was lower in cells expressing PRL-3 at both pH 7.4 and pH 6.5 compared to Mock cells, but more so under normoxic than hypoxic conditions. Additionally, at higher doses of uncoupling agents, the expression of HIF-1α was almost completely abolished, with a more pronounced effect seen in PRL-3 cells. Furthermore, PRL-3 was shown to trigger a Warburg effect independent of HIF-1α under normoxic conditions, further demonstrating its significance in metabolic rewiring in MM cells.

Lastly, mitochondrial membrane potential and superoxide production were examined following treatment with uncouplers. CCCP decreased mitochondrial membrane potential dose-dependently in both Mock and PRL-3 cells, with a stronger impact observed in PRL-3 cells. Although CCCP induced an increase in superoxide production, particularly at high concentrations, BAM15 did not exhibit a similar effect. We observed that PRL-3 enhanced basal superoxide production in cells, while also conferring resistance to further increases induced by uncouplers.

Sammendrag

Myelomatose er en type blodkreft som påvirker B-lymfocytter i benmargen (BM), og stammer fra kroppens plasmaceller som produserer antistoffer. Et kjennetegn ved kreftceller er omstilling av metabolismen mot aerob glykolyse, en fenomen der kreftceller foretrekker glykolyse over oksidativ fosforylering for å produsere ATP, selv i nærvær av tilstrekkelig oksygen. Mikromiljøet i beinmargen er komplekst, og kjennetegnes av sur pH og lavt oksygennivå, noe som er avgjørende for å forme kreftcellenes metabolisme, og i å fremme tumorutvikling. PRL-3, en metastase-assosiert fosfatase, er en viktig del av myelomatoses evne til å endre metabolismen, samt at det beskytter kreftcellene mot det sure miljøet i mikromiljøet.

I denne studien undersøkte vi effekten av avkoblerne BAM15 og CCCP, og glykolysinhibitoren 2-Deoxy-D-Glukose (2-DG) på energiproduksjon i INA-6 myelomatose (MM) celler. Avkoblere forstyrrer elektrontransportkjeden og ATP-syntese ved å transportere H+-ioner fra den mitokondrielle intermembranen til matrix, og kollapser dermed den elektrokjemiske gradienten som er nødvendig for å drive ATP-syntase. 2-DG, en glukoseanalog uten en kritisk OH-gruppe, akkumuleres under den første fasen av glykolysen, og blokkerer glukosemetabolismen og dermed reduserer ATP produksjon via glykolysen. I denne studien så var vårt mål å oppklare effekten av disse stoffene på å forstyrre metabolske prosesser som er avgjørende for kreftcellers overlevelse, med fokus på PRL-3s rolle og effektene av metabolsk acidose og hypoksi. Tidligere studier har vist at kreftceller som uttrykker PRL-3, har økt produksjon av ATP, og oppregulerer både oksidativ fosforylering og glykolyse sammenlignet med kontrollceller, noe som antyder en potensiell sårbarhet for målrettet behandling.

Våre funn indikerer at kreftceller som uttrykker PRL-3, viser forbedrede respiratoriske og glykolytiske aktiviteter, som dokumenteres ved økt oksygenforbruk og ekstracellulære acidifikasjonsrater. Ettersom hypoksi vanligvis fremmer glykolyse mens metabolsk acidose hemmer det, undersøkte vi samspillet mellom disse faktorene. Interessant nok opprettholdt PRL-3-celler lignende eller høyere nivåer av proliferasjon og levedyktighet under hypoksi og lav pH når de kun ble eksponert for avkoblere. Denne trenden ble reversert ved introduksjon av 2-DG, og endret betydelig levedyktigheten til PRL-3-uttrykkende celler, noe som understreker glukoseavhengighet som en potensiell svakhet.

Vi vurderte uttrykkene av viktige proteiner involvert i metabolisme og tilpasning til hypoksi og lav pH. Våre resultater viste at p-AMPK i PRL-3-celler hadde paradoksalt nok nedregulering under forhold som energistress, og at uttrykket av GLUT1 var lavere i celler som uttrykker PRL-3 ved både pH 7.4 og pH 6.5 sammenlignet med kontrollcellene, men mer under normoksiske forhold enn hypoksiske forhold. I tillegg, ved høyere doser av avkoblere, var uttrykket av HIF-1 nesten fullstendig nedregulert, med en mer påvist effekt sett i PRL-3-celler. Videre ble det vist at PRL-3 induserte en Warburg-effekt uavhengig av HIF-1 under normoksiske forhold, og demonstrerer ytterligere dens betydning i metabolsk omstilling i MM-celler.

Til slutt ble membranpotensial og superoksidproduksjon undersøkt etter behandling med avkobler. CCCP reduserte mitokondriell membranpotensial doseavhengig i både Mock- og PRL-3-celler, med en sterkere innvirkning observert i PRL-3-celler. Selv om CCCP induserte en økning i superoksidproduksjon, spesielt ved høye konsentrasjoner, viste ikke BAM15 en lignende effekt. Vi observerte at PRL-3 forsterket basal superoksidproduksjon i cellene, samtidig som det ga dyktighet mot ytterligere økninger indusert av avkoblerne.

Acknowledgements

This master's thesis was conducted at the 'Bone Marrow Microenvironment in patients with multiple myeloma' research group at the Center for Myeloma Research, Department of Cancer Research and Molecular Medicine at the Norwegian University of Science and Technology.

First of all, I would like to thank my supervisor, Prof. Magne Børset, for accepting me into his research group and for allowing me the freedom to pursue a very specific and specialized research topic under their supervision. Through his excellent guidance and academic knowledge, coupled with always being available for long discussions, he has both introduced and helped me in the ways of scientific research and critical thinking.

I would also like to thank my co-supervisor Sara Beate Stjern Årbogen for all the much needed help during the laboratory work. Your unwavering patience is greatly appreciated, as you had to suffer through teaching me everything from basic lab work to advanced techniques, as well as having to answer all of my inane questions.

Furthermore, I would like to thank the rest of the bone marrow group for their insights, tips, feedback, and comments during our Tuesday meetings. I learned quite a lot listening to your presentations, as it introduced me to the scientific process, getting a glimpse into how you conducted your own research and how you handled either setbacks or unexplained results. I especially extend my thanks to Eli Svorkdal Hess for her guidance and help, both in the laboratory and in answering my many questions.

Also, I would like to thank Hanne Hella for her technical help, optimism, and eagerness in trying to help solve my mysterious flow results, and Berit Fladvad Størdal for her technical assistance and help in the laboratory. Also, I extend my gratitude to Ingrid Aass Roseth for lending me her time, helping me with the Seahorse experiment.

Lastly, I thank my family, friends, and enemies. I probably could have done it without you.

Table of Contents

Abbreviations

2-DG 2-Deoxy-D-Glucose

AMP Adenosine monophosphate

AMPK AMP-activated protein kinase

ATP Adenosine triphosphate

BAM15 2-fluorophenyl)6-[(2-fluorophenyl)amino](1,2,5-oxadiazolo [3,4-e]pyrazin-5-yl) 2-fluorophenyl

BM Bone marrow

CA Carbonic anhydrase

CCCP Carbonyl cyanide m-chlorophenyl hydrazone

CSR Class switch recombination

CTG CellTiter-Glo

DCQ Dequalinium Chloride

ECAR Extracellular acidification rate

ETC Electron transport chain

GLUT Glucose transporter

HIF-1α Hypoxia-inducible factor 1-α

HK Hexokinase

MGUS Monoclonal Gammopathy of Undetermined Significance

MCT Monocarboxylate transporter

MM Multiple myeloma

mPTP Mitochondrial permeability transition pore

NHE1 Sodium-hydrogen exchanger 1

OCR Oxygen consumption rate

OXPHOS Oxidative phosphorylation

PPP Pentose-phosphate-pathway

PRL-3 Phosphatase of regenerating liver-3

PTP Protein tyrosine phosphatases

RLU Relative light units

ROS Reactive oxygen species

SMH Somatic hypermutations

STAT Signal transducer and activator of transcription

TME Tumor microenvironment

TMRM Tetramethylrhodamine, methyl ester

VEGF Vascular endothelial growth factor

1 Introduction

The heterogeneity observed in cancer presents perhaps the most significant challenge in finding a cure for this deadly and prevalent disease. This seemingly endless complexity, combined with an individual's genetic makeup, essentially renders every cancer unique and highly challenging to treat. Numerous strategies exist to combat cancer, including radiation therapy, chemotherapy, immunotherapy, and invasive surgery. Recent advances in CRISPR / Cas9 gene editing technology and the use of bispecific antibodies and CAR-T intervention also hold considerable promise for future therapeutic interventions.[1][2] However, these methods produce varying degrees of success due to the uniqueness of each tumor and its potential for metastasis.

1.1 Multiple Myeloma

Multiple myeloma (MM) is a form of hematologic malignancy that affects B lymphocytes in the bone marrow (BM) and originates from antibody-producing plasma cells in the body. The development of MM is caused and promoted by somatic mutations and is associated with secondary complications such as anemia, hypercalcemia, renal failure, and osteolytic lesions.[3] MM is driven by complex interactions of several pro-survival signaling pathways such as IL6/STAT3, PI3K/Akt/mTORC1, MAPK,[4] the extracellular matrix, and bone cells such as osteoblasts and osteoclasts, which control the formation and breakdown of bone tissue, respectively.[5]

The physiological development of B cells commences within the BM, where immature B lymphocytes undergo a series of maturation steps. This process, depicted in Figure 1.1, entails the differentiation of pro-B cells, followed by the rearrangement and maturation of heavy- and light-chain immunoglobulin (Ig) genes. Upon completion of this maturation process, mature B cells exit the BM and migrate to secondary lymphoid tissues such as lymph nodes and spleen. Within the germinal centers of lymph nodes, mature B cells undergo antigenic stimulation, leading to further differentiation into centroblasts or short-lived plasma cells.[6] Subsequently, centroblasts evolve into centrocytes through mechanisms such as somatic hypermutations (SMH) and class-switch recombination (CSR), culminating in the generation of memory B cells or plasmablasts equipped with high-affinity antibodies. Plasmablasts may migrate back to the BM via homing mechanisms and undergo further differentiation into plasma cells.

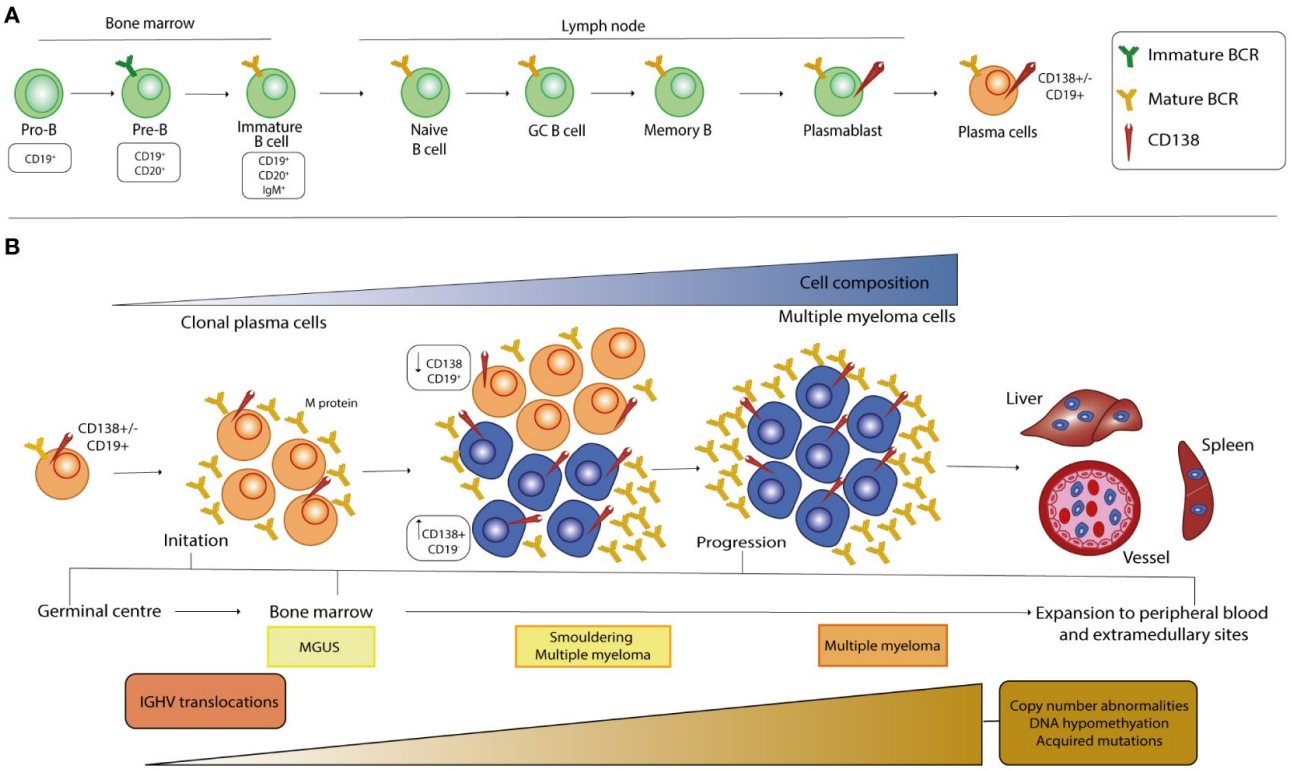

Figure 1.1: B cell development and MM pathogenesis: A) Development of B cells commences in the BM, where B cells undergo rearrangement of immunoglobulin heavy and light chains to express mature B cell receptors (BCRs) during the immature B cell stage. Upon migration to peripheral tissues, B cells reach full maturity, marked by the expression of CD138 on their cell surface. **B)** MM progresses through several stages, starting with Monoclonal Gammopathy of Undetermined Significance (MGUS), characterized by low levels of monoclonal protein (M-protein) produced by long-lived plasma cells. As MM progresses, transitioning to Smoldering multiple myeloma, malignant cells show a rise in CD138 surface levels while displaying an inverse relationship with CD19 levels. The final stage of MM involves the proliferation and expansion of the malignant clone, leading to organ infiltration and a poor prognosis. Adapted from Riccardi et al.[7]

An analysis of the Ig genes of MM cells by Bakkus et al.[8] unveiled distinct features characterized by SMH patterns lacking intraclonal variation and the absence of ongoing SMH or antigen selection. These findings suggest that primary MM cells originate from a subset of B cells that have undergone prior antigen-driven selection within the germinal center.

Monoclonal Gammopathy of Undetermined Significance (MGUS), an asymptomatic condition, serves as a precursor stage that precedes the development of MM.[9] Central to MGUS diagnosis is the presence of a monoclonal (M) paraprotein, generated from a clonal population of plasma cells, which produces an aberrant immunoglobulin (IgG, IgA, IgM, IgE, IgD, or light-chain only). This distinctive paraprotein is detectable via serum or urine protein electrophoresis, manifesting as a discernible 'band' or 'spike'. MGUS is characterized by three primary diagnostic criteria: **(i)** The existence of a monoclonal paraprotein in the serum, typically measuring <30 g/L. **(ii)** Proliferating clonal plasma cells within the BM, which make up $< 10\%$ of the BM. **(iii)** Lack of organ damage due to calcium elevation, renal dysfunction, anemia, and bone disease (CRAB criteria) associated with multiple myeloma. Upon detection of a monoclonal paraprotein, the possibility of an underlying hematologic malignancy is quickly investigated and excluded.[10] A higher level of paraprotein (>30 g/L), coupled with an increased percentage of plasma cells within the BM (>10 %), or the manifestation of end-organ damage related to plasma cell disease, suggests progression to smoldering multiple myeloma, which is the second stage. The development of MGUS is believed to involve various mechanisms, including cytogenetic alterations and changes in the BM microenvironment.

Chromosomal translocations are also frequently observed, often affecting regions responsible for the heavy-chain component of immunoglobulin. Among these, the t(11;14)(q13;q32) translocation, affecting Chromosome 14 (chr14), is prevalent and occurs in approximately 20% of MM patients.[11][12] This translocation leads to an increase in the expression of cyclin D1, a regulator of cell cycle progression that drives the G1/S phase transition. In general, approximately 40% of patients with MM exhibit translocations in the Ig heavy chain region located at chr14,[13] while the remaining 60% manifest hyperdiploidy, characterized by the gain of multiple odd-numbered

chromosomes, such as chr3, 11, 15, 19, and 21.[14] MM, while relatively uncommon, carries a global mortality rate of approximately 1% ,[15] constituting around 11% of all hematologic cancer cases in Norway as of 2022.[16] Although MM remains incurable, recent therapeutic advances have significantly improved treatment options, resulting in improved post-diagnosis survival rates,[17] with an expected 5-year survival rate of approximately 56% or higher.[18] For example, the ZUMA-7 study demonstrated that axi-cel, a form of CAR-T therapy, markedly enhanced both progression-free survival and overall survival.[19]

1.2 Bioenergetics

Every cell within the human body depends on energy for survival, maintenance, and proliferation. This energy facilitates cellular movement, transport of ions and other molecules across cell membranes, and the functioning of intricate signaling pathways that control gene expression, RNA and DNA synthesis, synaptic functions, and other essential activities. This concept is equally valid for cancer cells. Lacking energy, cancer cells are unable to initiate growth, multiply, or trigger pro-oncogenic genes, as these activities depend on energy for subsequent downstream signaling and function.[20]

Adenosine triphosphate (ATP) serves as the primary energy molecule in humans. Various pathways, including cellular respiration, glycolysis, degradation of ketone bodies, beta-oxidation of fatty acids, and protein catabolism, can synthesize ATP, and the choice of pathway often depends on metabolic conditions.[21] The specific ratio and nutrients required are affected by numerous factors, such as external influences of the tumor microenvironment, which is characterized by variable pH and oxygen levels, and internal factors such as the type of cancer cell, its genetic characteristics, and whether it is classified as solid or hematologic cancer.

1.2.1 Oxidative phosphorylation

Mitochondria serve as the primary ATP production site in eukaryotic organisms through the process of oxidative phosphorylation (OXPHOS). This process involves multiple complex redox reactions within the electron transport chain (ETC), which occur in the presence of molecular oxygen. The coenzymes NADH and $FADH_2$ are generated in the mitochondrial matrix via the citric acid cycle[22] and in the cytosol through glycolysis.[23] These coenzymes act as high-energy electron donors for OXPHOS. During this process, NADH and $FADH_2$ are converted to NAD^+ and FAD, respectively, each donating two electrons.

Electrons are transferred through a sequence of redox reactions within the ETC, which is composed of four distinct protein complexes (I, II, III, IV), coenzyme Q (CoQ), and the hemeprotein cytochrome c, all located in the lipid bilayer of the inner mitochondrial membrane.[24] For NADH, electrons are initially transferred to Complex I and subsequently pass through Complex I, CoQ, III, cytochrome c, and IV, until reaching the ultimate electron acceptor, molecular O_2. This sequence of transfers reduces molecular O_2 along with two H^+ ions to form H_2O. In contrast, $FADH_2$ bypasses Complex I, instead donating electrons directly to Complex II. These electrons continue through CoQ, III, cytochrome c, and IV, culminating in the reduction of O_2 to H_2O. These processes are depicted in Figure 1.2.

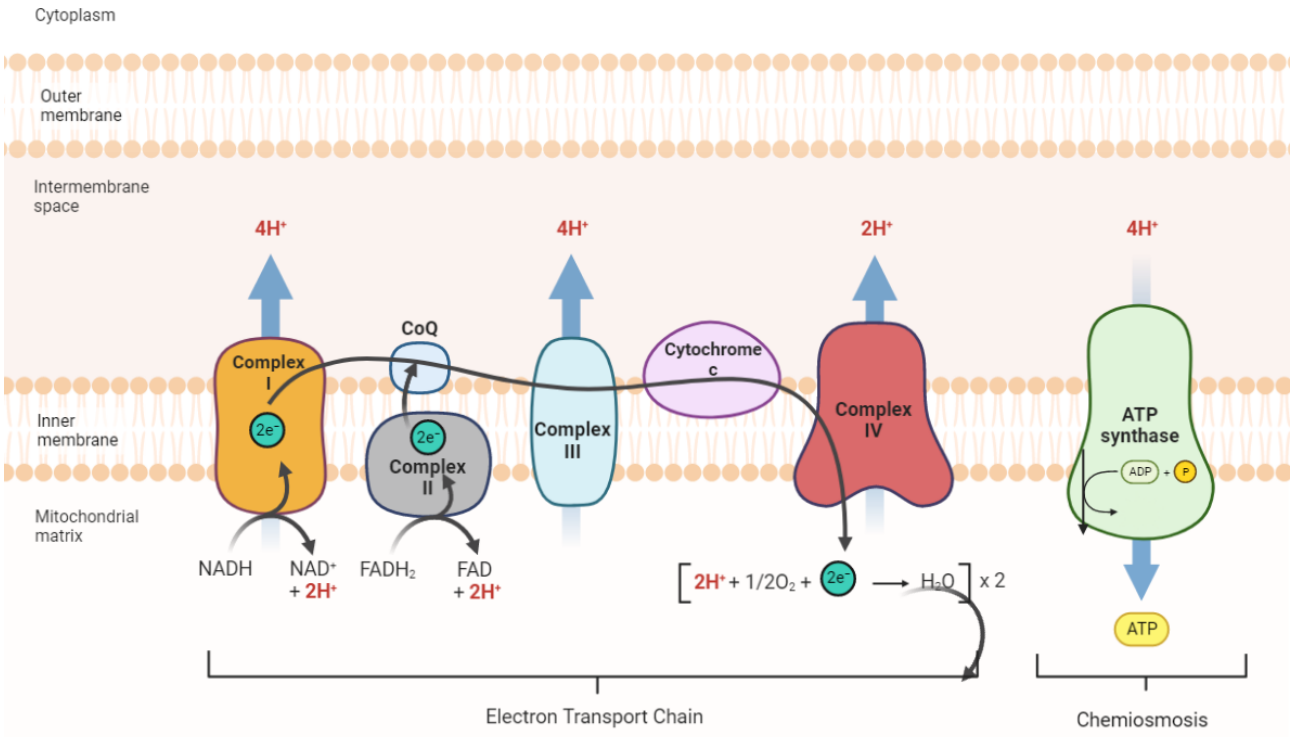

Figure 1.2: The process of oxidative phosphorylation: The Electron Transport Chain is shown on the left, consisting of the protein complexes I, II, III & IV, the hemeprotein cytochrome c and coenzyme Q. ATP synthase on the right utilizes the electrochemical gradient created by pumping H^+ protons into the intermembrane space and the energy from the diffusion of H^+ back into the mitochondrial matrix to drive protein rotors within the ATP synthase itself to form ATP. Figure made with Biorender and based on Shrestha et al.[25]

During the transfer of an electron along the ETC, the energy released from each redox reaction is utilized by Complexes I, III, and IV to actively transport H^+ ions from the mitochondrial matrix to the intermembrane space. This active transport of protons by the complexes results in an accumulation of H^+ ions in the intermembrane space, creating an electrochemical gradient. This gradient, known as the protonmotive force, is the basis for the process called chemiosmosis. ATP is then generated by chemiosmosis as protons from the intermembrane space diffuse back into the mitochondrial matrix[26] through ATP synthase.[27] While the production of ATP in mitochondria is a linked reaction involving the ETC and ATP synthase, a certain number of protons still re-enter the matrix by diffusing through the inner membrane, a process called proton leak, which accounts for approximately 20 - 25% of oxygen consumption in mammals.[28]

1.2.2 Glycolysis

Most cells in living creatures, such as mammals and vertebrates, use glucose as a source of energy and a basis for a number of biochemical reactions.[29] Glycolysis, a multistep process of chemical and biological reactions that occur in the cytosol, breaks glucose down into energy. This metabolic pathway converts glucose into its final molecule, pyruvate, through ten specific steps. Furthermore, this pathway does not require the presence of oxygen, making it an anaerobic source of energy.[30] Both anaerobic and aerobic glycolysis require glucose transporter proteins (GLUTs) to transport glucose to cells for uptake, because glucose is highly hydrophilic due to its hydroxyl group[31]

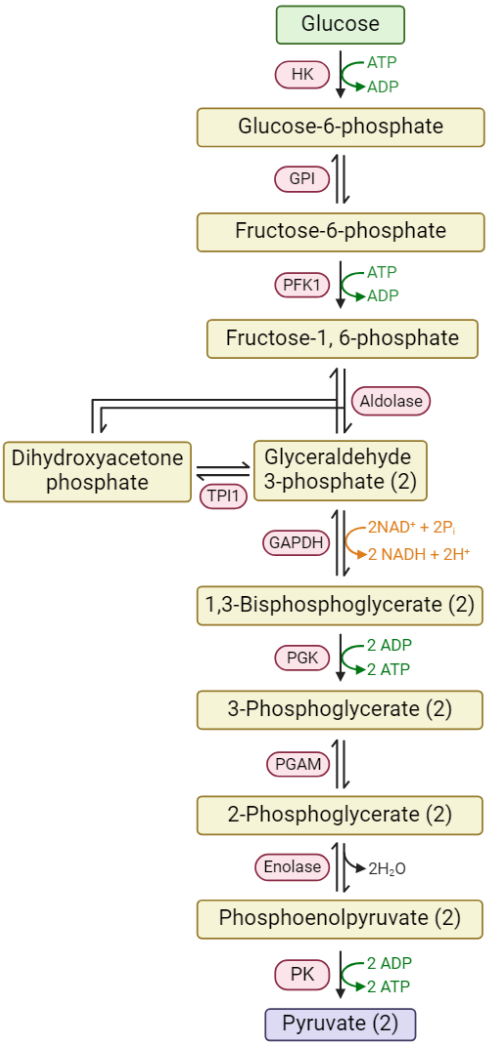

Figure 1.3: Glycolysis pathway: Schematic overview of glycolysis, highlighting the key enzymes involved in each conversion. Glycolysis is a central metabolic pathway that converts glucose into pyruvate, yielding ATP and NADH. Enzymes such as hexokinase, phosphofructokinase-1, and pyruvate kinase catalyze specific reactions, regulating the flow of metabolites through the pathway. The various intermediaries are in yellow, and the enzymes used are in red. Figure made with Biorender.

In glycolysis, as seen in Figure 1.3, one molecule of glucose forms two molecules of pyruvate, with the coinciding creation of two molecules of ATP. In cells under normoxic conditions, most of the pyruvate created by glycolysis is actively transported to the mitochondria. There, it is oxidized to acetyl coenzyme A by pyruvate dehydrogenase and subsequently enters the citric acid cycle.[32] In cancer cells, tumors, and other highly proliferating cell types, such as pluripotent stem cells and activated lymphocytes, the environment is often characterized by high degrees of hypoxia.[33] In such conditions, most of the pyruvate is not oxidized in the citric acid cycle. Instead, it is reduced in the cytosol to lactate by the enzyme lactate dehydrogenase (LDH) and the reducing agent NADH, a process known as lactate fermentation, as shown in Figure 1.4.

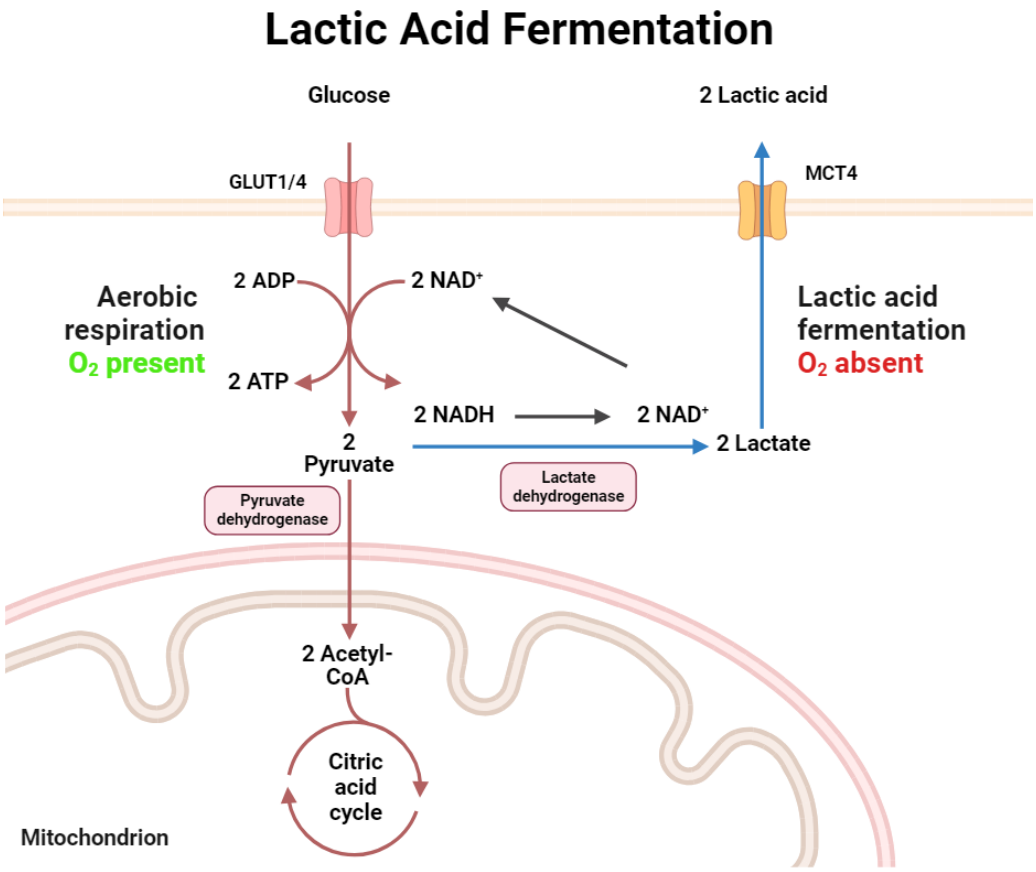

Figure 1.4: Lactic acid fermentation: The two fates of pyruvate during either aerobic respiration or anaerobic fermentation. When O_2 is present, pyruvate is transported into the mitochondria and is oxidized into acetyl-CoA by pyruvate dehydrogenase, and promptly joins the citric acid cycle. If O_2 is scarce, pyruvate is reduced to lactate by lactate dehydrogenase and is transported out of the cell via MCT4. Figure made with Biorender.

Glucose-6-phosphate (G6P) is the first product of glycolysis (Figure 1.3). It is formed in the cytosol when the enzyme hexokinase (HK) irreversibly phosphorylates glucose. G6P can then move to the pentose-phosphate pathway (PPP) and regenerate NADPH from $NADP^+$ and form intermediaries such as pentoses and riboses. NADPH is an important protective mechanism against genome mutations as it protects against highly deleterious reactive oxygen species (ROS).[34] The shift in metabolism facilitated by the PPP is also crucial for managing the diverse oxygen levels that tumors experience. When G6P and other carbon-based molecules venture through the PPP, a carbon flux is formed. This provides metabolic nutrients for nucleotide biosynthesis, used in DNA replication, RNA transcription, and maintaining a stable cellular redox state.[35]

1.2.3 The Warburg effect

In 1924, Otto Warburg published a revolutionary paper that shed light on cancer bioenergetics.[36] His work revealed a distinctive metabolic trait in cancer cells, wherein they preferentially utilize glycolysis over OXPHOS as their primary source of ATP generation. Unlike normal cells, which predominantly rely on OXPHOS to produce 36 ATP molecules per glucose molecule, cancer cells predominantly undergo glycolysis, yielding only 2 ATP molecules per glucose molecule. This metabolic adaptation, known as the "Warburg effect," is integral to the rapid proliferation and survival of cancer cells in the local microenvironment.

The term "aerobic glycolysis" is often used interchangeably with the Warburg effect, denoting the phenomenon in which cancer cells produce lactate through glycolysis even in the presence of adequate oxygen. Despite being energetically inefficient, many types of cancer exhibit a preference for aerobic glycolysis due to the increased demand for not only ATP but also macromolecules required for biosynthesis. This increased glycolytic flux leads to the augmented production of essential biomolecules necessary for the accelerated proliferation characteristic

of cancer cells.[37][38]

The molecular mechanisms driving the Warburg effect have been studied intensely through continuous research over the years and mostly been elucidated. Activation of oncogenic signaling pathways, including Myc, Ras, and Akt, coupled with inactivation of the tumor suppressor p53, orchestrates upregulation of glycolytic enzymes and glucose transporters, thus bolstering glycolytic activity.[39][40][41][42] In addition, certain glycolytic enzyme isotypes, such as the transition from other pyruvate kinase isotypes to PKM2Z play a contributing role.[43] Mutations affecting key enzymes in the citric acid cycle, such as succinate dehydrogenase, fumarate hydratase, and isocitrate dehydrogenase 2, along with alterations in mitochondrial DNA impacting the respiratory chain, further contribute to the Warburg effect.[44][45]

Another advantage gained by switching to aerobic glycolysis is the fact that glucose metabolism shows an increased regulation of apoptotic pathways, namely a redox reaction of glutathione (GSH) that inactivates cytochrome c. GSH is produced in glycolysis via PPP and is a potent reducing agent. By increasing the glycolytic flux, cancer cells increase the production of GSH which in turn downregulates the ability of cytochrome c to initiate apoptosis.[46] The trade-off between lower ATP production and increased nucleotide synthesis is a valuable compromise. DNA replication, RNA transcription, protein translation for cell division, and the synthesis of phospholipids for cell membranes are more important than the raw ATP output.

Glutamine is another source of fuel that cancer cells utilize. Glutamine is transported into the mitochondria and is utilized to refill and restore important metabolic intermediaries used in the citric acid cycle, or in the production of more pyruvate in a reaction with malic enzyme. The Warburg effect is driven by several signaling pathways, such as growth factor stimulation through PI3K / Akt and Ras. Akt promotes glucose transporter activity and has been shown to stimulate glycolysis by activating several important enzymes, such as HK and phosphofructokinase (PFK).

However, the Warburg effect is not absolute - not all types of cancer cells or tumors follow this metabolic reprogramming,[47] and much remains to be elucidated in this regard. Several studies have revealed that in numerous cancer cell lines, glycolytic ATP production never exceeds 64% of total ATP production and can be as low as $<$1% in some cell lines.[48] Evidence suggests that metabolic enzyme activity remains heterogeneous even within the same classes of tumors, and glycolytic enzymes can be up- or downregulated.[49]

There is also evidence that some types of cancer cells utilize lactate as a temporary citric acid cycle intermediate. This is achieved through the two monocarboxylate transporters MCT1 and MCT4.[50] Some also theorize that there is an intricate cooperative relationship in which cancer cells use aerobic glycolysis and OXPHOS symbiotically. The Lactate Shuttle Theory suggests a cooperative relationship between cells, wherein lactate produced by glycolytic cells is utilized as a substrate by neighboring cells for OXPHOS.[51][52] Furthermore, lactate has been implicated in a negative feedback loop, lowering the activity of key glycolytic enzymes, such as HK and phosphofructokinase (PFK), thus self-inhibiting aerobic glycolysis.[53]

1.2.4 2-Deoxy-D-Glucose

2-deoxy-D-glucose (2-DG) represents a synthetic glucose analogue, characterized by structural similarities to glucose with a notable distinction in one functional group. Specifically, the hydroxyl group at the 2-position of the sugar ring in glucose is substituted by a hydrogen atom in 2-DG, as shown in Figure 1.5. This structural and chemical modification is detrimental to glucose metabolism and glycolysis. Upon administration, 2-DG is swiftly internalized into cells, primarily facilitated by GLUT1 and GLUT4 through facilitated diffusion.[54] 2-DG is also capable of crossing the blood-brain barrier (BBB).[55] Following cellular uptake, 2-DG undergoes phosphorylation similar to glucose by HK. However, due to the absence of a hydroxyl group, 2-DG forms the electrically charged 2-deoxy-D-glucose-6-phosphate (2-DG-6P), bearing a net charge of $^{-2}$ owing to deprotonation of both phosphate groups. This imparts a charge imbalance, effectively sequestering 2-DG-6P within the cell and promoting its intracellular accumulation.[55]

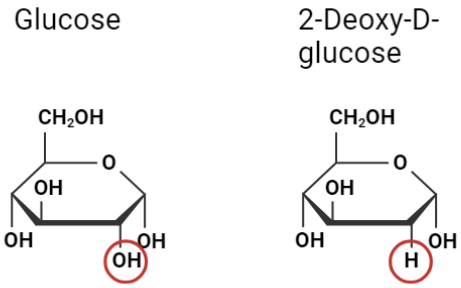

Figure 1.5: Structure of Glucose and its derivative 2-DG: Molecular structure of glucose and 2-Deoxy-d-Glucose. The structural alteration between each molecule is highlighted by the red circle. While both molecules share a similar backbone, 2-DG lacks the hydroxyl group at the 2-position present in glucose, which is replaced by a hydrogen atom. This substitution renders 2-DG unable to undergo further glycolysis, making it a competitive inhibitor of glucose metabolism.

Due to the absence of the vital hydroxyl group, 2-DG-6P cannot further isomerize to fructose-6-P. Consequently, it competitively inhibits glucose metabolism and therefore reduces glycolytic energy production.[56] This disruption of glycolysis by 2-DG operates at multiple levels. At one hand it reduces the amount of G6P available for subsequent utilization, thereby attenuating the metabolic flux throughout glycolysis and impeding its progression. Furthermore, 2-DG-6P serves as a non-competitive feedback inhibitor of HK, further impeding glucose phosphorylation.[57]

The hypoxic microenvironment prevalent in tumors is known to upregulate the expression of glycolytic enzymes, including HK and GLUTs. Since 2-DG competes with glucose for uptake by GLUTs and HK binding, its effect is enhanced by the intrinsic nature of cancer cells. This property renders 2-DG an intriguing candidate for exploiting the dysregulated metabolism of cancer cells. In addition, its relative non-toxicity and oral bioavailability enhance its attractiveness as a potential therapeutic agent.[58]

1.3 Tumor microenvironment

The tumor microenvironment (TME) is a complex structure composed of various components, including the extracellular matrix, tumor cells, immune cells such as macrophages, lymphocytes and granulocytes, endothelial cells, as well as an array of cytokines and chemokines. Insulin-like growth factor-1 (IGF-1) and interleukin-6 (IL-6) have been identified in particular as the main growth factors in MM.[59] In MM, the presence of malignant cells within the BM TME disrupts homeostasis among its various components. Instead of fostering equilibrium, these malignant cells instigate a cascade of events promoting proliferation, migration, drug resistance, and metastasis through intricate signaling pathways and intercellular interactions.[60]

1.3.1 Metabolic acidosis

The distinct metabolic rewiring observed in cancer cells, characterized by a shift toward aerobic glycolysis and subsequent accumulation of lactate, causes a profoundly altered TME. The expulsion of lactate by cancer cells results in the buildup of acidic substances in the extracellular environment, leading to a substantial proton gradient. Consequently, while cancer cells themselves maintain an alkaline intracellular pH, the TME outside of these cells becomes highly acidic.[61] The extracellular pH within the TME exhibits a wide range, with reported values as low as 5.8 to 7.0, in stark contrast to the slightly alkaline pH range of 7.2 to 7.4 typically observed in normal cell environments.[62][63]

Interestingly, this acidic microenvironment exerts a regulatory influence on cancer cell metabolism. Acidosis inhibits glycolysis, thus transitioning cancer cells from aerobic glycolysis to OXPHOS.[64] The mechanisms leading to the inhibition of glycolysis by protons are multifaceted. In part, there is a clear downregulation in the glycolytic enzymes HKII and PFK1, which are highly sensitive to H^+ inhibition due to the effects of pH on enzyme activity. The conformational change, protonation of the active site, and changes in the ionization state lead to a considerable

reduction in the glycolytic flux and the rate of glycolysis.[64] Secondly, the mass action ratio of LDH-catalyzed reactions is close to equilibrium due to the increase in cytosolic lactate concentration, which causes forward and backward reactions to have almost the same rate.[65]

Because acidosis does not suppress the expression of HKII, PFK1, and GLUTs, the inhibition of glycolysis mainly arises from proton inhibition and the change in LDH equilibrium. However, glycolysis is not the sole contributor to the excessive proton build-up in the TME. ATP hydrolysis, amino acid metabolism, and glucose utilization are also associated with increased proton flux.[66] Proton transporters such as vacuolar ATPases (V-ATPases), monocarboxylate transporters (MCTs), sodium-hydrogen exchangers (NHEs), and carbonic anhydrases (CAs) facilitate proton efflux and intracellular pH regulation in cancer cells. These transporters intrinsically protect cancer cells from drugs and molecules due to the high rate of protonation that occurs in the TME, thereby diminishing the efficacy of therapeutic interventions.[67][68]

In MM cells, as the disease progresses, the cells alter the microenvironment of the BM, forming the distinctive pathophysiology of MM that involves a high degree of drug resistance and aggressiveness. MM cells disrupt bone metabolism in favor of bone destruction, and there is a complex interplay between MM cells and the TME of bone lesions, essentially creating a relentless positive feedback loop of cancer growth and bone degradation.[69][70] As mentioned earlier, MM cells also produce a large quantity of lactate and consequently protons, lowering the pH of the TME by a huge margin compared to normal cells. Kato et al.[71] measured the extracellular pH of osteoclasts and found that it was as low, or even lower than pH 5.5. As a result, the interaction between MM cells and osteoclasts, in particular, leads to the creation of an extremely acidic TME. This acidity is caused by the production of lactate from anaerobic glycolysis and the secretion of protons by osteoclasts.[72]

1.3.2 Hypoxia

During the initial stages of cancer development, rapid proliferation often surpasses the capacity for oxygen diffusion, resulting in regions of hypoxia within the TME. This phenomenon arises due to the chaotic and disorganized nature of the vasculature in solid tumors, leading to inadequate oxygen supply to certain areas. Consequently, hypoxic sectors emerge within the TME, triggering an adaptive response characterized by increased expression of the transcription factor hypoxia-inducible factor (HIF). Hypoxia is a prominent feature of the TME and is crucial in regulating angiogenesis, metabolic processes, and immune responses, spanning both solid and hematologic malignancies. Hypoxia drives the upregulation of vascular endothelial growth factor (VEGF), a key signaling protein implicated in angiogenesis.[73] Notably, the synergistic interplay between hypoxia and aerobic glycolysis further exacerbates the acidic TME. HIF orchestrates the upregulation of GLUTs and glycolytic enzymes by binding to hypoxia-responsive elements (HREs) located in the promoter regions of oxygen-sensitive genes. This molecular cascade results in enhanced glycolytic activity and lactate efflux, thereby fueling the metabolic demands of cancer cells under hypoxic conditions.[74]

In contrast to most other organs, the BM is inherently hypoxic from a physiological standpoint. Spencer et al.[75] conducted *in vivo* assessments of intravascular oxygen tension (pO_2) in live mice, revealing BM oxygen levels to range between 15-30 mmHg (with a mean of 23 mmHg), equivalent to approximately 3% oxygen saturation. Additionally, extravascular pO_2 measurements indicated a range of 10-25 mmHg (with a mean of 17 mmHg), corresponding to 2% oxygen levels, notably lower than the 40-60 mmHg range observed in well oxygenated organs.[76] Within the framework and structure of BM, there are significant variations in the degree of hypoxia, characterized by two distinct areas. Located closer to the bone itself, the endosteal niche is believed to be the more hypoxic region, with a greater concentration of HIF-1α positive cells compared to the more centrally located vascular niche.[77]

1.3.3 Hypoxia-inducible factor 1α

Hypoxia-inducible factor 1α (HIF-1α) serves as a critical master transcription factor (TF) essential for cellular adaptation to hypoxic conditions commonly observed in tumor and cancer cells. As a heterodimeric TF, HIF-1α

forms a complex with HIF-1β, constituting helix-loop-helix proteins that function as biological oxygen sensors. Under normoxic conditions, HIF-1α undergoes rapid degradation via the ubiquitin/proteasomal pathway. Upon proline hydroxylation, HIF-1α binds to the von Hippel-Lindau protein (VHL) E3 ligase complex, prompting ubiquitination and subsequent proteasomal degradation. However, in hypoxic environments or following exposure to hydroxylase inhibitors like cobalt chloride, HIF-1α degradation is impeded, leading to its stabilization and accumulation.

HIF-1α exerts diverse biological effects by binding to HREs situated in the promoters of target genes, thereby activating transcription of various metabolic genes. These genes govern critical processes such as angiogenesis, erythropoiesis, cell cycle regulation, metabolism, and apoptosis.[78]

A pivotal function of HIF-1α under hypoxia is the promotion of angiogenesis. By inducing the expression of VEGF, a potent angiogenic factor, HIF-1α facilitates the formation of new blood vessels. This process improves the delivery of oxygen and nutrients to hypoxic tissues, thereby promoting cell survival and maintaining tissue homeostasis within the hypoxic TME. Another crucial adaptation orchestrated by HIF-1α in response to hypoxia is the metabolic shift from OXPHOS to glycolysis. HIF-1α upregulates glycolytic metabolism while simuultaneously downregulating OXPHOS, rendering cancer cells more reliant on glycolysis for energy production. This metabolic reprogramming is achieved through the upregulation of key glycolytic enzymes such as HKII, pyruvate kinase M2 (PKM2), and lactate dehydrogenase A (LDHA), which enhance glucose uptake and lactate production.[79]

Hypoxia exerts an inhibitory effect on metabolism, particularly on the citric acid cycle, which typically relies on the conversion of glucose to pyruvate and the subsequent conversion to acetyl-CoA. Under hypoxic conditions, the HIF pathway is activated, leading to the upregulation of pyruvate dehydrogenase kinase 1 (PDK1) by HIF-1α. PDK1 phosphorylates and inactivates pyruvate dehydrogenase, the enzyme responsible for converting pyruvate to acetyl-CoA. Consequently, pyruvate is directed toward LDH for conversion to lactate, rather than entering the citric acid cycle, thus inhibiting mitochondrial metabolism.[80][81] Additionally, HIF-1α plays a role in the regulation of the expression of genes involved in glucose transport and metabolism, such as GLUT1 and GLUT3. By promoting the expression of these transporters, HIF-1α enhances glucose uptake into cells, ensuring a sustained supply of glycolytic substrates to compensate for partial shutdown of OXPHOS under hypoxic conditions. Another consequence of HIF-1α stabilization is increased expression of MCT4 through transcriptional regulation. MCT4 is responsible for the export of lactate that is created through glycolysis and therefore HIF-1α also has a role in acidifying the TME.[82]

1.4 Phosphatase of Regenerating Liver-3

Protein tyrosine phosphatases (PTPs) are crucial enzymes that regulate cellular functions by removing phosphate groups from tyrosine residues in proteins, thus modulating signaling pathways. In the context of the TME, the activation of PRL-3 plays a significant role in promoting the survival and aggressiveness of MM cells.[83] PRL-3, encoded by the PTP4A3 gene, is a small (20 kDa) oncogenic PTP with dual-specificity capabilities, enabling it to target both tyrosine and serine/threonine residues.[84]

First identified in 1998 by Zeng et al.,[85] PRL-3 stands out due to its unique structural feature - a CAAX motif at its C-terminal tail. This motif facilitates the prenylation of PRL-3, anchoring it to the plasma membrane, a characteristic that is uncommon among other PTPs.[86] In particular, PRL-3 overexpression has been strongly associated with tumorigenesis, metastasis, and poor prognosis in cancer patients. Saha et al.[87] explored the molecular basis of metastasis and found that PRL-3 was expressed at elevated levels in all 18 metastases studied, as seen in Figure 1.6, and that numerous copies of the PRL-3 gene were present in a small region on the 8q24.3 chromosome.[87]

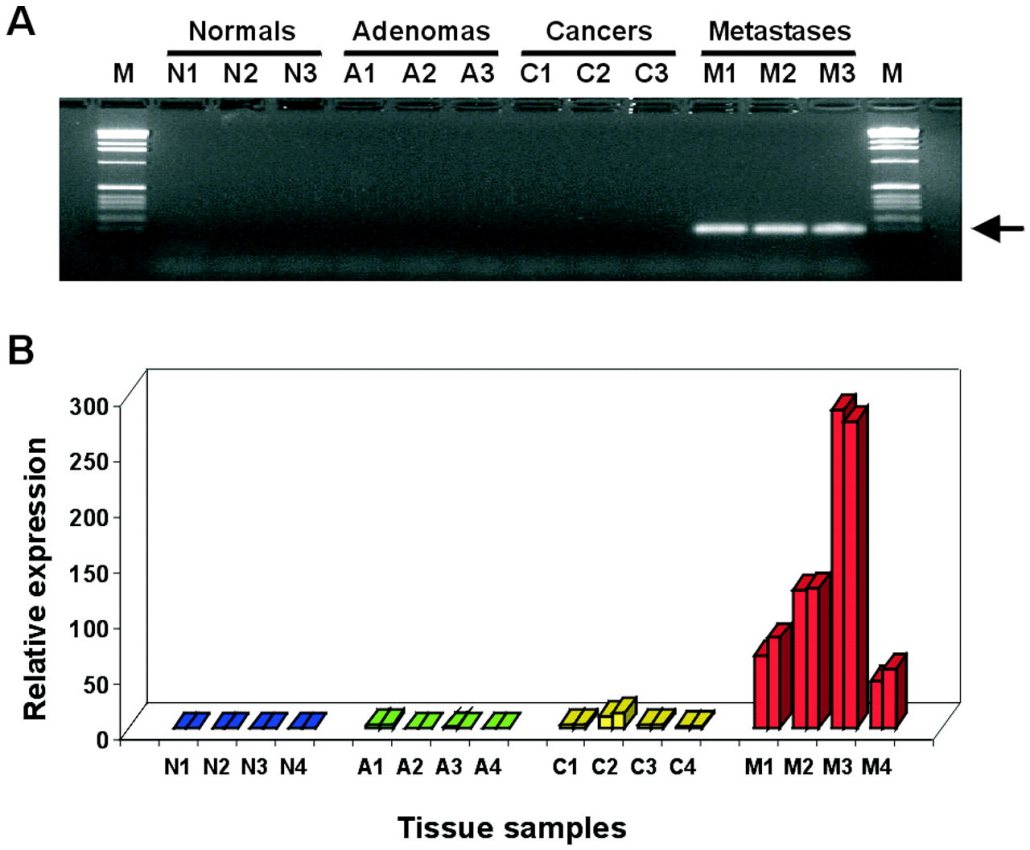

Figure 1.6: PRL-3 expression at different stages in colorectal cancer: The expression of PRL-3 at different stages in colorectal tumors in humans. RT PCR was used to evaluate the expression and compared to the β-amyloid precursor protein (APP) gene. Adapted from Saha et al.[87]

The expression of PRL-3 is regulated by various pathways and mechanisms. Sequencing of exon 10 from acute myeloid leukemia samples with elevated PRL-3 levels did not show somatic mutations or gene amplifications, suggesting that expression is governed at the transcriptional, translational, post-translational level, or by a combination of the three.[88] At the transcriptional level, P53, a tumor suppressor protein, has been linked to PRL-3 activation,[89] although the rate of occurrence of PRL-3 in certain types of cancer exceeded that of P53 mutations, indicating that additional regulators also control PRL-3 expression.[90] A study of the effects of transforming growth factor β (TGF-β) supported this theory, showing it to be an inhibitor of PRL-3 transcription. TGFβ was shown to facilitate the interaction of TFs Smad2 and Smad3 with the PRL-3 promoter.[91]

Snail, a C2H2-type zinc finger family TF, was also demonstrated to possess the ability to attach to the PRL-3 promoter, thus amplifying its transcription and subsequently increasing its protein levels in human colon cancer cells.[92] Two other important proteins that play a role in the regulation of PRL-3 expression are VEGF and signal transducer and transcription 3 activator (STAT3). In a study by Xu et al. (2011), a novel model was introduced in which cancer cells exhibiting elevated PRL-3 levels showed increased VEGF release, thus stimulating angiogenesis.[93] VEGF, in turn, triggers the expression of myocyte enhancer transcription factor 2 (MEF2), which binds to the PRL-3 promoter, increasing its transcription. STAT3, on the other hand has been linked with PRL-3, as shown by Lazo et al.[94] who demonstrated that inhibiting PRL-3 led to a decline in STAT3 levels in ovarian cancer. STAT3 has also been shown to require IL-6 stimulation to regulate PRL-3. Upregulation of STAT3 was observed in cancer cell lines that were IL-6 dependent and independent, accompanying the increase in PRL-3 levels at protein and mRNA levels.[95]

In particular, PRL-3 protein levels in various types of cancer, such as colon, breast, and lung cancer, did not consistently correspond to its mRNA levels, implying that PRL-3 regulation extends beyond transcriptional control. Wang et al.[96] demonstrated that poly(C)-binding protein 1 (PCBP1), a member of the hnRNP family of RNA- and DNA-binding proteins, interacted with the 5′-UTR region of PRL-3 mRNA, leading to its translational downregula-

tion. However, PCBP1 was also shown to not completely suppress PRL-3 translation, suggesting the presence of other mechanisms that negatively regulate PRL-3 when protein levels are low despite the presence of mRNA.[96]

Post-translational modifications (PTMs) also influence PRL-3, increasing the complexity of its regulation. PTMs are vital for maintaining cellular homeostasis by affecting the function, activity, destination, structure, and stability of proteins. Consequently, PTMs are considered mechanisms of both protein turnover and destruction.[97] The most elucidated and studied PTMs for PRL-3 include oxidation and reduction,[98] prenylation, although contradictory ,[99][100] and ubiquitination.[101][102] Cysteine residues within the active or regulatory sites of phosphatases are particularly susceptible to oxidation because of the chemical properties of the sulfur atom within the cysteine side chain.[103]

The thiol (-SH) functional group of cysteine residues is highly nucleophilic and critical for catalysis by participating in nucleophilic attacks on phosphate groups during dephosphorylation. However, the thiol group of cysteine in PRL proteins is also highly susceptible to oxidation,[104] which can lead to the formation of intramolecular disulfide bonds between Cys-104 and Cys-49, or other oxidized forms such as sulfenylamide bonds, thus decreasing or affecting phosphatase activity.[105][106] However, intracellular enzymes such as thioredoxin (TRX) reverse these oxidative modifications by utilizing NADPH,[107] donating electrons from TRX-reductase or GSH to break disulfide bonds and restore cysteine residues to their reduced state.

In terms of prenylation, there exist two modifications, namely farnesylation and geranylgeranylation, catalyzed by the farnesyltransferase enzyme (FT) and geranylgeranyl transferases (GGT I or GGT II), respectively. PRL-3 has been shown to be farnesylated,[99] whereas the case of geranylgeranylation remains unclear.[100] Farnesylation anchors PRL-3 to the plasma membrane, as previously mentioned, but also to early endosomes and to the Golgi apparatus.[108] Binding of PRL-3 to these structures is essential for it to exert its biological functions, particularly in cell signaling pathways involved in cancer progression and metastasis.[99][109]

Regarding PRL-3 and ubiquitination, ubiquitination serves as a mechanism to regulate its turnover and maintain cellular homeostasis. The process involves the sequential action of three enzymes: ubiquitin-activating enzyme (E1), ubiquitin-conjugating enzyme (E2), and ubiquitin ligase (E3). Initially, ubiquitin is activated by E1 in an ATP-dependent manner and transferred to an E2 enzyme. The E3 ligase then facilitates the transfer of ubiquitin from the E2 enzyme to specific lysine residues on the target protein, forming an isopeptide bond between the C-terminal glycine of ubiquitin and the -amino group of the target lysine. Once ubiquitinated, PRL-3 can be degraded via proteasomal or autophagy pathways Figure 1.7.[102][110][101]

One of the molecular mechanisms by which PRL-3 exerts its effects is through the regulation of the CNNM4 protein (Cyclin and CBS domain divalent metal cation transport mediator 4) and TRPM (transient receptor potential melastatin).[112] CNNM proteins are evolutionarily conserved Mg^{2+} transporters that selectively bind to the TRPM7 channel, stimulating cation flux.[113] Increased intracellular Mg^{2+} levels lead to upregulated proliferation, regulation of energy metabolism,[112] and metastasis, although the mechanism behind this is poorly understood. PRL-3 has also been found to interact with TRPM channels, particularly TRPM7. TRPM7 is a divalent cation-permeable channel with kinase activity involved in cancer metastasis. PRL-3-mediated regulation of TRPM channels influences intracellular Ca^{2+} and Mg^{2+} levels, affecting cell migration, invasion, and metastasis. Furthermore, TRPM7 kinase activity phosphorylates substrates involved in cytoskeletal dynamics, cell adhesion, and migration, further contributing to cancer metastasis.

Clarification on whether PRL-driven oncogenesis was dependent on phosphatase activity or CNNM-binding activity was attained by Kozlov et al. (2020),[114] who showed that replacing Cys with Asp (CD mutation) the active site of PRL-3, thus rendering PRL-3 enzymatically inactive, had no influence on the interaction between CNNM-PRL. Similarly to wildtype PRL-3, this mutant CD form effectively suppressed CNNM4-mediated Mg^{2+} efflux in cells. Thus, these results demonstrated that phosphatase activity is not required to promote oncogenesis, but rather that CNNM4 binding is the driving factor. Increased intracellular ATP levels also result from rising Mg^{2+} levels. Increased ATP levels in cells from B16 melanoma mice led to steady proliferation under glucose-poor conditions, which are found prominently in malignant tumors.[115] Concomitantly, elevated ATP levels also influenced signaling pathways such as AMP-activated protein kinase (AMPK) and mammalian target of rapamycin (mTOR).

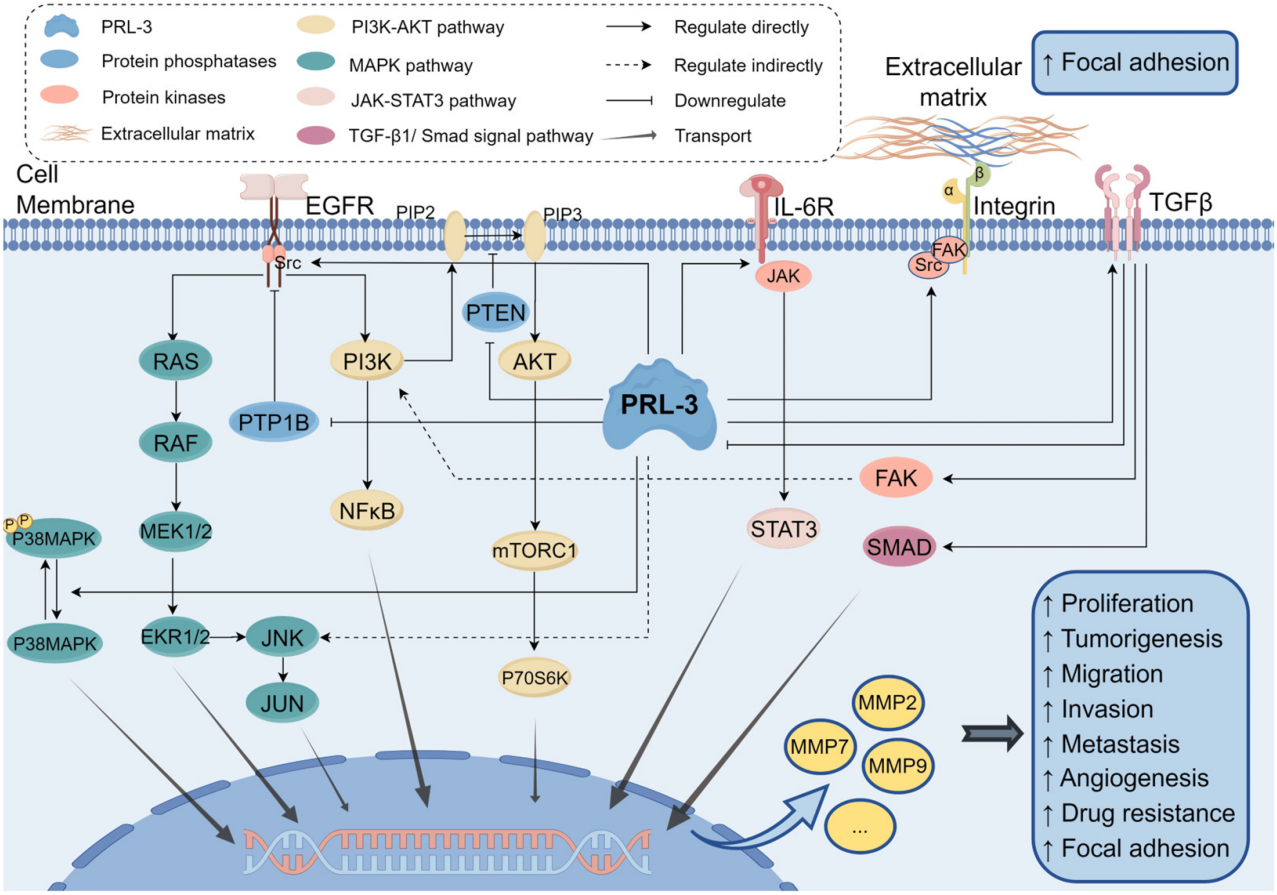

Figure 1.7: The multifaceted role of PRL-3 in promoting cancer progression: PRL-3, a phosphatase enzyme, exerts its oncogenic effects by activating various signaling pathways implicated in cancer development and metastasis. It enhances cell proliferation, survival, migration, and invasion by modulating key signaling molecules such as Src, ERK, and -catenin. Additionally, PRL-3 promotes angiogenesis, epithelial-mesenchymal transition, and immune evasion, fostering an environment conducive to tumor growth and metastasis. Adapted from Liu et al.[111]

AMPK, usually activated when the ratio of ATP:ADP is low, was found to be suppressed, whereas mTOR activity was high. Inhibition of CNNM also increased the rate of electron transfer in the electron transport chain (ETC), leading to excess ATP and an increase in reactive oxygen species (ROS).[116]

In MM, PRL-3 is induced by various signaling pathways such as IL-6 and other growth factors,[117] providing protection against the hypoxic and acidic conditions of the TME through several mechanisms. One such protective mechanism was proposed by Funato et al.[118] who revealed that PRL-3, overexpressed in kidney cancer cells, provided protective functions through H^+ extrusion and lysosomal exocytosis.[118] This protective mechanism leads cells expressing PRL-3 to become 'addicted' to the low- pH environment characteristic of the TME. The mechanism of lysosomal exocytosis stems from PRL binding to CNNM4, leading to a simultaneous increase in ATP and ROS due to augmented Mg^{2+} levels. ROS triggers the activation of transient receptor potential mucolipin (TPRml), a localized Ca^{2+} channel. This release of Ca^{2+} into the cytosol causes lysosomal exocytosis and H^+ extrusion.[119] A CRISPR/Cas9 knockout study of TRPml showed that PRL-3-induced lysosomal exocytosis was counteracted, as well as the change in optimal pH in cells from B16 melanoma mice.[120]

1.5 Metabolic rewiring in multiple myeloma

Like most cancers, MM also undergoes a radical change in terms of metabolic processes. MM cells are highly susceptible to glycolysis inhibitors due to their dependence on glucose, which is a result of the aforementioned phenomenon of aerobic glycolysis.[121] An observed increase in the expression of rate-limiting enzymes, such as HKII and LDHA, in the glycolysis pathway correlates with a poorer prognosis.[122] It is noteworthy that MM cells can import lactate exogenously via MCT1, which contributes to driving the reverse Warburg effect.[123] MM cells have been shown to metabolize through OXPHOS after inhibition of glycolysis. This is achieved primarily through glutaminolysis, indicating a compensatory mechanism in which the limitation of glycolysis is offset by increased dependence on OXPHOS.[124] The most studied metabolic pathways in MM are glycolysis and glutaminolysis, but also the PPP and folate pathway have been shown to regulate MM to a certain degree.[125]

Both HKII and LDHA are upregulated to a greater degree in relapsed MM patients compared to those newly diagnosed with the disease.[126] PRL-3 also alters MM cell metabolism, evident by the fact that MM cells with a PRL-3 vector had a higher rate of glycolysis, OXPHOS, and ATP production compared to cells with an empty control vector (Mock).[83] Both glucose uptake and lactate excretion are increased in cells with PRL-3 compared to Mock cells, but the glutamine / glucose uptake ratio was markedly lowered, pointing to a change in metabolism away from glutamine and toward aerobic glycolysis.[127]

1.6 AMP-activated protein kinase

AMP-activated protein kinase (AMPK) is a cellular energy sensor found in eukaryotic cells. Its primary function is to maintain the homeostasis of cellular energy. It achieves this by sensing changes in the ratio of AMP:ATP, which reflects the energy status in both the whole body and cells.[128][129] AMPK activation occurs when the ATP that is bound in its regulatory γ subunit is replaced by either ADP or AMP. This switch induces a conformational change in AMPK that elicits allosteric activation and phosphorylation of catalytic subunits by upstream kinases. A drop in ATP and an increase in ADP from various energy processes in the cell shift the reaction equilibrium of myokinase (2 ADP $\rightarrow$ AMP + ATP) heavily to the right. This produces a high AMP:ADP ratio, subsequently activating AMPK.[130]

Intracellular Ca^{2+} can also activate AMPK through non-canonical mechanisms, independent of AMP/ADP levels. This occurs when certain conditions are met, such as DNA damage and glucose starvation through non-canonical mechanisms independent of AMP / ADP.[131][132] When AMPK phosphorylate downstream targets that control catabolic pathways and simultaneously turn off anabolic pathways, combined with the abrogation of several energy-consuming processes related to the cell cycle, AMPK regulates not only the synthesis of ATP but also the proliferation and growth of cells upon activation.

1.7 Reactive oxygen species

A consequence of the incomplete coupling between the ETC and ATP production is what is called an electron leak.[133] Electron leak occurs when single electrons, in the ETC, undergo electron transfer between different complexes. Instead of reaching their final electron acceptor, molecular O_2, electrons escape the respiratory chain, partially reducing O_2, creating $O_2^{\bullet -}$ (superoxide). Superoxide serves as a dangerous precursor to more potent reactive oxygen species (ROS), which are oxygen-derived molecules with one unpaired electron. The superoxide anion is rapidly converted to hydrogen peroxide (H_2O_2) through a dismutation reaction with the enzyme superoxide dismutase.

H_2O_2, although not traditionally categorized as a ROS, is commonly regarded as such due to its involvement in oxidative processes. The superoxide anion, if not rapidly converted through this dismutation, can lead to more dangerous reactive oxygen species, such as the hydroxyl radical $OH^{\bullet}$, if H_2O_2 reacts with free Fe^{2+}, which is known as the Fenton reaction.[134]

Normal cellular function relies on intrinsic defense mechanisms against ROS, collectively known as antioxidants. These defenses encompass a variety of enzymes, including superoxide dismutase, peroxidases, and catalases, as well as molecules such as GSH and vitamins C and E.[135] However, when ROS production, often generated during OXHPOS, exceeds the antioxidant capacity, oxidative stress occurs.[136] Oxidative stress is implicated in cellular damage and is linked to various diseases, including those associated with aging.[137] ROS possess potent oxidative capabilities, rendering them capable of damaging lipids, proteins, and nucleic acids, particularly mitochondrial DNA, which lacks the protective histone layer found in nuclear DNA.[138][139]

ROS are inherent to cellular processes and serve as secondary messengers in signaling pathways associated with cell proliferation and differentiation, as evidenced in growth factor signaling pathways.[140][141] However, ROS also play a role in cancer development, contributing to tumorigenesis, angiogenesis, chemoresistance, DNA damage, mutagenesis, and modulation of apoptosis.[142] Cancer cells show elevated levels of ROS and antioxidants compared to normal cells,[143] and maintain a specific tumorigenic-favorable homeostasis by balancing these two species. Increased ROS levels in cancer cells often stimulate tumor growth by activating TFs like NF-κB and AP-1, which promote proliferation and inhibit apoptosis.[144]

1.8 Mitochondrial uncouplers

Mitochondrial uncouplers disrupt the normal functioning of OXPHOS by transporting H^+ ions from the intermembrane space back into the mitochondrial matrix, thereby dissipating the electrochemical gradient crucial for driving ATP synthase.[26] This essentially interrupts the coupling between electron transport and ATP synthesis. Although protons continue to be actively pumped out of the mitochondrial matrix in the presence of an uncoupler, the coupling process with ATP synthase is hindered.

As a result, the energy derived from redox reactions, in the form of the proton gradient, is not effectively utilized by ATP synthase, as the uncoupling agent facilitates the translocation of H^+ ions across the inner mitochondrial membrane independently of ATP synthase. This uncoupling of OXPHOS frees a considerable amount of energy in the form of heat, which can have adverse effects on cellular function due to the intricate interaction between biochemical processes and temperature. The mechanism of action of uncoupling agents is schematically depicted in Figure 1.8, illustrating how protons are transported back into the mitochondrial matrix, circumventing ATP synthase.

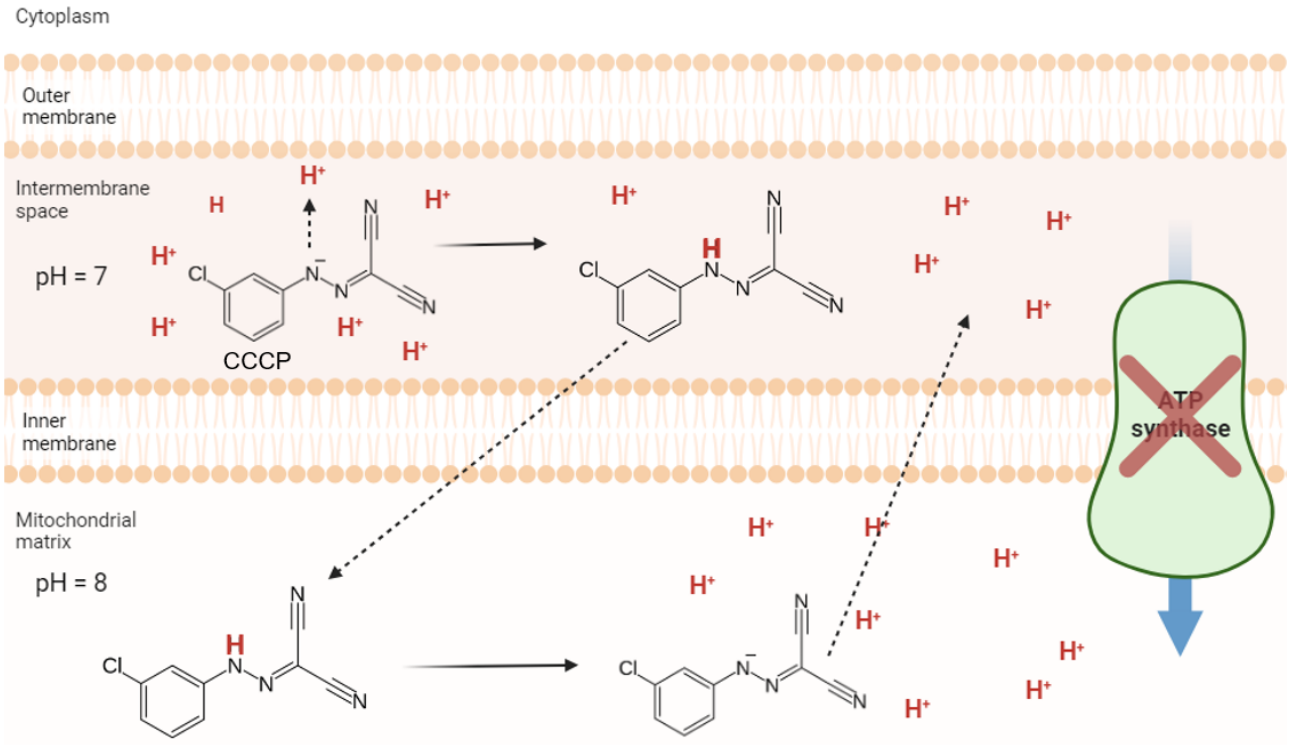

Figure 1.8: Mechanism of a classic chemical uncoupler: Structure of CCCP and its mechanism as a protonophore. The deprotonated form of CCCP in the intermembrane space picks up a proton and subsequently is protonated. The protonated form of CCCP feels an electrical attraction to the basic environment of the mitochondrial matrix and thus diffuses through the inner mitochondrial membrane, taking the H^+ ions with it. Inside the mitochondrial matrix, CCCP is deprotonated due to its chlorine and nitrogen atoms that act as electron-withdrawing groups. In its deprotonated state inside the mitochondrial matrix, CCCP feels an attraction to the acidic environment of the intermembrane space, and diffuses back through the inner membrane, where this process is repeated, leading to a decoupling of oxidative phosphorylation. Figure made with Biorender.

Exogenous uncouplers, predominantly protonophores, exhibit hydrophobic properties and possess weak acidic characteristics.[145] The pH gradient resulting from the active transport of protons from the mitochondrial matrix to the intermembrane space facilitates the preferential accumulation of protonated, weakly acidic molecules within the relatively basic environment of the matrix. Upon entry into the matrix these uncouplers release the dissociable proton, assuming their anionic form. Subsequently, uncouplers experience an electrochemical attraction towards the more acidic intermembrane space. As a result, they readily traverse the membrane to acquire another H^+ ion. This cyclic process persists until the exogenous uncoupler is fully metabolized.

1.8.1 Carbonyl cyanide m-chlorophenyl hydrazone

Carbonyl cyanide m-chlorophenyl hydrazone (CCCP) is a classical chemical uncoupler known to disrupt the electrochemical gradient across the mitochondrial inner membrane, thereby uncoupling OXPHOS. This pertubation results in reduced ATP production and an increase in cellular respiration as mitochondria attempt to compensate for the loss of ATP. CCCP exhibits cytotoxic effects in various cancer cells through multiple mechanisms. These include reversible opening of the mitochondrial permeability transition pore (mPTP) and mitochondrial swelling,[146] induction of apoptosis through ligands such as TNF-related apoptosis-inducing ligand and ROS, reduction in mitochondrial membrane potential ($\Delta\psi$),[147] fas-triggered cell death,[148] or reduction in ATP levels.[149] CCCP targets both the mitochondrial and plasma membranes, allowing it to shuttle protons across both.[150] CCCP has been shown to activate AMPK independently of mTORC1,[151] and inhibit NADH-dependent respiration in tumor cells by activating mitochondrial Ca^{2+} efflux.[152] It's structure is seen in Figure 1.9.

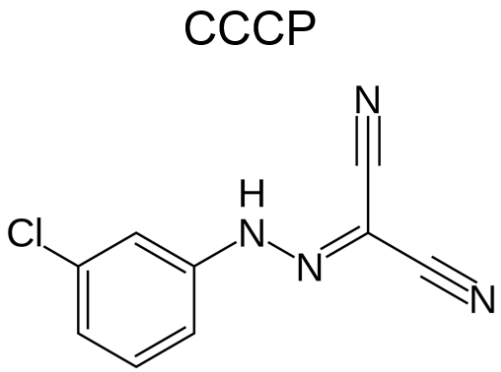

Figure 1.9: Structural Representation of Carbonyl Cyanide m-Chlorophenyl Hydrazone (CCCP): The figure illustrates the molecular structure of Carbonyl Cyanide m-Chlorophenyl Hydrazone (CCCP), a potent chemical uncoupler. CCCP disrupts the proton gradient across mitochondrial membranes, effectively decoupling oxidative phosphorylation and ATP synthesis. The structure comprises a central hydrazone moiety (R-NH-N=R'), a cyanide group (-CN), and a chlorinated phenyl ring (m-chlorophenyl). This unique configuration allows CCCP to efficiently transport protons across lipid membranes, leading to a collapse of the proton motive force.

1.8.2 2-fluorophenyl)6-[(2-fluorophenyl)amino](1,2,5-oxadiazolo [3,4-e]pyrazin-5-yl)

2-fluorophenyl)6-[(2-fluorophenyl)amino](1,2,5-oxadiazolo [3,4-e]pyrazin-5-yl (BAM15) is a novel mitochondrial protonophore (Figure 1.10 similar to CCCP mechanistically. However, what distinguishes BAM15 from CCCP and other traditional uncouplers is its specific targeting of mitochondria, thereby avoiding plasma membrane depolarization and minimizing off-target effects. BAM15 initiates vital energy signaling pathways, such as AMPK and peroxisome proliferator-activated receptor gamma coactivator 1-α (PGC-1α).[153] An increase in PGC-1α activation causes an upregulation of specific genes involved in mitochondrial biogenesis, mitochondrial respiration, and certain antioxidant genes such as manganse superoxide dismutase, catalase, thioredoxin 2, and thioredoxin reductase, all of which collectively prevent mitochondrial dysfunction.[154]

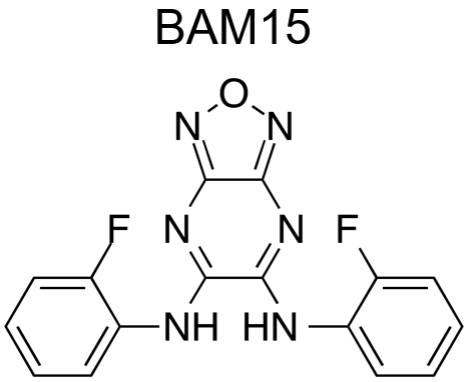

Figure 1.10: Molecular Structure of the Mitochondrial Uncoupler BAM15: The figure depicts the molecular structure of BAM15, a mitochondrial uncoupler known for its selective protonophoric activity. BAM15 exhibits a unique structure featuring, pyrazine, oxadiazole, and fluoro-substituted phenyl rings. This configuration enables BAM15 to facilitate proton transport across the mitochondrial inner membrane, effectively dissipating the proton gradient

BAM15 has demonstrated efficacy in decreasing ROS.[155] Under normoxic conditions, prolyl hydroxylase marks HIF-1α for degradation. However, ROS inhibits prolyl hydroxylase, leading to the stabilization of HIF-1α. Reduced ROS levels would therefore diminish the inhibition of prolyl hydroxylase, resulting in less stabilization of HIF-1α. ROS inhibition occurs through the oxidation of Fe(II) to Fe(III), which interferes with the enzymatic activity of prolyl hydroxylase.[156] Ascorbic acid can rescue this reaction by reducing Fe(III) back to Fe(II).

1.9 Electrical properties of cancer cells

Mitochondria are pivotal in the cell cycles of eukaryotic organisms, influencing both cellular survival and apoptosis.[157] Protons are actively pumped out of the inner mitochondrial membrane, generating an electrochemical gradient essential for ATP synthesis (Figure 1.2.1). Enzymatic oxidation of fatty acids and glucose by processess in the citric acid cycle and in glycolysis establishes both a proton gradient and a pH gradient across the inner mitochondrial membrane, creating a membrane potential (Ψ_m) ranging from -80 to -120 mV,[158] and a pH gradient of 0.5 to 1.0 pH units.[159]

Maintaining a hyperpolarized voltage across the inner mitochondrial membrane (Ψ_{IMM}) is critical for the viability of eukaryotic cells. Failure to maintain this voltage leads to cell death through the opening of the mPTP, triggering the release of cytochrome c and initiating apoptosis.[160] Notably, tumor cells often exhibit a more hyperpolarized Ψ_{IMM} compared to normal cells, along with a depolarized plasma membrane (Ψ_{PM}), rendering them particularly susceptible to voltage fluctuations.[161] This altered voltage gradient also enhances the accumulation of lipophilic anions within tumor cells, with a much higher affinity compared to normal cells, especially considering the substantial voltage difference (60 - 80 mV), supposing that the ion has a single charge. This effect increases by a factor of 10^2 if the ion has a double-charge.[162] Hyperpolarization also scales with the severity of cancer, meaning that the more dangerous / invasive cancer, the more hyperpolarized its Ψ_{IMM} is (certain cancers can be up to 130 mV more hyperpolarized[163]), leading to an even greater affinity, which can be calculated using the Nernst equation, for the mitochondrial matrix by lipophilic ions.[164]

In contrast, cancer cells tend to depolarize their Ψ_{PM} compared to normal cells, potentially as an adaptive response to metabolic acidosis resulting from aerobic glycolysis. As lactate and protons accumulate extracellularly, the proton motive force (Δp) increases. However, cancer cells strive to maintain a neutral Δp.[165][166] The Δp in the Ψ_{PM} consists of two components: $\Delta\Psi_m$ and ΔpH, which can be calculated using the following formula:

$$\Delta p = \Delta\Psi - 2.3RT/F\Delta pH \tag{1.1}$$

Where $\Delta\Psi$ = Ψ_{in}- Ψ_{out}, Δ pH = pH_{in} - pH_{out}, R is the gas constant, T is the temperature in Kelvin, and F is the Faraday constant. This becomes the following equation after simplifying the terms and assuming a temperature of 300K:

$$\Delta p = \Delta\Psi - 59\Delta pH \tag{1.2}$$

For a normal cell, assuming a $\Delta\Psi$ of -70 mV,[167] extracellular pH = 7.4[168] and intracellular pH = 7.2[168]

$$\Delta p = 70mV - (59(7.4 - 7.2)) = 58mV \tag{1.3}$$

For a cancer cell, assuming a $\Delta\Psi$ of -10 mV,[167] extracellular pH = 6.5[168] and intracellular pH = 7.2[168]

$$\Delta p = 10mV - (59(7.2 - 6.5)) = 51mV \tag{1.4}$$

Hence, Δp for both normal and cancer cells is similar. This would not have been the case had the cancer Ψ_{pm} not been depolarized:

$$\Delta p = 70mV - (59(7.2 - 6.5)) = 111mV \tag{1.5}$$

This would lead to an extremely high Δp, forcing protons back into the cancer cell, reducing its pH.
The rate of ATP/ADP exchange at steady-state is influenced by the mitochondrial membrane potential ($\Delta\Psi_m$). Figure 1.11 illustrates that as $\Delta\Psi_m$ decreases, the rate of ATP efflux also decreases, exhibiting an almost linear relationship.[169] A decline in ATP efflux implies reduced availability of free ATP for cellular processes, indirectly leading to ATP deprivation.

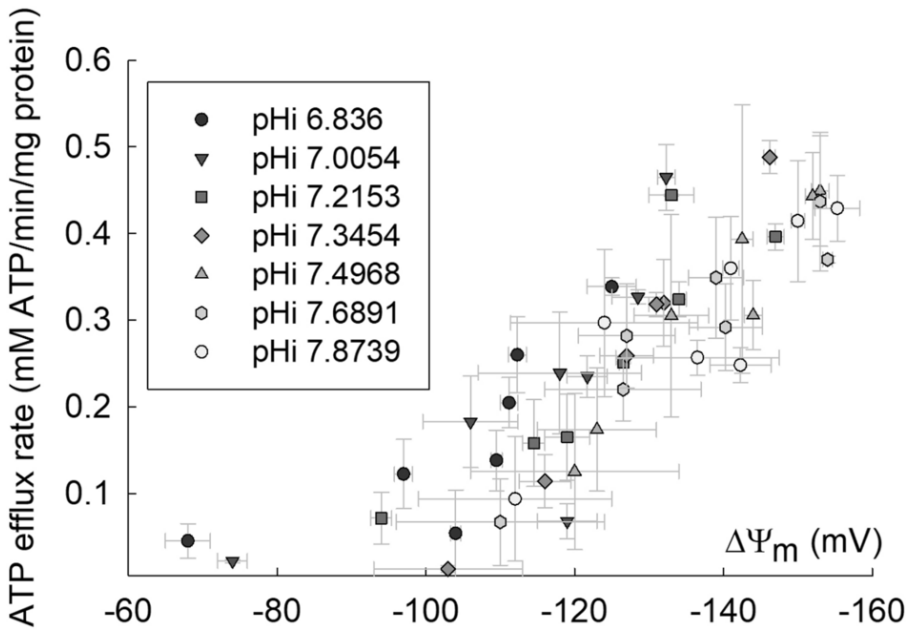

Figure 1.11: Relationship between Mitochondrial Membrane Potential and ATP Efflux via ANT: The relationship between mitochondrial membrane potential ($\Delta\Psi_m$) and the rate of ATP efflux from the mitochondrial matrix to the cytosol through the Adenine Nucleotide Translocase (ANT) protein. As $\Delta\Psi_m$ increases, facilitated by the proton gradient across the inner mitochondrial membrane, the electrochemical driving force for ATP export via ANT intensifies. This leads to an elevated rate of ATP efflux into the cytosol, where ATP serves as a critical energy currency for various cellular processes. Adapted from Chinopoulos et al.[169]

1.9.1 Dequalinium Chloride

Dequalinium chloride (DCQ) is a bis-quaternary ammonium salt compound with antiseptic properties, commonly used in various drugs and pharmaceuticals. Its efficacy against bacteria, viruses, and fungi, coupled with its ability to enhance cell permeability and inhibit enzyme activity, renders it a valuable compound in medical applications.[170]

DCQ primarily influences bacterial cell permeability through two mechanisms. Initially, it adsorbs onto the cell surface of the microorganism, facilitating diffusion through the cell wall. Subsequently, it binds to the cytoplasmic membrane, resulting in protein precipitation and complex formation. At higher concentrations, DCQ may induce cell membrane lysis, disrupting osmotic balance.[171][170] Upon penetration of the cell wall, DCQ interferes with metabolic processes primarily by protein denaturation, thereby inhibiting cell metabolism. Additionally, it disrupts ATP synthesis by impeding glucose metabolism and interfering with F1-ATPase activity.[172][173] One caveat worth noting is that the doses required to inhibit metabolic processes are substantially higher than those needed to alter cell permeability.[174]

From a cancer perspective, DCQ is significant due to its capacity to target energy production in cancer cells.[175][176] Its chemical properties, particularly its $^{2+}$ cationic state in solution, enable DCQ to accumulate in the mitochondria of cancer cells, exploiting their hyperpolarized mitochondrial membrane.[161] Due to this $^{2+}$ cationic state, DCQ acts synergistically when administered alongside anionic uncouplers or other negatively charged compounds, thereby enhancing their effects.[177] DCQ has also been observed to increase the formation of ROS and deplete GSH, resulting in elevated cellular oxidative stress.[178] Moreover, it interferes with several signaling pathways such as ERK1/2 and PI3K/Akt, leading to their downregulation.[179]

2 Aim and hypotheses

The primary objective of this Master's thesis is to investigate the response of PRL-3-expressing MM cells to ATP deprivation by mitochondrial uncoupling agents and an inhibitor of glycolysis, and the influence of the BM microenvironment on their metabolic adaptations. Specifically, we aim to elucidate the regulatory role of PRL-3 in both OXPHOS and glycolysis in MM cells, as highlighted in previous studies by Abdollahi et al.[127]

Hypotheses:
i:) PRL-3-expressing cells are hypothesized to display sensitivity to metabolic stressors such as uncoupling agents and glycolysis inhibitors. PRL-3 may confer an advantage in cancer cells by enhancing glycolytic flux, but also potentially create a vulnerability when glycolysis is inhibited.

ii:) The TME, characterized by low pH and hypoxia, is hypothesized to accentuate the metabolic advantages conferred by PRL-3. PRL-3-expressing cells are expected to show enhanced survival, metabolic efficiency, and adaptability in response to the acidic and hypoxic conditions of the TME compared to Mock cells.

iii:) That proteins crucial for metabolism, pH balance, and hypoxia response undergo changes in expression in MM cells, due to the action of mitochondrial uncoupling agents and 2-DG during conditions of energy and environmental stress.

iv:) We predict changes in both mitochondrial membrane potential and production of reactive oxygen species in MM cells following treatment with uncoupling agents, and that these alterations will have anti-tumorigenic effects.

By methodically investigating the interactions of bioenergetics, chemical inhibition, PRL-3 expression, and the TME, our research aims to gain more knowledge of the dynamic processes of metabolic adaptations under energy stress, and to uncover novel vulnerabilities in MM cells that can be targeted for therapeutic intervention.

3 Materials and methods

3.1 Cell line and culture medium

INA-6 cell line used in this research originates from a German patient and was harvested several decades ago. These cells were grown and maintained in RPMI 1640, supplemented with L-glutamine (0.68 mM), Fetal Calf Serum (10%) and IL-6 (1 ng/ml). For experiments pertaining to normal oxygen conditions, cells were cultured in an atmosphere of 5% CO_2 at 37 °C, while experiments conducted under hypoxic conditions were carried out in a galaxy incubator (New Brunswick™ Galaxy 48R) at 5% CO_2, 2% O_2 at 37 °C. For experiments at pH 7.4, the RPMI 1640 medium was unchanged from baseline and then measured with a pH meter to verify its pH.
For experiments under acidic conditions, RPMI 1640 medium was prepared as normal, but to it, hydrochloric acid (HCl) was added until the desired pH was reached, then measured and verified with a pH meter. The acidic medium was prepared and sterile filtered on the day of the experiments, due to the tendency of the RPMI to oxidize when exposed to air and for CO_2 to diffuse out of the medium, increasing the pH of the medium.

3.2 INA-6 CellTiter-Glo proliferation assay

The proliferation of INA-6 cells following treatment with CCCP, BAM15, 2-DG, or their combination was assessed using the CellTiter-Glo® (CTG) 2.0 Cell Viability Assay. This assay quantifies the levels of ATP produced by metabolically active cells within a culture. Luminescence outputs, recorded in relative light units (RLU), correlate directly with ATP concentration, which in turn reflects the number of viable cells in the culture with a linear correlation ($r^2 > 0.99$). The CTG reagent consists of the protein luciferin, which is promptly catalyzed by the enzyme Luciferase together with ATP, Mg^{2+}, and O_2, which oxygenates Luciferin, turning it into oxyluciferin together with luminescence formation with a half-life of nearly 5 h. The process is depicted in Figure 3.1.

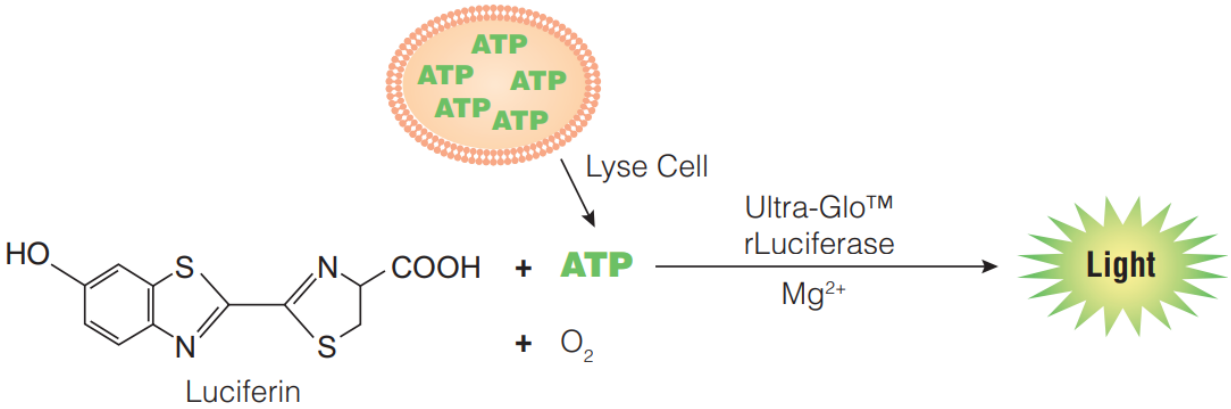

Figure 3.1: Chemical reaction between Luciferin and ATP, O_2, Mg^{2+} and Luciferase: In this reaction, luciferin reacts with ATP, O_2 , and Mg^{2+} in the presence of the luciferase enzyme. The reaction leads to the formation of oxyluciferin, AMP, inorganic pyrophosphate (PPi), carbon dioxide (CO2), and light emission. This luminescent reaction serves as a sensitive indicator of ATP concentration[180]

CellTiter-Glo® 2.0 cell viability assay was purchased from Promega (Madison, WI). The reagent was aliquoted according to the Promega technical manual provided in 15 ml centrifuge tubes and stored at -20 °C.

3.2.1 CTG assay procedure

INA-6 cells were cultured in RPMI 1640 supplemented with L-glutamine (0.68 mM), Fetal Calf Serum (10%) and IL-6 (1 ng/ml). Following centrifugation, the cells were resuspended in 1 ml of RPMI medium and counted. The cells were then allocated to a 96-well plate with a white bottom, 50 µl of medium with cells at a density of 10,000 cells/well. Subsequently, 50 µl of either an uncoupler or a 2-DG was added to achieve a final volume of 100 µl

per well. The plate was incubated for 24, 48, or 72 h prior to addition of 50 µl of CTG reagent to each well, and protected from light with aluminum foil. The plate was then placed on a shaker at 200 rpm for 2 min, followed by another 10 min at rest. The plate was then loaded into the FLUOstar® Omega (BMG Labtech) plate reader, configured for luminescence signal and ran accordingly.

3.3 Flow cytometry-based cytotoxicity assay

Flow cytometry serves as a high precision tool when the goal is to obtain a detailed analysis of individual cells based on their characteristics, such as cell size, complexity in terms of granularity and the presence of specific molecules or fluorescent markers. Flow cytometry allows for the quantitative analysis of individual cells within a heterogeneous population by measuring physical and chemical properties. The technique operates on the principles of optics and fluidics, utilizing lasers and detectors to examine cells as they flow in a fluid stream, passing the laser, which interacts with each cell one by one. When cells pass through the focused laser beam within the cytometer, the cells scatter light in different directions and emit fluorescence if labeled with fluorescent probes. This interaction provides information about the size, structure, internal complexity, and molecular composition of cells.

Light scattering in flow cytometry occurs in two main directions: Forward Scatter (FSC): This measures the intensity of light scattered in the forward direction, which correlates with cell size or volume. Larger cells scatter more light in the forward direction than smaller cells. Side Scatter (SSC): This measures the intensity of light scattered perpendicular to the laser beam, providing information about the granularity or internal complexity of the cells. Cells with more internal structures or granularity scatter more light sideways. Combining the information from FSC and SSC, these measurements can help characterize different cell populations from a macro-level point of view.

The second way to detect cells is by fluorescence emission. Many biological molecules, such as proteins, nucleic acids, and lipids, exhibit intrinsic fluorescence. In flow cytometry, cells are often labeled with fluorescent dyes or antibodies conjugated to fluorophores. When the electrons in these molecules get excited by the laser beam, these fluorophores emit light at specific wavelengths, allowing for the detection and quantification of cellular components, such as cell surface markers, DNA content, or intracellular proteins.

Choosing the appropriate fluorescent probe or dye is critical in flow cytometry to minimize interference from autofluorescence, which is intrinsic fluorescence emitted by cellular components such as flavins and lipofuscins. Autofluorescence can mask the signal from fluorescent labels or probes, leading to inaccurate measurements and misinterpretation of the data. To mitigate this problem, compensation controls are usually run in advance. By measuring the spillover of fluorescence signals into adjacent detection channels, compensation controls ensure reliable quantification of each signal, even in the presence of autofluorescence.

To assess the apoptotic and necrotic status of plasma cells after 24 h of ATP starvation, Annexin V, Alexa647, and Propidium Iodide (PI) were used. Annexin V binds with high affinity to phosphatidylserine, a phospholipid normally located on the inner part of the plasma membrane. During apoptosis, phosphatidylserine translocates to the outer part of the membrane, exposing it to the extracellular environment. Thus, Annexin V, conjugated with the fluorophore Alexa647, can specifically bind to phosphatidylserine on the outer membrane of apoptotic cells, enabling their detection by flow cytometry. In contrast, PI is utilized to detect dead or necrotic cells. PI cannot penetrate the intact plasma membranes of healthy cells, thus resulting in no binding. However, in cells with compromised membranes, PI can enter and bind to DNA. When PI is bound to DNA, it undergoes a conformational change, leading to enhanced fluorescence. Therefore, PI fluorescence serves as an indicator of late apoptotic and necrotic cells.[181]

3.3.1 Flow cytometry setup and procedure

The day prior to the assay, compensation controls were prepared. INA-6 wild-type (WT) and INA-6 Mock / PRL-3 cells were put aside. The following day INA-6 cells were seeded out in either pH 7.4 or pH 6.5 RPMI 1640, L-

glutamine (0.68 mM), Fetal Calf Serum (10%) and IL-6 (1 ng/ml). The cells were then spun and resuspended in 1 ml of RPMI medium and counted. 2 ml with 150,000 cells / well was seeded in a 24-well plate with a white bottom. The appropriate concentration of the uncoupling agent and 2-DG was added to each well, depending on the given experiment, and then incubated for 24 h in normoxia or hypoxia. The next day, a box of ice was prepared and 1 ml of each cell sample was pipetted and transferred to a flow tube, washed in cold PBS and spun at 4 °C, 448 x g for 5 min. Each flow tube was then decanted, the last drop dried on cellulose paper and then gently shaken on a rack to loosen the pellet.

During spin-down, Binding buffer (BB) was diluted 1:10 in deionized water. A total of 350 µl was required for each sample, along with five additional samples to account for compensation controls and potential volume loss during pipetting. Three Eppendorf tubes were filled with 350 µl of the diluted BB + water solution for use as compensation samples. To prepare compensation samples, three flow tubes were set up. The first tube contained INA-6 WT with 300 µl of BB and water solution, the second tube included INA-6 Mock/PRL-3 with a small quantity of INA-6 WT plus 350 µl of BB and water solution, and the third contained Annexin/alexa647 beads. Following the setup of these samples, 0.5 µl of Annexin/Alexa647 stock solution was added to the leftover BB and water solution. Subsequently, 300 µl of this mixture was distributed to each sample, which was then gently mixed by hand, protected from light, and placed in an ice-filled box to incubate for 55 min.

During the incubation phase, the Annexin/alex647 compensation mixture was prepared. The container with beads was briefly vortexed and then a single drop of beads was transferred into the flow tube. Subsequently, cold PBS was added and the tube was centrifuged at 4 °C and 448 x g for 5 min. After the supernatant was removed and the last drop dried on cellulose paper, the tube was gently shaken. Next, 1 µl of Alexa647 antibody was added to the remaining contents of the tube and the mixture was incubated on ice for 30 min. After incubation, the tube was washed with cold PBS and centrifuged at 4 °C and 448 x g for 5 min. Finally, the contents were resuspended in 350 µl of diluted BB + water, excluding the previously prepared Annexin/Alexa647 stock solution in the Eppendorf tube.

Following the incubation period of the samples, a predetermined volume of BB + water mixed with the Annexin/Alexa647 stock solution (50 µl $\times$ number of samples) was transferred to a new Eppendorf tube, to which (2 µl $\times$ number of samples) of Propidium Iodide (PI) was added. Next, 50 µl of this BB + PI mixture was distributed in each sample, and 2 µl of PI was added to the INA-6 WT compensation sample, followed by incubation for 5 min. Subsequently, the samples were examined using a BD LSR II Flow Cytometer (BD Biosciences) set to 488 nm and equipped with filters for Green fluorescent protein (GFP). Compensation samples for GFP, PI, and Annexin/alexa647 were performed, and the flow cytometer was adjusted for spectral overlap before analyzing the experimental samples. Viable cells were identified in the lower left quadrant (annexinV^-/PI^-), while cells in early apoptosis were located in the lower right quadrant (annexinV^+/PI^-), and those in late apoptosis or necrosis were in the upper right quadrant (annexinV^+/PI^+).

3.4 Protein expression elucidation by Western blotting

Western blotting, also called protein immunoblotting, is a fundamental technique used in research to detect, quantify, and characterize specific proteins within a sample. Western blotting, at its core, is a technique that is based on the principles of protein separation, transfer, detection, and analysis, respectively. The initial step in Western blotting is sample preparation, which involves protein extraction by cell lysis. This is done by resuspending a cell culture in IP lysis buffer, centrifuging, and extracting the supernatant. From here on, Bradford assay, a colorimetric technique based on the shift in absorbance of Coomassie brilliant blue G-250 dye, is usually performed. The dye changes form and color whether it is anionic, neutral, or cationic,[182] arising from the presence or absence of charged amino acids. Bradford assay is implemented to ensure that an equal amount of protein levels is present in each sample.

The next step is protein separation, which involves the separation of proteins according to their molecular weight. This is achieved through dodecyl sulfate-polyacrylamide gel electrophoresis (SDS-PAGE). SDS-PAGE de-

natures the protein in the sample and gives the protein a negative charge, allowing for separation solely on the basis of the size of the proteins. The proteins then migrate through the gel, toward the positive anode, in response to an electric field. Dithiothreitol (DTT), which is a reducing agent, is also added to the samples. DTT reduces the disulfide bonds within the proteins, helping the proteins to fully denature, avoiding unwanted structures to form during electrophoresis. Smaller proteins migrate through the gel matrix faster, while larger proteins move more slowly, resulting in their separation according to their molecular weight.

Following electrophoresis, proteins are transferred (blotted) from the gel onto a membrane substrate, typically made of nitrocellulose or polyvinylidene difluoride (PVDF), either via wet or dry blotting. This transfer step ensures the immobilization of proteins in a single layer, preserving their spatial arrangement and enabling subsequent antibody detection. The next steps involve the binding of antibodies. After transfer, the membrane is blocked to prevent nonspecific binding and then incubated with a specific primary antibody for the protein of interest. The primary antibody recognizes and binds to the target protein, and after a series of washes to remove unbound primary antibodies, the membrane is then incubated with a secondary antibody conjugated to an enzyme or a fluorophore.[183]

The secondary antibody binds to the primary antibody, amplifying the signal and allowing for its detection. Enzyme-linked secondary antibodies are often used in conjunction with substrates that produce a chemiluminescent or chromogenic signal during enzymatic reaction, whereas fluorophore-conjugated antibodies allow direct visualization of the target protein under appropriate excitation.[183] One or several molecular weight ladders of known proteins are often added to the membrane, such as SeeBlue and MagicMark, which makes for quick comparisons.

3.4.1 Reagents and procedure for Western blot analysis

INA-6 cells were cultured in RPMI 1640 supplemented with L-glutamine (0.68 mM), 10% Fetal Calf Serum, and interleukin-6 (IL-6) at a concentration of 1 ng/ml. Subsequently, cells were harvested from culture plates and centrifuged in 50 ml polypropylene vials at 4 °C, 448 x g for 5 min. After discarding the supernatant, the cells were resuspended in 400 µl of Phosphate-buffered saline (PBS) and transferred to Eppendorf tubes. Following a second centrifugation step at 4 °C, 1000 x g for 6 min, the supernatant was carefully removed and the cell pellets were lysed using a prepared lysis buffer.

The lysis buffer was prepared according to the protocol and consists of NP40 (1%), NaCl (150 nM), Trizma hydrochloride (50 mM), Glycerol (10%), cOmplete™ Mini EDTA-free Protease Inhibitor Cocktail (10 ml), Sodium Fluoride (50 mM), and Sodium Orthovanadate (1 mM). NP40 is a non-ionic detergent that helps with solubilization of non-polar insoluble proteins. NaCl ruptures cell membranes and prevents the aggregation of proteins. Trizma hydrochloride acts as a pH buffer. Glycerol is added for general stabilization. Both Sodium Fluoride and Sodium Orthovanadate are phosphatase inhibitors. The lysis buffers are stored in aliquots of 445 µl, without Sodium Fluoride and Sodium Orthovanadate. 50 µl of Sodium Fluoride, and 5 µl Sodium Orthovanadate were added to the buffer when performing Western blotting. The lysis buffer was then added to the pellets in volumes of 40 µl buffer per 1 million cells, resuspended well to break up the pellet and kept on ice for 15-20 min. The tubes were then briefly vortexed, before spinning at 4 °C, 17005 x g for 15 min.

The protein contents of the lysates were quantitatively analyzed using the Bradford assay (Sigma-Aldrich), by making a standard curve of BSA (Sigma-Aldrich). The plate was then placed on a BioRad microplate and absorbance was measured at 595 nm. Using absorbance readouts, each sample was diluted according to the lowest concentration sample in lysis buffer. 5 µl DTT 10% (PanReach AppliChem) in NuPAGE® LDS 4X (ThermoFisher) sample buffer was also added in preparation for gel electrophoresis, making each Eppendorf tube contain a total volume of 20 µl.

The samples were then heated at 70 °C for 10 min and briefly centrifuged for approximately 15 s. The gel chambers were then prepared by adding MOPS or MES buffer (depending on the size of the protein) and submerging the NuPAGE™ 4-16 %, Bis-Tris gel, 1.0 mm (Invitrogen) in the locked chambers of the Xcell Surelock Mini-Cell (NuPage, Life Technologies). 15 µl of each sample was then added to a lane, with 3 µl of SeeBlue™ Plus2 (Invitro-

gen) in the first and penultimate lane and 1 µl of MagicMark™ XP (Invitrogen) in the last lane, as protein ladders. The gel was then connected to a Power Ease 500 (Invitrogen), and ran at Program 1: 30 min 80 V, 30 min 150 V, 30 min 180 V.

After the end of the electrophoresis, the gel was dry blotted using a nitrocellulose membrane (iBlot™ 2 Transfer Stacks, nitrocellulose, Invitrogen) and ran in an iBlot™ 2 Gel Transfer Device (ThermoFisher Scientific). After completion, the membrane was blocked with TweenTris Buffered Saline (500 ml of 1M Tris HCL pH 7.5, 300 ml of 5M NaCl, 100 ml 10% Tween 20, and H_2O) blocking buffer for 1 h, and subsequently the primary antibody was applied and left overnight at 4 °C on an orbital shaker.

The next day, after removing the primary antibody and washing the membrane in TBS-T 3x5 min, secondary antibody incubation was carried out for 1 h at room temperature, also on an orbital shaker. Subsequently, the membrane was washed 4x5 min in TBS-T, before 3 µl of SuperSignal™ West Femto Maximum Sensitivity Substrate (1.5 µl peroxide buffer and 1.5 µl luminol enhancer solution) was mixed in a vial and applied to the membrane. After 3 min with this solution, the membrane was placed on a plastic film and inserted into a Licor Odyssey FC (LI-COR Biosciences, NE, USA) for imaging.

3.5 Seahorse XF energy phenotype assay

The Agilent Seahorse XF Analyzer is an instrument that enables real-time measurement of cellular bioenergetics by analyzing the oxygen consumption rate (OCR) and the extracellular acidification rate (ECAR) of living cells. Using the principle of measuring changes in dissolved oxygen and pH in the microenvironment surrounding adherent or suspension cells, the analyzer utilizes specialized solid-state sensor probes integrated into a microplate. These probes form a temporary 200 µm microchamber on top of the cells that allows the simultaneous measurement of OCR and ECAR, providing a comprehensive view of cellular metabolic activities. The biosensor cartridge contains two fluorophores, one quenched by O_2 and one sensitive to protons.

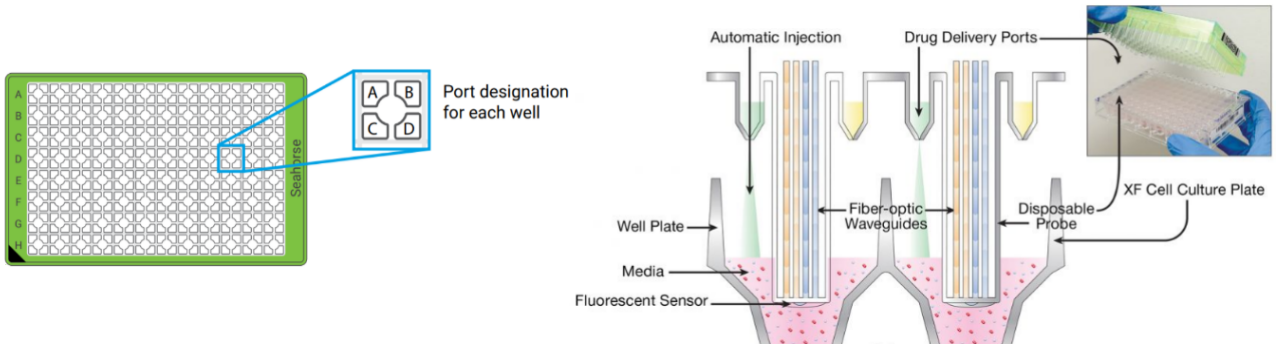

Figure 3.2: Seahorse assay setup: The plate and sensor probes on a Seahorse XF Pro Analyzer. Each plate has four different loading ports per well. In this experiment, 20 µl of a mix containing BAM15 and Oligomycin was loaded into every port 'A' of the injection port of the sensor cartridge. Each well contained 180 µl of XF assay media and 25,000 cells. During the assay, the sensor probes would routinely mix the contents of each well, ensuring proper oxygenation, before measuring OCR and ECAR. In the stress-part of the assay, each drug delivery port would inject part of the stressor mix into the XF assay media containing cells, then subsequently measure the changes in OCR and ECAR. The cycle of mixing, injecting and measuring was repeated five times.

During measurements, light excites the two fluorophores, leading to excitation of the encapsulated fluorophores. The sensors then detect and measure the change in the level of fluorescent emission resulting from the change in the level of oxygen and protons. Plate layout, and sensor probes can be seen in Figure 3.2. When cells are seeded onto the microplate, their metabolic activities, such as OXPHOS and glycolysis, influence the surrounding oxygen and pH levels. The consumption of oxygen by cells leads to a decrease in dissolved oxygen levels, while metabolic processes such as glycolysis result in the production of lactate and protons, leading to extracellular acidification. By modulating cellular metabolism with compounds such as mitochondrial inhibitors and glycolytic substrates, the Agilent Seahorse XF Analyzer enables the evaluation of key metabolic parameters, including ATP production, mitochondrial respiration, and glycolytic capacity.

3.5.1 Seahorse setup and method

On the day prior to the experiment, all wells in an Agilent Seahorse cell culture 96-well plate were coated in 30 µl Poly-D-Lysine (100 µg/ml) for 20 min. Afterwards, the Lysine was aspirated from the wells and the wells were washed twice with 200 µl of sterile water and subsequently air dried for a minimum of 30 min. The plate was then put in a plastic bag and stored at 4 °C overnight. The 96 wells on the Agilent Seahorse XF Sensor Cartridge plate were hydrated with 200 µl of sterile water, before the XF sensor cartridges were submerged in sterile water and placed in a 37 °C incubator without CO_2 for the night.

The following day, the sterile water in the XF sensor cartridge plate was replaced with 200 µl of Seahorse Calibrant Solution, before the plate was put back in the incubator for another 60 min prior to the assay. Subsequently, 25 ml of Seahorse XF assay medium was made and prepared according to the manufacturer's protocol. 23.0 ml of Seahorse XF Base Medium (102353-100, Seahorse Bioscience) was measured in a 50 ml tube and 2.5 ml of Pyruvate (5 mM), 0.25 ml D-Glucose (1 M), and 0.25 ml Glutamine (200 mM). The medium was then heated to 37 °C before adjusting the pH to pH 7.4 with NaOH. Then, the stock compounds BAM15 and oligomycin (mitochondrial complex V inhibitor) were prepared at their final concentrations.

A 15 ml tube was used to prepare the master stressor mix, which included assay medium, BAM15, and Oligomycin. 20 µl of this mix was then loaded into every port A of the sensor cartridges (Figure 3.2), based on the premade "Energy phenotype" template on the Agilent Seahorse XF Pro Analyzer. The cells were then harvested, counted, and resuspended in warm assay medium at the correct density (25,000 cells/well). 50 µl of cell-free assay medium was added to the four outer wells at each corner. 50 µl of assay medium with cells was added to all remaining wells. The plate was then centrifuged on an XF carrier tray at 300 x g for 1 min without braking. 130 µl of assay medium was carefully added to the side of the wells, bringing the total volume to 180 µl. The cell culture plate was then placed in the 37 °C incubator without CO_2 for approximately 30-45 min, before performing the assay. The software protocol consisted of 12 min of calibration, then three steps of: 3 min mixing, 3 min measuring, for baseline readouts. Then, the stressor mixes were injected into their respective wells, with five cycles of: 3 min mixing, 3 min measuring. The result data was then analyzed with Agilent Seahorse Wave Pro software.

3.6 Quantification of superoxide production

Fluorescence is a physical phenomenon that involves the emission of light by a substance upon excitation by another form of energy, such as photons or electrons. The wavelengths of peak emission and excitation are denoted by λ_{em} and λ_{ex}, respectively. These wavelengths vary among different fluorescent molecules and are crucial for distinguishing fluorescent substances. Common techniques for detecting fluorescence include fluorescence spectrophotometry, the use of fluorescence microscopy for visual observation, and, more commonly, flow cytometry. The methods utilize a beam of photons (either ultraviolet or visible) that excites fluorescent molecules, leading them to emit light at a lower energy, often but not exclusively, visible light.

In fluorescence-based methods for detecting ROS, a probe specific for fluorescence detection is mixed with the ROS-producing system (such as enzymes, cells, or tissues) and the emitted fluorescence from the reaction is measured to assess the ROS levels. Typically, the probes used in fluorescence-based ROS detection are either non-fluorescent or faintly fluorescent, but produce brightly fluorescent products when they react with ROS. These fluorescence-based probes offer a much higher sensitivity for detecting ROS compared to other methods such as ultraviolet/visible (UV/vis) spectrophotometry. In addition, flow cytometry provides real-time data on cellular populations. A significant limitation of fluorescence-based methods is their limited selectivity towards different reactive species, which can complicate the detection of ROS in biological systems. However, when used properly and combined with other assays, fluorescence-based flow cytometry can provide valuable insights into ROS dynamics.

Flow cytometry can be used to quantify superoxide production in mitochondria using MitoSOX superoxide indicators.[184] These indicators permeate living cells and specifically localize to mitochondria. They quickly react

with superoxide, but not with other types of ROS or reactive nitrogen species (RNS), resulting in a brightly fluorescent product. MitoSOX indicators can help differentiate between artifacts in isolated mitochondrial samples and the actual production of superoxide in live cell mitochondria. They also serve as an important resource for studying compounds that affect oxidative stress in different diseases.

3.6.1 MitoSox Red protocol

For the detection of mitochondrial ROS, INA-6 Mock and INA-6 PRL-3 MM cells under standard culture conditions were incubated for 5 min at 37 °C, 5% CO_2. After the addition of an uncoupling agent at various concentrations (2,8,32 µM), the cells were incubated for 5 min, then subsequently treated with MitoSox Red (5 µM) and protected from light for 15 min. After the incubation period, the dye was removed through two washes with warm PBS at 20 °C at 448 x g, followed by resuspension in warm PBS for analysis. The detection of MitoSoX Red occurred at an excitation/emission of 405/610 nm with a BD LSR II flow cytometer (BD Biosciences) using FACS Diva software (BD Biosciences).

3.7 Plasma cell mitochondrial membrane potential

To measure the mitochondrial membrane potential of MM cells, the MitoProbeTM TMRM Assay for flow cytometry (Invitrogen) was used. MitoProbe™ TMRM Assay for Flow Cytometry is designed to measure the mitochondrial membrane potential in cells ($\Delta\Psi_m$), using the fluorescent dye tetramethylrhodamine methyl ester (TMRM). TMRM selectively accumulates in active mitochondria with intact membrane potential. The dye accumulates in mitochondria on the basis of the negative charge across the inner mitochondrial membrane, which is maintained by the proton gradient generated during OXPHOS.

Therefore, the TMRM fluorescence intensity is directly proportional to the mitochondrial membrane potential. In healthy, polarized mitochondria, TMRM fluorescence is high as a result of its accumulation within the mitochondrial matrix. In contrast, depolarized or dysfunctional mitochondria exhibit reduced TMRM fluorescence. By measuring TMRM fluorescence using flow cytometry, changes in the mitochondrial membrane potential of cells can be assessed and monitored under various experimental conditions.

3.7.1 TMRM procedure

To evaluate mitochondrial membrane potential, INA-6 Mock and INA-6 PRL-3 myeloma cells under standard culture conditions were incubated for 5 min at 37 °C and 5% CO_2 after the addition of an uncoupling agent at various concentrations (2,4,8,16 µM) and then stained with TMRM (20 nM) in serum-free RPMI for 30 min at 37 °C, 5% CO_2. Subsequently, the cells were washed twice with PBS at 448 x g, 4 °C, then resuspended in PBS for analysis by flow cytometry on a BD LSR II instrument (BD Biosciences) using FACS Diva software (BD Biosciences). TMRM fluorescence was monitored at specific excitation and emission wavelengths of 548/584 nm, respectively. The results were then analyzed with FlowJo 10.2. To ensure data accuracy, our results were initially gated by assessing the expression of GFP and FSC/SSC to exclusively select live cells, as apoptotic or dead cells would also exhibit a diminished TMRM signal.[185]

3.8 Statistics

The propagation of uncertainty of the experimental data was treated in a statistical manner according to the following:

$$Mean = \overline{X} = \frac{\sum_{i=1}^{n} X_i}{n} \tag{3.1}$$

Standard deviation (SD) =

$$\Delta X = \sqrt{\frac{\sum_{i=1}^{n} (X_i - \overline{X})^2}{n-1}} \tag{3.2}$$

Standard error of the mean (SEM) = Standard error (SE)

$$SEM = SD(\overline{X}) = \frac{SD(X)}{\sqrt{n}} = \frac{SD}{\sqrt{n}} = \frac{X}{\sqrt{n}} \tag{3.3}$$

From this, the combination of errors of functions with more than one variable relates as follows:

$$Z = X + Y \rightarrow (\Delta Z)^2 = (\Delta X)^2 + (\Delta Y)^2 \tag{3.4}$$

$$Z = X - Y \rightarrow (\Delta Z)^2 = (\Delta X)^2 + (\Delta Y)^2 \tag{3.5}$$

$$Z = X \times Y \rightarrow \left(\frac{\Delta Z}{Z}\right)^2 = \left(\frac{\Delta X}{X}\right)^2 + \left(\frac{\Delta Y}{Y}\right)^2 \tag{3.6}$$

$$Z = X/Y \rightarrow \left(\frac{\Delta Z}{Z}\right)^2 = \left(\frac{\Delta X}{X}\right)^2 + \left(\frac{\Delta Y}{Y}\right)^2 \tag{3.7}$$

The standard error of the mean can then be used to find the confidence intervals of the unknown samples, assuming that the distribution is normally distributed. The confidence intervals 95% for both limits are given as: $\overline{X} \pm 1.96 \times$SEM. Statistical analyzes were performed with GraphPad Prism 10.2.1, using two-way ANOVA together with Tukey's multiple comparison test. The results were deemed statistically significant if $p < 0.05$. The notation is as follows: ns $p > 0.05$, * $p \leq 0.05$, ** $p \leq 0.01$, *** $p \leq 0.001$, **** $p \leq 0.0001$. All results were presented as normalized to the control group, with error bars given as $2\times$SEM, unless stated otherwise.

4 Results

4.1 PRL-3 increases ATP production and viability in acidic conditions

Cells expressing PRL-3 (INA-6 PRL-3) and those without PRL-3 (INA-6 Mock) were cultured in identical RPMI media, albeit under varying pH conditions for a duration of 72 h. Subsequent to the incubation period, ATP production was evaluated using the CTG assay at intervals of 24, 48 and 72 h (see Figure 4.1). The findings indicate that PRL-3-expressing cells exhibited elevated ATP production relative to their Mock counterparts in both pH 7.4 and pH 6.5 environments. In addition, increased cell viability was observed among PRL-3-expressing cells, particularly evident under acidic conditions (Figure 4.1C). The y-axis is reported in Relative Light Units (RLU), which quantifies the amount of photons emitted by the chemical reaction involving Luciferin which is detected by the instrument.

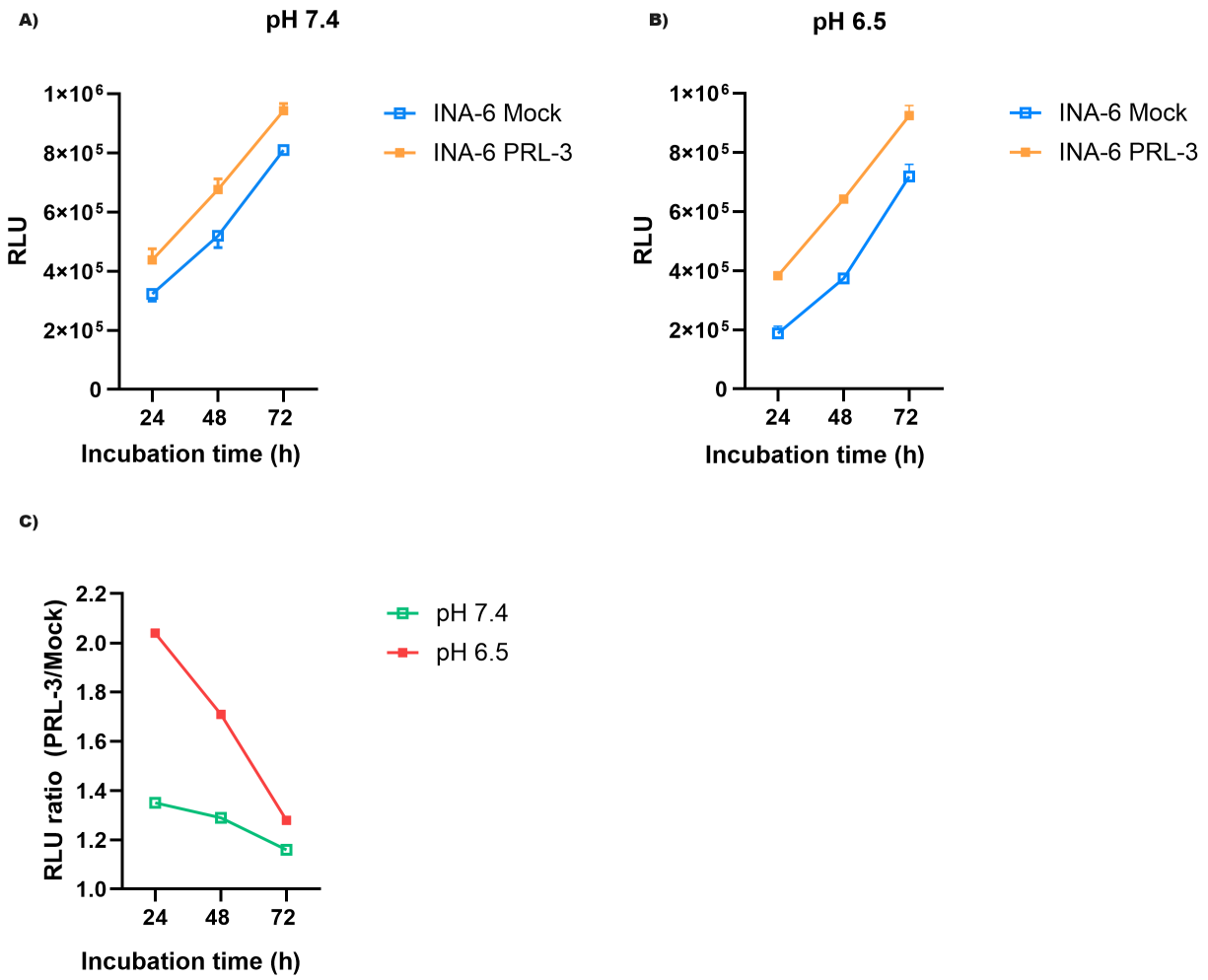

Figure 4.1: PRL-3 causes favorable viability in acidic environment: A-C) Mock and PRL-3 cells were cultured in different pH for 1-3 days, and measured for ATP content. **A)** Cells cultured in pH 7.4 with ATP measurements each day. **B)** Cells cultured in pH 6.5 with ATP measurements each day. **C)** The ratio of the RLU intensity between PRL-3/Mock at pH 7.4 and pH 6.5, measured by CTG assay. Data is shown as mean ± 2×SEM.

Figure 4.1C depicts the RLU ratio between PRL-3 and Mock cell populations. Specifically, under physiological pH conditions, PRL-3-expressing cells exhibited a RLU 1.35 times higher than that of Mock cells after 24 h. This RLU difference declined to 1.29 and 1.16 at 48 and 72 h, respectively. Similarly, under acidic conditions, the initial RLU at 24 h was 2.09-fold higher, gradually diminishing to 1.71 at 48 h, and 1.28 at 72 h.

4.2 INA-6 Mock and PRL-3 metabolic profiles

We investigated the metabolic profiles of INA-6 Mock and PRL-3 cells under different conditions to understand their energy demands and adaptations. Specifically, we measured basal OCR and ECAR in cells cultured under normoxic conditions at pH 7.4 and under hypoxic conditions at pH 6.5. Given that OCR is closely related to ATP production via OXPHOS, and ECAR predominantly mirrors the rate of glycolysis, both of these pathways were determined with a Seahorse XF Pro Analyzer. Through comparative analysis of these metabolic parameters across different levels of pH and oxygenation in the two cell populations, insights were obtained about the potential impact of PRL-3 expression on cellular metabolism and responses to variations in the microenvironment.

4.2.1 Hypoxia and low pH severely affects OXPHOS and Glycolysis

PRL-3-expressing cells exhibited elevated levels of both OCR and ECAR relative to their corresponding Mock controls at pH 7.4, both under basal conditions and in response to stress induced by BAM15 and oligomycin, as depicted in Figure 4.2. Particularly noteworthy was the significantly heightened baseline glycolytic flux observed in PRL-3-expressing cells compared to Mock cells under normoxic conditions.

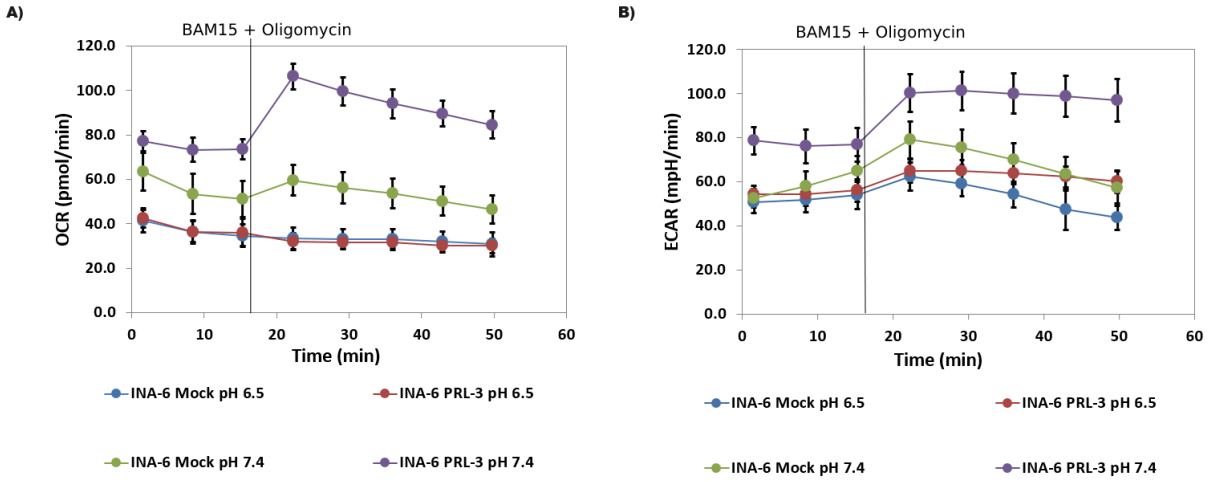

Figure 4.2: PRL-3 controls OCR and ECAR in MM cells: (A-B) The oxygen consumption rate and extracellular acidification rate were measured by an Agilent Seahorse XF Pro Analyzer. **A)** The rate of OCR in Mock and PRL-3 cells at pH 7.4 under normoxia, and at pH 6.5 under hypoxia. **B)** The rate of ECAR in Mock and PRL-3 cells at pH 7.4 under normoxia, and at pH 6.5 under hypoxia. Results show one representative out of three independent experiments, each with 20-24 technical replicates. Data is shown as mean $\pm$ 2$\times$SEM.

However, a notable decline in both OCR and ECAR was evident under hypoxic conditions at pH 6.5 for both Mock and PRL-3 cells, with PRL-3 cells displaying a more pronounced reduction in OCR and ECAR relative to Mock cells, as depicted in Figure 4.2. Although OCR levels in PRL-3 cells decreased to a level comparable to that observed in Mock cells, ECAR remained moderately elevated in PRL-3 cells. The energy phenotype and metabolic potential of both cell types are shown in Figures 4.3A and 4.3B. Metabolic potential is defined as the percentage increase in stressed OCR relative to baseline OCR, and stressed ECAR relative to baseline ECAR, thereby reflecting the cell's ability to meet energy demands through OXPHOS and glycolysis, respectively. Under stressed conditions, PRL-3-expressing cells exhibited a notable increase in both OXPHOS and glycolytic activity, surpassing the more modest increase observed in Mock cells. Moreover, both PRL-3 and Mock cells cultured at pH 6.5 under hypoxic conditions demonstrated a decrease in OCR, accompanied by an elevation in ECAR upon exposure to the stressor mix.

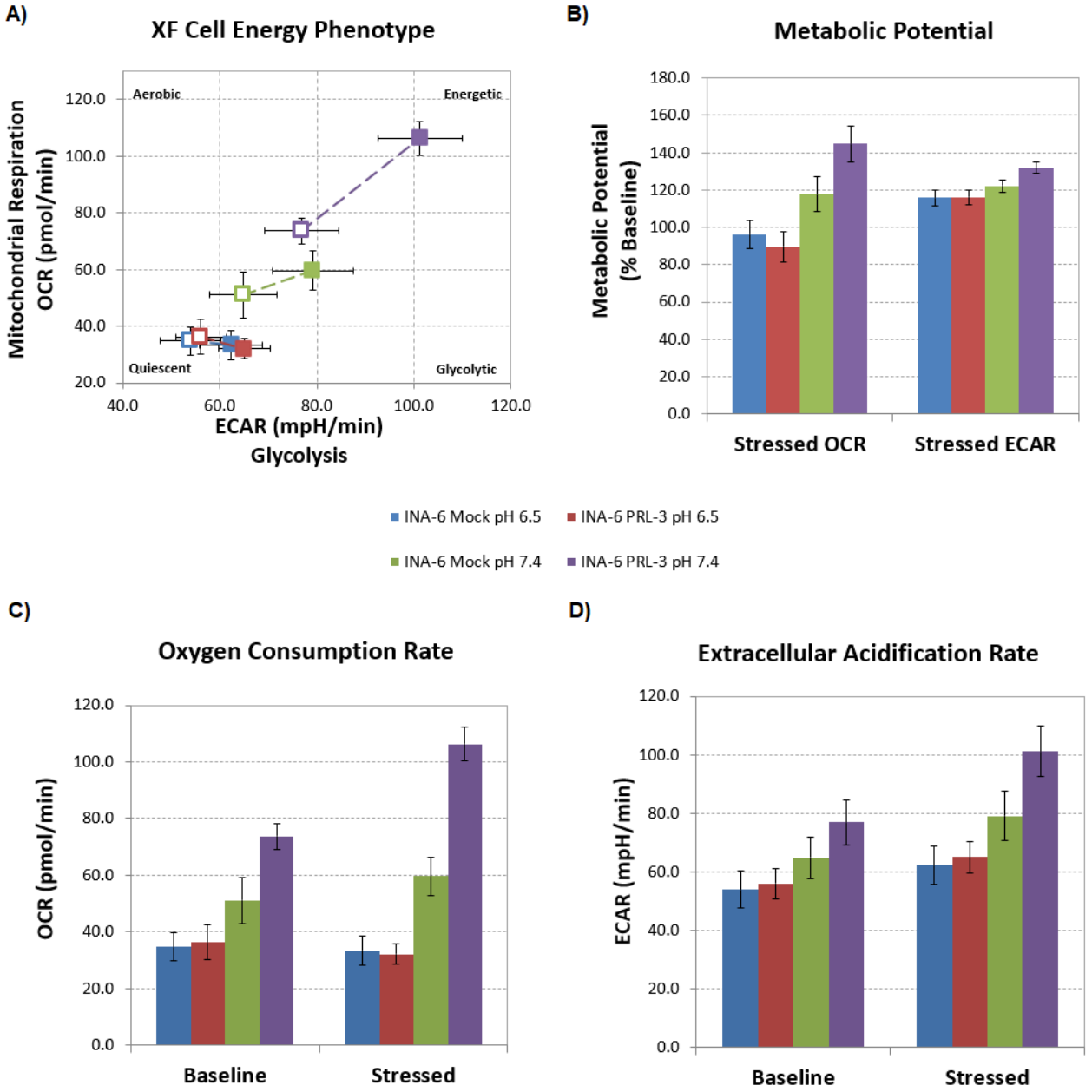

Figure 4.3: INA-6 cell energy phenotype and metabolic adaptations at different incubating conditions: A-D) Energy diagram, metabolic potential, OCR and ECAR for INA-6 Mock and INA-6 PRL-3 cells incubated under varying oxygen and pH conditions. **A)** Cell energy phenotype diagram depicting basal OCR and ECAR (hollow squares) and stressed rates (full squares) for MM cells cultured at pH 7.4 and normoxia, and at pH 6.5 and hypoxia. **B)** The metabolic potential of the cells for each condition. Metabolic potential is the increase in OCR / ECAR between stressed and basal, given as a percentage. **C)** The OCR at baseline and stressed conditions for the different conditions. **D)** The ECAR at baseline and stressed conditions for the different conditions. Data is shown as mean $\pm$ 2$\times$SEM.

4.3 Key proteins related to metabolism and pH regulation show differences in expression between pH 7.4 and pH 6.5

We conducted Western blot analysis to investigate the protein expression profiles of key regulators involved in cellular metabolism and pH regulation. Our analysis focused on discerning the expression levels of selected proteins important for metabolic pathways and pH homeostasis under various experimental conditions. The aim was to gain insight into how PRL-3 influences these proteins under conditions of limited ATP availability, particularly within the harsh environment of the TME.

The expression of PRL-3 decreased with increasing doses of uncouplers, but these results cannot be taken at face value, since the overexpression of PRL-3 in the INA-6 cell line used in these experiments is controlled by retroviral transduction.[186]

4.3.1 CCCP and BAM15 regulate expression of HIF-1α

The expression and regulation of HIF-1α play important roles in cellular responses to hypoxic conditions, facilitating adaptive mechanisms vital for cell survival and metabolic homeostasis. In this study, we sought to explore the potential influence of mitochondrial uncouplers on HIF-1α expression levels under hypoxic conditions at pH 7.4. Our results provide insight into the dose-dependent modulation of HIF-1α by these compounds, highlighting their capabilities as regulators of cellular adaptations to hypoxic conditions.

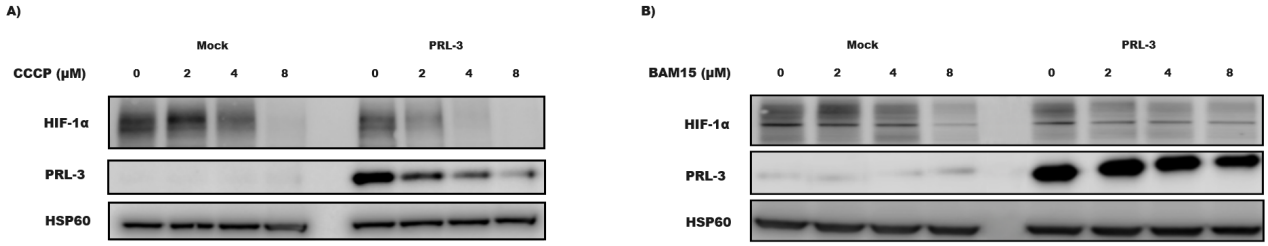

Figure 4.4: Expression of HIF-1α is diminished by the application of CCCP and BAM15: A-B) Expression levels of HIF-1α and PRL-3 for cells treated with **A)** CCCP or **B)** BAM15 for 24 h after 24 h pre-incubation in hypoxic conditions and immunoblotted with antibodies for HIF-1α and PRL-3.

Higher expression of HIF-1α was observed in the untreated Mock control group compared to the PRL-3 control, as shown in Figure 4.4. In Mock cells, 2 μM CCCP barely affected HIF-1α expression. HIF-1α exhibited partial reduction at 4 μM CCCP and a significant decrease at 8 μM CCCP compared to control cells (Figure 4.4A). In contrast, in PRL-3-expressing cells, treatment with 2 μM CCCP induced a pronounced inhibition of HIF-1α, with further reductions observed at 4 and 8 μM CCCP, resulting in nearly complete abrogation of HIF-1α expression. Notably, both Mock and PRL-3 cells required a concentration of 8 μM BAM15 to achieve a significant reduction in HIF-1α expression (Figure 4.4B). Furthermore, PRL-3 was neither related nor regulated by HIF-1α, since Mock cells incubated under hypoxic conditions did not induce any changes in PRL-3 expression (Figure 4.4), and conversely, cells expressing PRL-3 did not exhibit stabilization of HIF-1α under normoxic conditions (Figure 4.5).

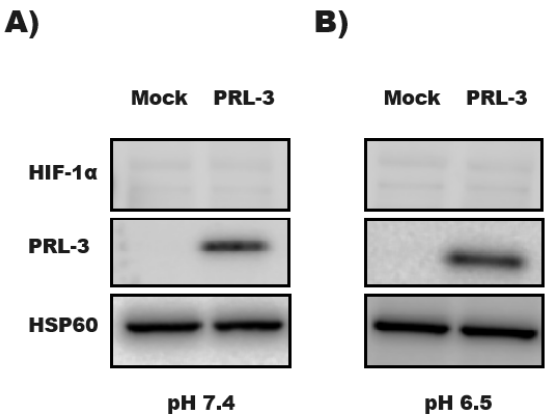

Figure 4.5: PRL-3 does not stabilize HIF-1α under normoxic conditions: INA-6 Mock and INA-6 PRL-3 cells were grown under normoxic conditions for 24 h at **A)** pH 7.4 and **B)** pH 6.5, and immunoblotted with antibodies for HIF-1α and PRL-3.

4.3.2 PRL-3 downregulates p-AMPK, but fails to overcome proton inhibition from metabolic acidosis under normoxic conditions

PRL-3 is known to participate in various metabolic regulations[187] and plays a crucial role in adapting to the TME in MM cells. This led us to examine the expression of several proteins at pH 7.4 and pH 6.5 under normoxic conditions, aiming to ascertain whether metabolic acidosis affects PRL-3's ability to regulate metabolism through these proteins. Our results, depicted in Figure 4.6, revealed intriguing findings.

Surprisingly, PRL-3-expressing cells treated with a combination of uncoupler and 2-DG, regardless of concentration, exhibited severe suppression of p-AMPK expression, an energy sensor activated under low ATP conditions. In contrast, Mock cells showed upregulation of p-AMPK to the combination at pH 7.4, but not at pH 6.5 compared to the control group.

NHE1, a sodium-hydrogen antiporter pivotal in pH regulation that shuttles H^+ out of cells and Na^+ in, displayed higher expression levels in PRL-3 cells compared to Mock cells in the untreated control group at both pH 7.4 and pH 6.5. Notably, NHE1 expression remained largely consistent across various concentrations of uncouplers and 2-DG, except for a significant increase observed in PRL-3 cells exposed to 2 µM uncoupler and 500 µM 2-DG, particularly pronounced at pH 6.5. Interestingly, NHE1 expression appeared lower in PRL-3 cells at pH 6.5 with the highest concentration of uncoupler and 2-DG compared to the control group.

The expression of MCT4, which is involved in lactate efflux, was not significantly upregulated in PRL-3-expressing cells. Mock cells exhibited higher levels of MCT4 at pH 7.4 compared to PRL-3 cells when treated with various concentrations of CCCP and 2-DG. However, there was a slight increase in MCT4 expression at pH 6.5 for both Mock and PRL-3 cells, although levels remained comparable to those of the untreated control group.

GLUT1, which facilitates glucose transport into cells, showed upregulation in Mock and PRL-3 cells when treated with drug combinations at pH 7.4, albeit to a smaller extent in PRL-3-expressing cells. At lower pH, the expression of GLUT1 in untreated cells was slightly upregulated compared to the unstimulated control group at pH 7.4, but partially inhibited in both Mock and PRL-3 cells when treated with uncoupler and 2-DG. Moreover, at pH 7.4, untreated Mock cells had a more pronounced expression of GLUT1 compared to PRL-3 cells, whereas at pH 6.5 this was reversed, with control PRL-3-expressing cells exhibiting stronger expression.

HKII, responsible for glucose phosphorylation in glycolysis, demonstrated moderate upregulation in Mock and PRL-3 cells treated with 2 µM uncoupler and 500 µM 2-DG at pH 7.4, although this trend was not seen to the same degree when the uncoupler concentration doubled to 4 µM. At pH 6.5, HKII levels in Mock cells at both 2 and 4 µM were equal or partially downregulated, respectively, compared to control cells, while PRL-3 cells saw a large increase in expression at 2 µM, but a decrease in expression at 4 µM in comparison to untreated cells.

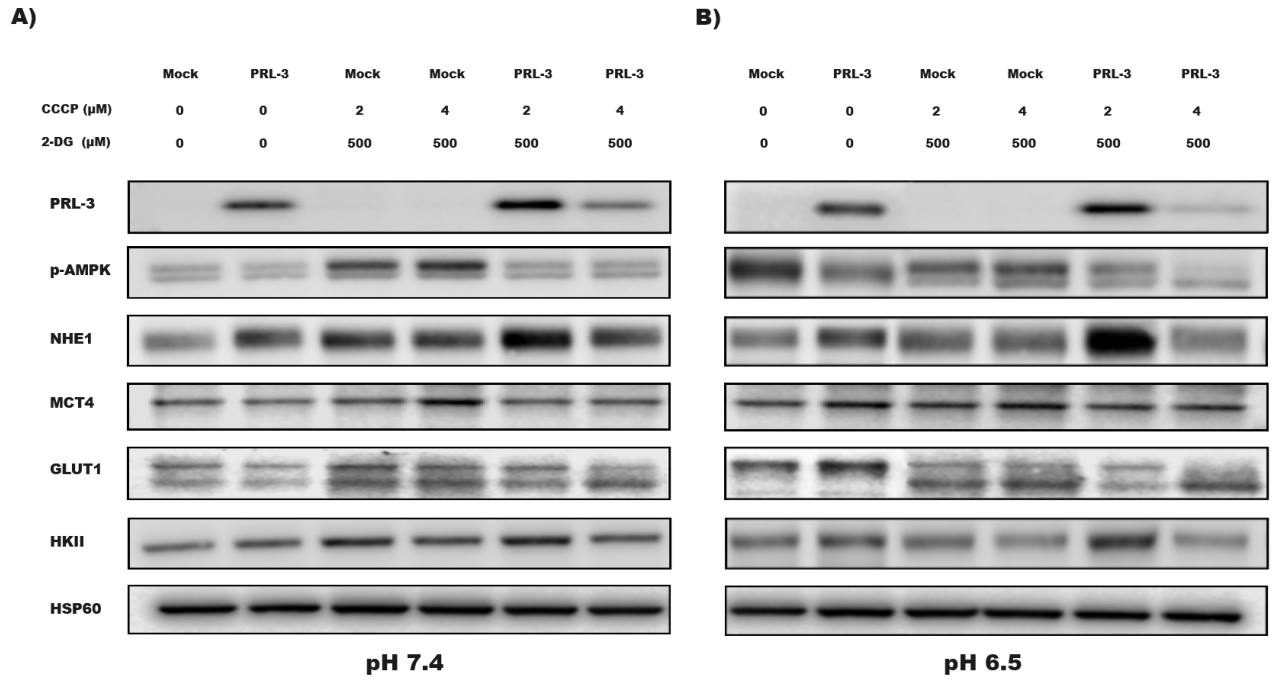

Figure 4.6: PRL-3 modulates the expression of metabolic proteins involved in glycolysis and pH regulation: INA-6 Mock and INA-6 PRL-3 cells were immunoblotted using the specified antibodies and allotted concentrations of CCCP and 2-DG. Originally it is one whole blot, but is shown as two separate blots to easier distinguish between **A)** pH 7.4 and **B)** pH 6.5.

4.3.3 Hypoxia-driven upregulation of metabolic proteins is attenuated by PRL-3

In response to hypoxia, cancer cells undergo profound molecular alterations, including changes in proteins involved in metabolism and pH regulation.[188] Based on our investigation of protein regulation under normoxic conditions (Figure 4.6), our aim was to elucidate the impact of hypoxia on these proteins and the role of PRL-3 in adapting to reduced oxygen levels.

Untreated Mock cells (Figure 4.7) at pH 7.4 exhibited significantly heightened activation of p-AMPK. In particular, p-AMPK expression peaked in Mock cells when treated with 4 μM CCCP and 500 μM 2-DG at pH 7.4, while expression levels generally decreased for all drug concentrations at pH 6.5. PRL-3-expressing cells exhibited lower levels of p-AMPK in hypoxia and pH 7.4 compared to Mock cells, and expression remained largely unchanged regardless of drug treatment or pH.

NHE1 exhibited a similar pattern to p-AMPK in both Mock and PRL-3 cells under hypoxic conditions, although PRL-3 cells showed a small decrease in NHE1 expression when treated with 2 μM CCCP and 500 μM 2-DG compared to normoxia, which was observed at both pH 7.4 and pH 6.5.

Unlike normoxia, the expression of GLUT1 in Mock cells exhibited a contrasting pattern between pH 7.4 and pH 6.5 under hypoxic conditions. At physiological pH, expression levels were upregulated in both the control group and at the highest concentration of uncoupler and 2-DG, while at lower drug concentrations, expression was downregulated. Conversely, under acidic conditions, the opposite trend was observed. In PRL-3-expressing cells, GLUT1 expression remained relatively stable across all conditions, with a slight increase observed at pH 6.5 for cells treated with 4 μM CCCP and 500 μM 2-DG.

Furthermore, HKII demonstrated a similar trend, with expression nearly abolished in Mock cells at pH 6.5 and the highest drug concentration, while in PRL-3-expressing cells, HKII levels decreased dose-dependently when treated with CCCP and 2-DG, with expression being slightly lower at pH 6.5.

However, by examining the HSP60 loading control (Figure 4.7), some, if not all of the observed patterns could be explained by irregular protein level for each sample.

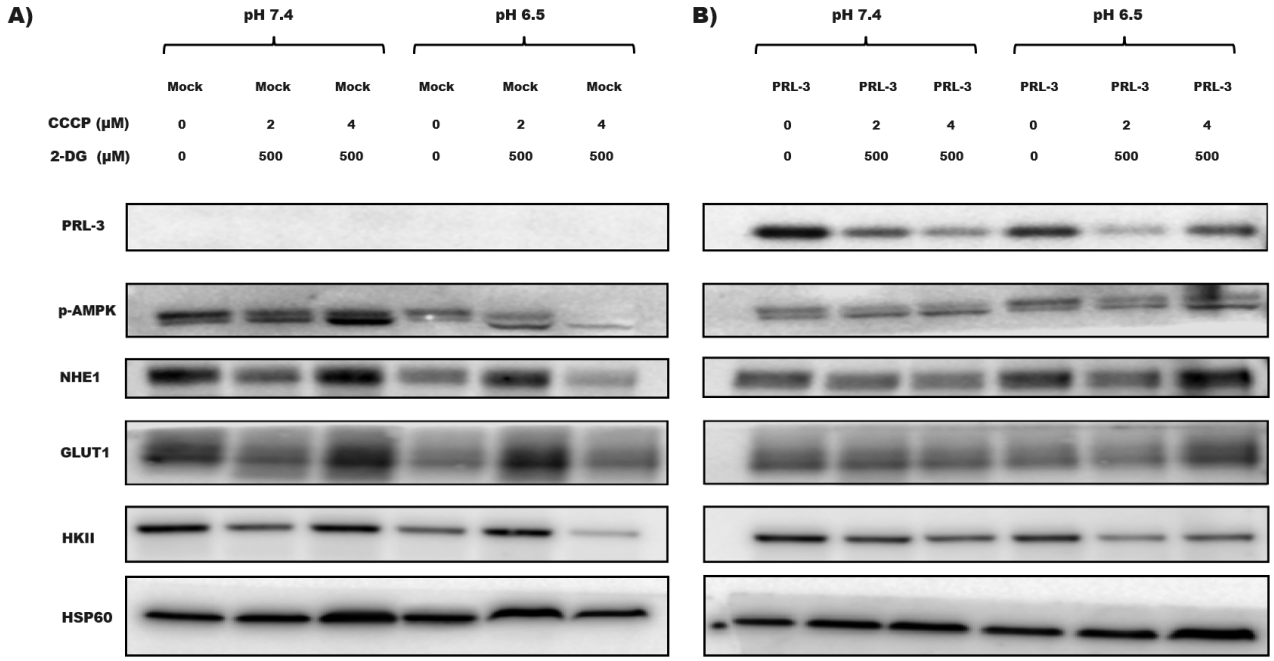

Figure 4.7: PRL-3 attenuates hypoxia-induced upregulation of proteins: Lysates were harvested from INA-6 Mock and INA-6 PRL-3 cells incubated under hypoxic conditions at pH 7.4 and pH 6.5 for 24 h, and immunoblotted against the shown antibodies.

4.4 Mitochondrial uncoupling lowers membrane potential in MM cells

Mitochondrial membrane potential ($\Delta\Psi_m$) serves as a critical indicator of mitochondrial integrity and cellular bioenergetics, crucial for understanding cellular metabolism, apoptosis, and metabolic disorders. To assess the state of $\Delta\Psi_m$ in MM cells, we employed Mitoprobe TMRM, a fluorescent dye-based method. This assay allowed us to assess changes in mitochondrial membrane potential before and after administration of mitochondrial uncouplers.

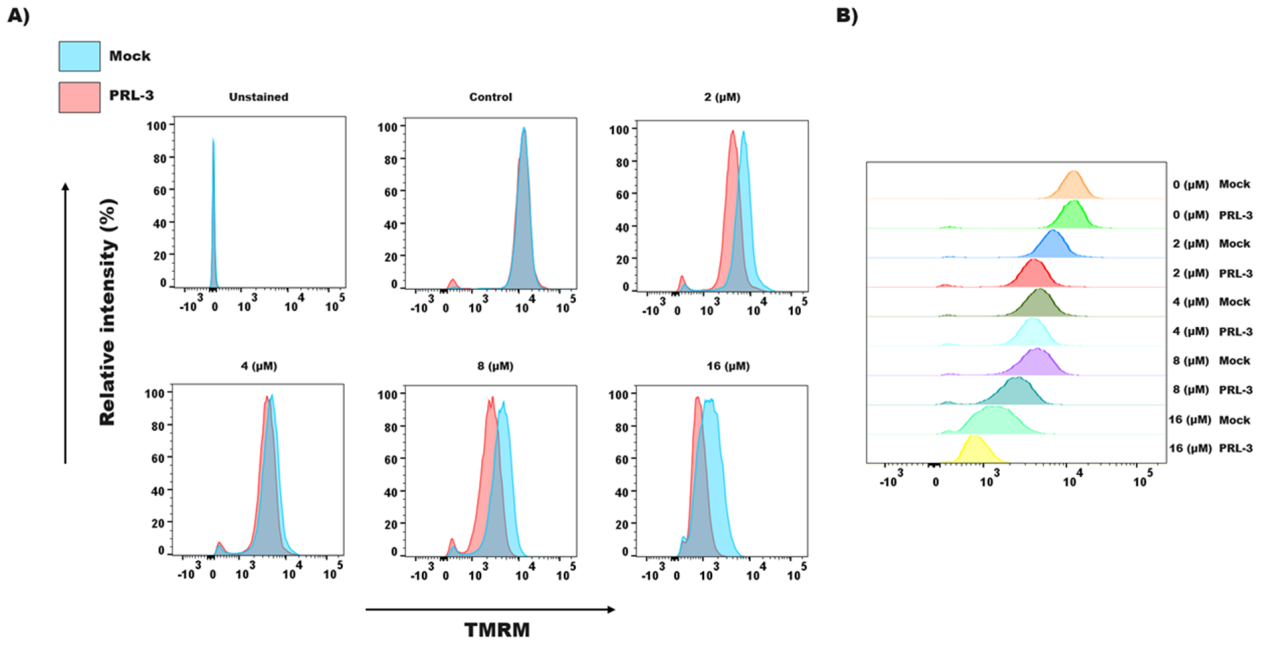

Figure 4.8: Cells expressing PRL-3 see greater amount of depolarization when treated with uncoupling agent: A-B) The mitochondrial membrane potential in INA-6 Mock and INA-6 PRL-3 cells after administering different concentrations of BAM15. **A)** TMRM signal for unstained, control, 2,4,8, and 16 μM BAM15 for Mock cells (Blue) and PRL-3 cells (Red). Cells were first incubated for 5 min after administering the uncoupler, then a subsequent 30 min incubation after staining with TMRM. **B)** Comparative diagram showing the effect of BAM15 in depolarizing the mitochondrial membrane. A weaker TMRM signal indicates a more depolarized membrane.

Utilizing TMRM, MM cells were characterized based on their mitochondrial membrane potentials. The unstained control group exhibited a negative TMRM signal (Figure 4.8), while the stained control group displayed a strong signal, indicative of a healthy and polarized membrane. Treatment with 2 μM BAM15 led to a reduction in $\Delta\Psi_m$ in both Mock and PRL-3 cells, with a more pronounced decrease observed in PRL-3 cells. This trend persisted across doses of 4, 8, and 16 μM BAM15. Notably, at all concentrations (Figure 4.8B), PRL-3 cells exhibited a weaker TMRM signal compared to Mock cells, suggesting a more depolarized membrane potential. Furthermore, the disparity between Mock and PRL-3 cells increased with higher concentrations of the uncoupler. Gating can be seen in Figure 6.7.

4.5 PRL-3 induces intrinsically higher levels of superoxide, but less affected by chemical elevation by uncoupling agents

The generation of superoxide, a ROS, occurs when molecular oxygen accepts a single electron. Subsequently, these superoxide species can subsequently give rise to more aggressive compounds such as the hydroxyl radical and peroxynitrite ($ONOO^-$) through processes such as the Fenton reaction, and interactions with nitric oxide (NO).[189] To assess intracellular superoxide generation, cells treated with CCCP or BAM15 were examined using Mitosox Red as a fluorescent marker. The experiments included varied doses of the uncouplers, ranging from 2 to 32 μM, aiming to elucidate whether there exists a dose-dependent effect on superoxide production in both Mock and PRL-3-expressing cells.

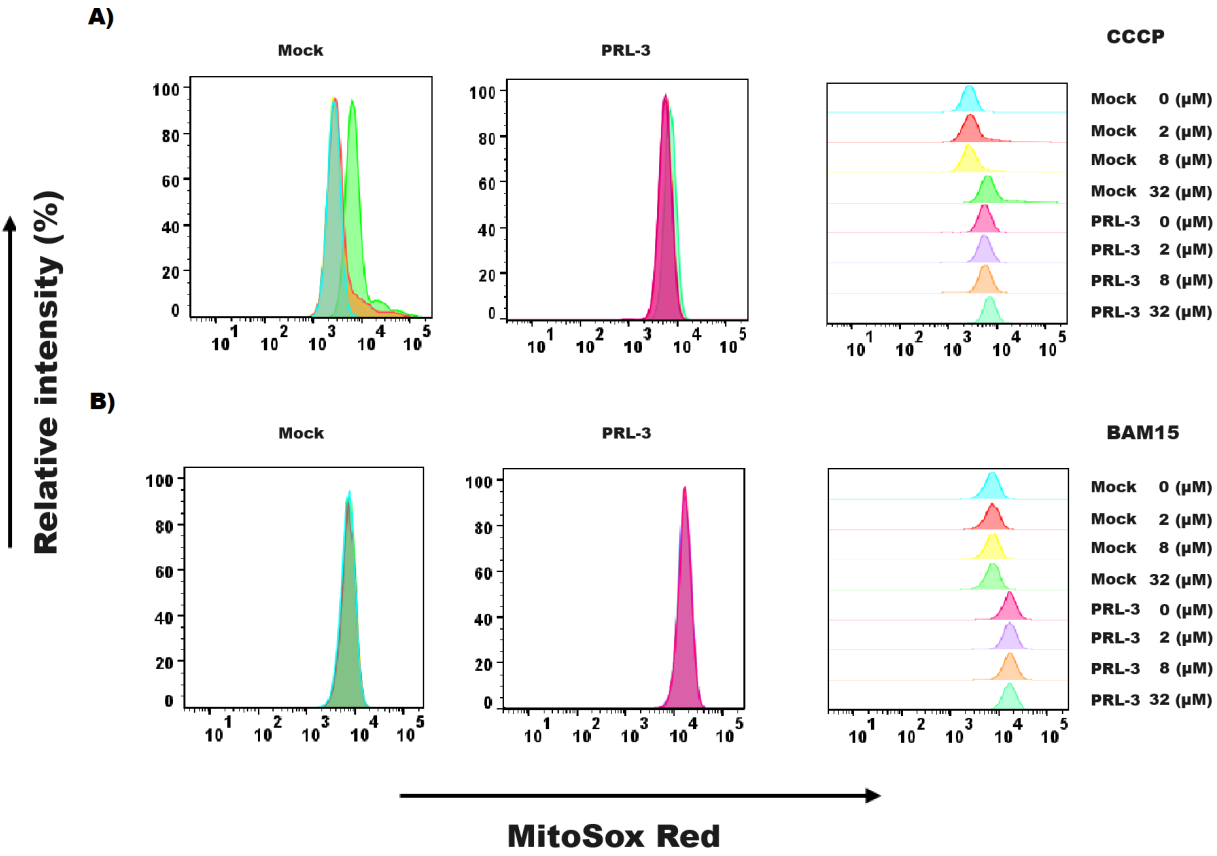

Figure 4.9: PRL-3 has higher amount of superoxide formation than Mock cells: (A-B) Superoxide measurements in INA-6 Mock and INA-6 PRL-3 cells after treatment with various concentrations of CCCP or BAM15. **A)** The superoxide levels in INA-6 Mock and INA-6 PRL-3 treated with CCCP. Cells were stained with MitoSox Red and incubated for 15 min after treating cells with 2, 8, or 32 μM CCCP. **B)** The superoxide levels in INA-6 Mock and INA-6 PRL-3 treated with BAM15. Cells were stained with MitoSox Red and incubated for 15 min after treating cells with 2, 8, or 32 μM BAM15. A stronger MitoSox Red signal signifies a higher superoxide concentration.

Figure 4.9 depicts that the baseline levels of superoxide in PRL-3-expressing cells were higher than those in Mock cells. In Mock cells, concentrations of 2 or 8 μM CCCP had no discernible effect on ROS levels compared to the untreated control; only at 32 μM CCCP did an increase in superoxide production become evident. Conversely, in cells overexpressing PRL-3, no significant alterations in superoxide concentration were observed during CCCP administration. Even at 32 μM CCCP, only a slight, albeit trivial, rise in superoxide formation was noted. Treatment with BAM15 showed no noticeable impact on superoxide levels, even at concentrations of 32 μM. However, cells expressing PRL-3 exhibited elevated superoxide levels compared to the Mock cells. Gating is shown in Figure 6.6.

4.6 Effect of uncoupling agents and 2-DG on cell proliferation

Cell proliferation is a fundamental process that is tightly regulated under both physiological and pathological conditions. In our study, we investigated the impact of CCCP and BAM15, in combination with the glycolysis inhibitor 2-DG, on the proliferation of MM cells using the CTG assay. Mitochondrial uncouplers are known to influence cellular metabolism and energy production, suggesting potential roles in modulation of cell proliferation. Given the limited literature on the effects of uncoupling agents specifically on MM cell lines, their impact had to be experimentally evaluated. Following an initial phase of trial and error, we determined the IC50 values and relevant concentrations of the uncouplers and 2-DG.

The working concentrations of CCCP and BAM15 were selected at 2 μM and 4 μM, respectively, in conjunction with a concentration of 500 μM of 2-DG. These concentrations were chosen based on their alignment with the sig-

moidal dose-response curves observed in preliminary experiments. To allow for comparison between Mock and PRL-3 expressing cells, the experimental values were normalized against the control group. This normalization was deemed necessary since PRL-3 expressing cells are known to exhibit enhanced ATP production compared to Mock cells, as discussed in Section 1.5. The concentration curves for CCCP, BAM15, 2-DG, and Dequalinium Chloride from the initial experiments can be found in the appendix section (Figures 6.1, 6.2 , 6.3, 6.4, 6.5).

4.6.1 Combination of uncoupling agents and 2-DG is required to counter PRL-3-induced metabolic effects

To assess the impact of inhibiting ATP production in both Mock and PRL-3 cells under standard physiological conditions, both cell types were subjected to a 24 h incubation period under normoxic conditions at pH 7.4. Throughout this incubation period, they were exposed to the designated combinations of drugs, as shown in Figure 4.10.

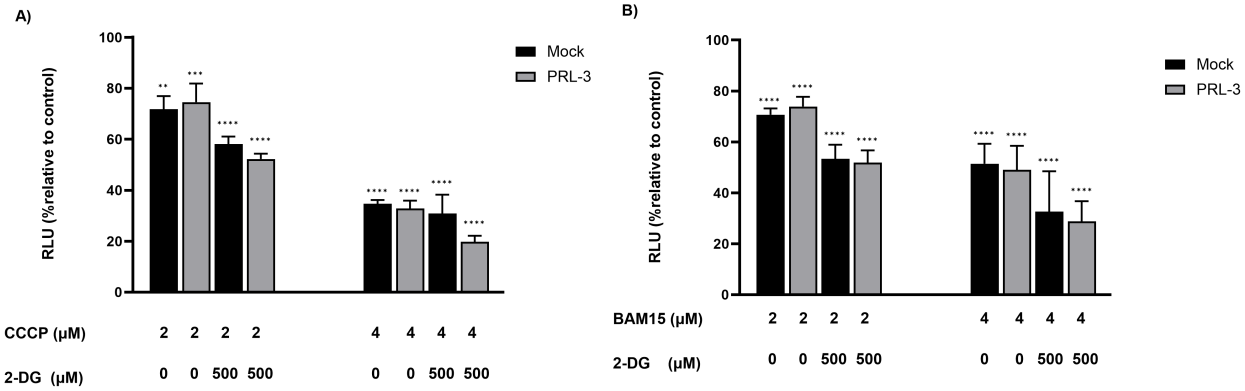

Figure 4.10: PRL-3 sensitizies cells to glycolytic inhibiton: The cell proliferation of INA-6 Mock and INA-6 PRL-3 when treated with either CCCP, CCCP + 2-DG, BAM15, or BAM15 + 2-DG in culture medium at pH 7.4 under normoxic conditions. **A-B)** CTG experiment for CCCP, BAM15 and 2-DG. Cells were incubated for 24 h with the given concentrations of CCCP, BAM15 and 2-DG. CCCP or BAM15 together with 2-DG reduced the proliferation of cells in a dose-dependent manner. The data is given as mean $\pm$ 2$\times$SEM, normalized against the untreated control group. The significance of the data was calculated by two-way ANOVA, where **** $p \leq 0.0001$.

Both concentrations of the uncoupling agents resulted in decreased proliferation in both Mock and PRL-3 cells, with no significant differences observed between the two cell types. Treatment with 2 µM CCCP or BAM15 led to a 30% reduction in proliferation, while 4 µM reduced proliferation by approximately 65% for CCCP and approximately 45% for BAM15. Inclusion of 2-DG further intensified these effects in both cell types, however, cells expressing PRL-3 exhibited an average decline in proliferation of about 18%, in contrast to Mock cells, which had a decrease of 8%.

The subsequent experiment aimed to assess the cell response under hypoxic conditions while maintaining pH at 7.4, to investigate the possible impact of metabolic rewiring by PRL-3, particularly in relation to reduced expression of HIF-1α, and variable expression of glycolytic proteins such as HKII and GLUT1 on cell proliferation.

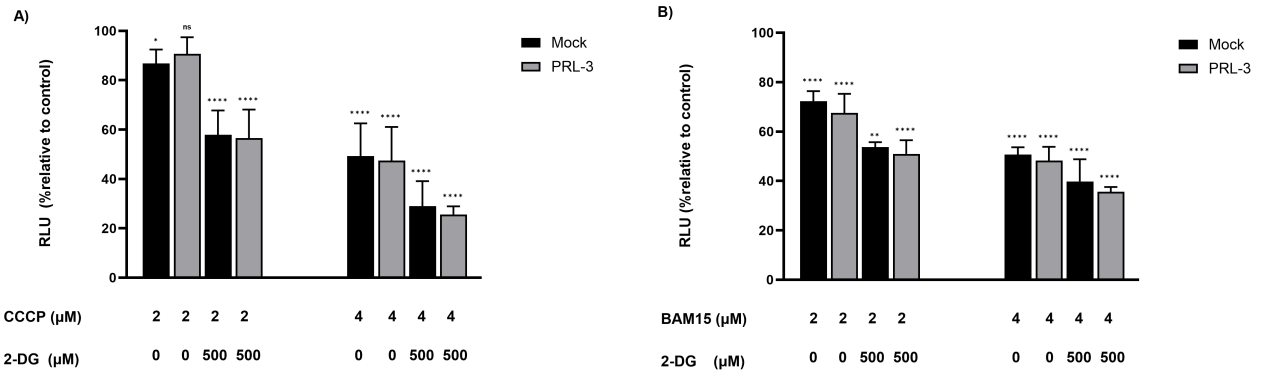

Figure 4.11: Hypoxia has negligible impact on proliferation in both Mock and PRL-3 cells at pH 7.4: A-B) Cell proliferation for INA-6 Mock and PRL-3 cells after 24 h of incubation in hypoxic conditions and treatment with **A)** CCCP or **B)** BAM15. The data is given as mean ± 2×SEM, normalized against the control group. The significance of the data was calculated by two-way ANOVA, where **** $p \leq 0.0001$.

Similar to the findings illustrated in Figure 4.10, under hypoxic conditions, the application of uncoupling agents and 2-DG led to a dose-dependent decrease in the proliferation of both cell types, as demonstrated in Figure 4.11. Treatment with 2 µM CCCP or BAM15 resulted in a reduction in proliferation ranging from 10% to 25%. When 2-DG was administered alongside 2 µM CCCP, a sharp drop in proliferation was observed by almost 50%, while BAM15 led to a reduction of 15-20%. At higher doses of 4 µM of the uncoupling agents, proliferation was further decreased by almost 50% for both CCCP and BAM15, with an additional 10-20% reduction after the addition of 2-DG.

4.6.2 Metabolic acidosis severely halts cell proliferation under both normoxic and hypoxic conditions

The subsequent investigation aimed to determine the impact of acidosis on plasma cells under both normoxic and hypoxic conditions. Metabolic acidosis has been shown to inhibit glycolysis, thereby shifting cellular reliance towards OXPHOS. Hence, we explored the inverse relationship between hypoxia-induced glycolysis upregulation and acidosis-induced OXPHOS upregulation. The pH of the medium was lowered from 7.4 to 6.5 by adding HCl to the culture medium, followed by a 24 h incubation period. The results of these experiments revealed a notable reduction in proliferation for both cell types when the pH was decreased from 7.4 to 6.5, particularly with the introduction of 2-DG. Interestingly, incubation under normoxic or hypoxic conditions had a minimal impact on overall proliferation rates. These findings are presented in Figure 4.12 and Figure 4.13, respectively.

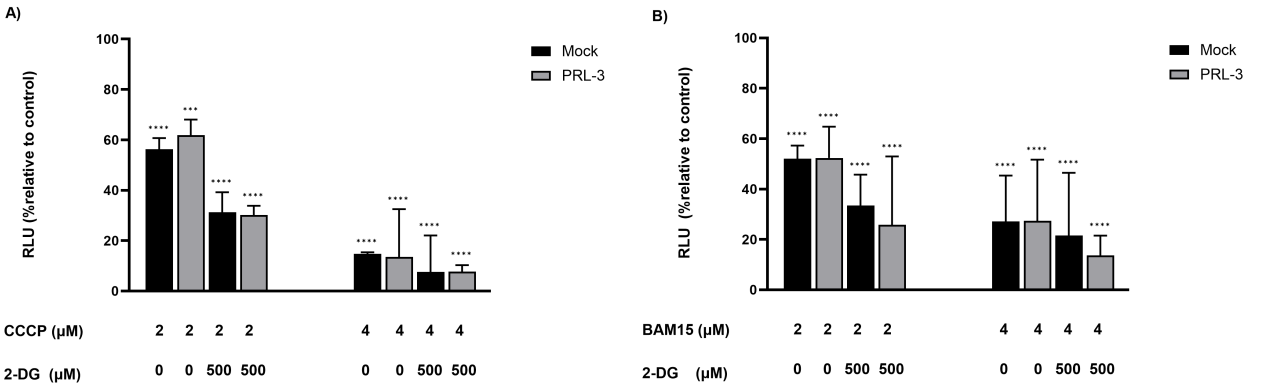

Figure 4.12: Culturing in acidic pH lowers proliferation significantly: A-B) Proliferation for INA-6 Mock and INA-6 PRL-3 cells after 24 h incubation at pH 6.5 under normoxic conditions. **A)** Treatment with CCCP in MM cells. **B)** Treatment with BAM15 in MM cells. The data is given as mean ± 2×SEM, normalized against the non-treated control group. The significance of the data was calculated by two-way ANOVA, where **** $p \leq 0.0001$.

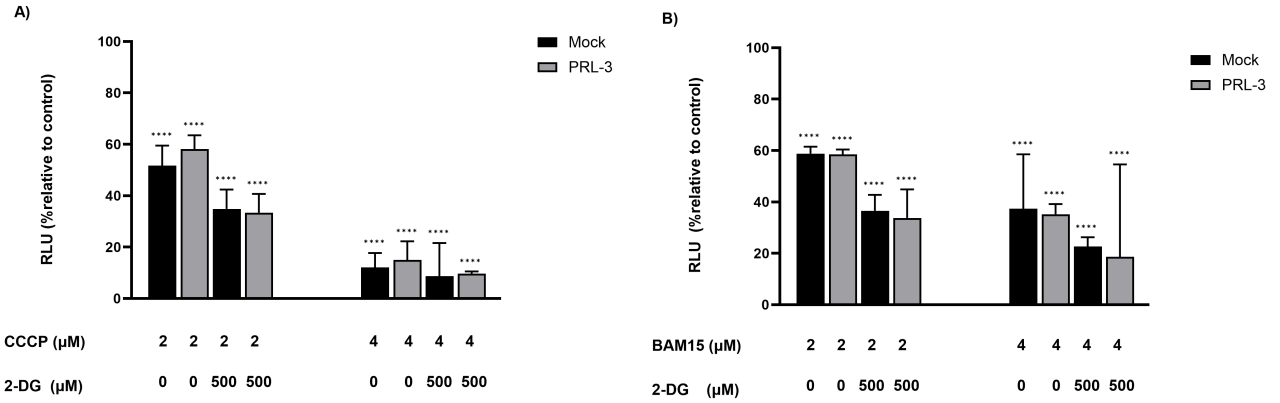

Figure 4.13: Acidic pH and low oxygen does not lead to any change in viability between INA-6 Mock and INA-6 PRL-3 cells: A-B) MM cells treated with the given concentrations of **A)** CCCP or **B)** and cultured at pH 6.5 under hypoxic conditions for 24 h. The data is given as mean ± 2×SEM, normalized against the unaltered control group. The significance of the data was calculated by two-way ANOVA, where **** $p \leq 0.0001$.

Incorporation of 2-DG resulted in a significant decrease in proliferation, reducing it by nearly 50% in cells treated with 2 μM CCCP or BAM15. However, this effect was not observed at the 4 μM dose in either cell type, regardless of oxygen conditions. The difference in proliferation between cells treated with uncoupler alone versus uncoupler combined with 2-DG at 4 μM remained consistent under normoxic and hypoxic conditions. The addition of the glycolysis inhibitor had minimal overall impact on proliferation. When comparing Mock and PRL-3 cells, there were marginal differences in proliferation, with PRL-3 cells exhibiting slightly lower proliferation rates, albeit with a larger SEM.

4.6.3 Dequalinium Chloride strongly amplifies the effect of uncoupling agents on cell proliferation

DCQ, classified as a cationic enhancer due to its $^{2+}$ cationic state and its inherent propensity to accumulate specifically within mitochondria, stands out as a potent chemical agent. This property renders it particularly attractive for negatively charged uncoupling agents such as CCCP and BAM15. Additionally, owing to its added impact on glucose metabolism and F1-ATPase, DCQ further enhances its potential as a therapeutic agent. The introduction of 3 μM DCQ along with CCCP or BAM15 resulted in a substantial reduction in proliferation compared to the application of uncoupling agents alone, as illustrated in Figure 4.14.

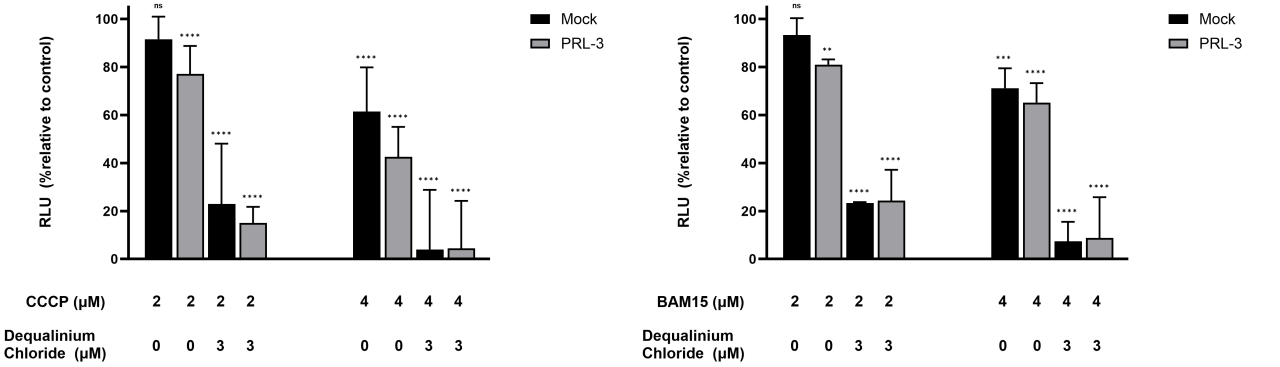

Figure 4.14: Dequalinium Chloride increases potency of uncouplers: Figure shows the proliferation of MM cells treated with CCCP **A)** or BAM15 **B)** with or without the cationic molecule Dequalinium chloride, and incubated at pH 7.4 under normoxia for 24 h. The data is given as mean ± 2×SEM, normalized against the unaltered control group. The significance of the data was calculated by two-way ANOVA, where **** $p \leq 0.0001$.

At 2 µM CCCP or BAM15, proliferation was measured at 85-80% compared to the control. However, with DCQ coadministration, proliferation decreased to 20% of the control. A further reduction was evident at 4 µM after the addition of DCQ, resulting in a critical decrease in proliferation in both cell types.

4.7 Induction of cell death by shutting down ATP production

In these experiments, we examined the cytotoxic effects induced by inhibiting OXPHOS and glycolysis. Since the CTG assay does not provide information on whether cells are apoptotic, necrotic, or dead, we employed simultaneous staining with Annexin V and propidium iodide (PI) to assess the cytotoxic effects of energy crisis in INA-6 cells. Our investigation aimed to evaluate the impact of uncoupling agents and 2-DG on cell viability under varying pH and oxygen conditions. Cells were cultured at pH 7.4 under normoxia to replicate physiological conditions and at pH 6.5 under hypoxia to mimic the acidic TME. The respective accumulation of cells in Q1, Q2, Q3, and Q4 quadrants can be seen in Figures 6.8, 6.9, 6.10, and 6.11.

4.7.1 PRL-3-expressing cells have reduced viability at pH 7.4 when subjected to ATP starvation

To elucidate the cellular state of INA-6 cells following 24 h of incubation with the uncoupling agents and glycolysis inhibitor at pH 7.4 and under normoxic and hypoxic conditions, cell viability was measured using flow cytometry.

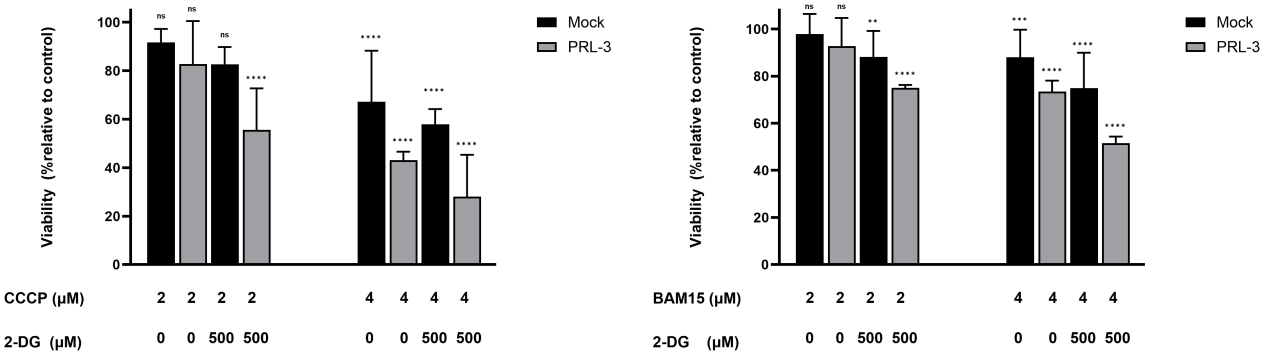

Figure 4.15: Viability of PRL-3-expressing cells is reduced more by a combination of inhibitors than Mock cells in normoxia: INA-6 Mock and INA-6 PRL-3 cells were treated with the specified concentrations of **A)** CCCP, or **B)** BAM15 and cultured under normoxia for 24 h. Cell viability was assessed by flow cytometry by Annexin V/PI-staining. The data is given as mean $\pm$ 2$\times$SEM from at least two independent experiments, results are normalized against the untreated control group. The significance of the data was calculated by two-way ANOVA, where **** $p \leq 0.0001$.

In normoxic conditions, both CCCP and BAM15 induced cell death in a dose-dependent manner (Figure 4.15). The viability of Mock and PRL-3 cells was approximately 70-80% compared to control cells when treated with 2 µM of uncoupling agents, with a further 20% reduction observed in combination with 2-DG.

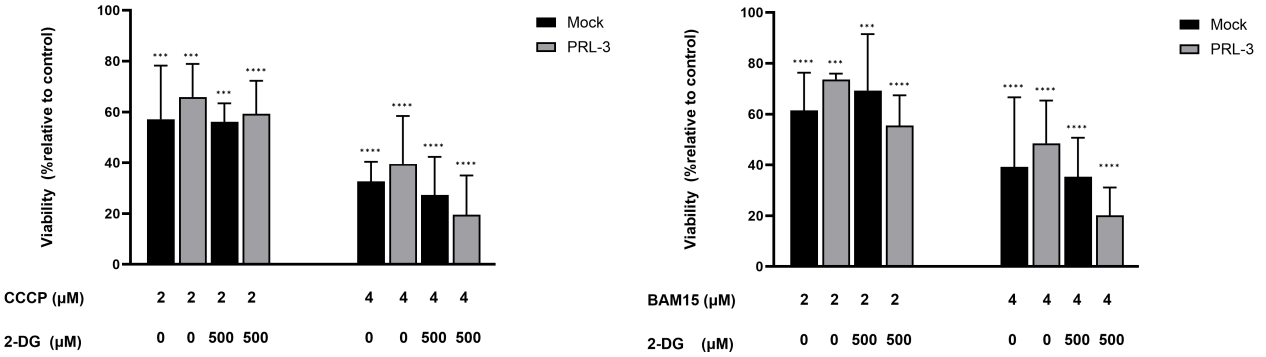

Figure 4.16: Hypoxia renders PRL-3 cells more susceptible to glycolysis inhibition than Mock cells: INA-6 Mock and INA-6 PRL-3 cells were treated with the indicated concentrations of **A)** CCCP, or **B)** BAM15 and cultured under hypoxic conditions for 24 h. Cell viability was assessed by flow cytometry by Annexin V/PI-staining. The data is given as mean ± 2×SEM from at least two independent experiments, results are normalized against the untreated control group. The significance of the data was calculated by two-way ANOVA, where **** $p \leq 0.0001$.

For cells incubated under hypoxic conditions, the viability of both Mock and PRL-3 cells treated solely with an uncoupling agent was approximately 60-65% (Figure 4.16) compared to the non-treated control group. Upon the addition of 2-DG, viability decreased by an additional 5-10% at most, with PRL-3 cells exhibiting a greater susceptibility to glycolysis inhibition. Viability was further reduced when cells were treated with 4 µM uncouplers„ with viabilities in the range of 35-40 % compared to the control cells, and with the addition of 2-DG, viability went down to 25-20%, with PRL-3-expressing cells exhibiting a larger decrease compared to Mock cells.

4.7.2 Low extracellular pH leads to unfavorable outcomes in MM cells

Metabolic acidosis significantly impedes cell proliferation, as shown in Figure 4.17. This reduction in viability aligns with the findings observed in cell proliferation (Figures 4.12 and 4.13). When cells were incubated under normoxia at pH 6.5, the viability of Mock cells decreased to approximately 60% compared to control cells, while PRL-3 cells exhibited an even lower viability of approximately 40% when treated with 2 µM of CCCP or BAM15. Upon combining the uncoupling agent with 2-DG, viability was further diminished by 5-20%. Notably, at 4 µM of the uncoupling agent, with or without 2-DG, viability plummeted to levels as low as 5-10% of the control.

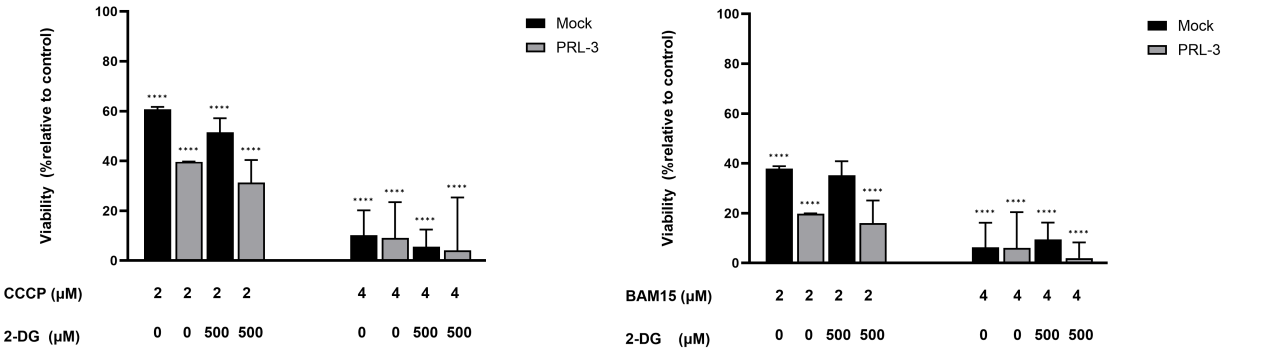

Figure 4.17: An acidic environment is a disfavor for PRL-3-expressing cells exposed to uncouplers and 2-DG: INA-6 Mock and INA-6 PRL-3 cells were treated with the given concentrations of **A)** CCCP, or **B)** BAM15 and cultured under normoxia for 24 h. Cell viability was assessed by flow cytometry by Annexin V/PI-staining. The data is given as mean ± 2×SEM from at least two independent experiments, results are normalized against the untreated control group. The significance of the data was calculated by two-way ANOVA, where **** $p \leq 0.0001$.

Similar to the findings under normoxic conditions (Figure 4.17), hypoxic conditions also resulted in substantial cell death for both Mock and PRL-3 cells when treated with mitochondrial uncoupling agents and 2-DG. Viability when treated with 2 µM of CCCP or BAM15 was approximately 50% compared to the control group. With the

addition of 2-DG, viability further decreased by another 20%. At a dose of 4 µM, a reverse trend was observed between the viability of Mock versus PRL-3 expressing cells when transitioning from incubating under normoxia to hypoxia. Mock cells exhibited a clear advantage in normoxia, whereas PRL-3 cells demonstrated enhanced viability in hypoxia, both for cells treated with CCCP or BAM15 (Figure 4.18).

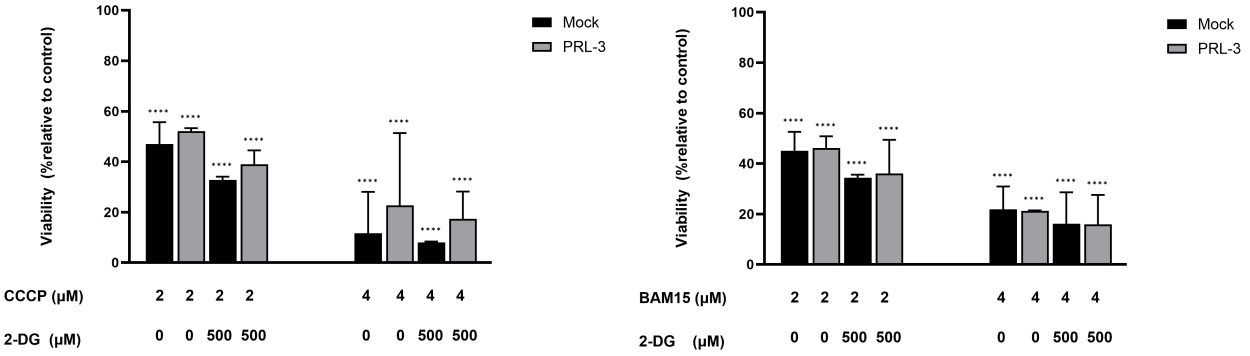

Figure 4.18: Hypoxia favors PRL-3-expressing cells under low pH conditions: INA-6 Mock and INA-6 PRL-3 cells were treated with the indicated concentrations of **A)** CCCP, or **B)** BAM15 and cultured under normoxia for 24 h. Cell viability was assessed by flow cytometry by Annexin V/PI-staining. The data is given as mean $\pm$ 2$\times$SEM from at least two independent experiments, results are normalized against the untreated control group. The significance of the data was calculated by two-way ANOVA, where **** $p \leq 0.0001$.

5 Discussion

5.1 PRL-3 offers advantages in an acidic environment

Low extracellular pH is a hallmark of the TME in MM cells.[190] PRL-3 has been identified as integral in regulating cancer cell metabolism and adaptation to an acidic environment. Studies have revealed that PRL-3 contributes to the acidification of the microenvironment through increased lactate production. Interestingly, cells overexpressing PRL-3 demonstrate better tolerance to acidic conditions by preventing intracellular acidification in low pH environments.[118] This adaptive capacity to thrive in an acidic milieu is further supported by research demonstrating that PRL-3 promotes glucose uptake, lactate excretion, and enhances proteins involved in glycolysis and the serine/glycine synthesis pathway, a sub-branch of glycolysis.[83]

In our study, we observed that cells with forced overexpression of PRL-3 exhibited a higher relative rate of ATP production and viability at pH 6.5 compared to Mock cells. Specifically, we observed that PRL-3-expressing cells displayed a RLU ratio twice as high as that of Mock cells after 24 h of incubation when the pH was set at 6.5, whereas the ratio was only 1.35 times higher at pH 7.4, indicating a 50% increase in the ratio between pH 6.5 and pH 7.4. However, as depicted in Figure 4.1C, these ratios diminished with increasing incubation time. This decline could possibly be attributed to the limited volume of medium in which the cells were incubated in. Given that PRL-3-expressing cells have been shown to exhibit increased OCR and ECAR compared to Mock cells at both pH 7.4 and pH 6.5, the amount of nutrients accessible for exponential cell division becomes a crucial factor. PRL-3-expressing cells metabolize at a faster rate than Mock cells, thereby more rapidly, both figuratively and literally eat through the sustenance provided by the growth medium.

The steeper decline in the ratio at pH 6.5 can also be explained by the same rationale. Since we showed that PRL-3 cells have a higher ECAR, the rate of lactate production and subsequent acidification of the medium will be much faster for PRL-3-expressing cells. Although the optimal pH for cells expressing PRL-3 has been shown to be around pH 6.5, there is a rapid reduction in viability in cells below this pH, as shown by Funato et al.[118]

5.2 Normoxia favors OXPHOS while hypoxia favors glycolysis

In our experiments, we observed that cells incubated under normoxia and pH 7.4 displayed higher levels of OCR compared to those incubated under hypoxia and pH 6.5. Especially PRL-3 cells, particularly under normoxic conditions, exhibited nearly double the basal OCR compared to both Mock and PRL-3 cells incubated under hypoxia and low pH, and nearly triple the OCR under stress induced by the BAM15/oligomycin stressor mix. These observations align with established knowledge regarding the influence of normoxia on cellular redox balance, which favors mitochondrial OXPHOS respiration over anaerobic glycolytic processes due to favorable redox states.[191] Under normoxic conditions, the abundance of oxygen facilitates the maintenance of redox balance, thereby promoting electron transfer from NADH and FADH2 to molecular oxygen through a cascade of redox reactions in the ETC.

In contrast, under hypoxic conditions, there is a metabolic shift toward glycolysis. Interestingly, while the OCR rates for Mock and PRL-3 cells are comparable under hypoxia and low pH, a significant disparity emerges under normoxia. This contrast may be partially explained by examining the ECAR rates, which reveal that PRL-3-expressing cells under hypoxia and treated with BAM15 and oligomycin over time exhibit ECAR levels nearly equivalent to Mock cells under normoxia, suggesting that the increase in glycolysis compensates for the offset in OXPHOS. Michl et al.[192] proposed that although the Warburg effect upregulates glycolysis in cancer cells, glycolytic flux would still decrease considerably in an acidic environment due to the aforementioned sensitivity to proton inhibition. In response, cancer cells adapt by altering metabolism towards increased reliance on OXPHOS, glutamine, and fatty acid metabolism.[193]

Our results demonstrate a different scenario in a hypoxic and acidic environment. Here, OXPHOS was comparably reduced for Mock and PRL-3 cells, while glycolysis, albeit also reduced compared to pH 7.4 and normoxia, remained relatively more active in PRL-3-expressing cells. Although the exact influence of PRL-3 on this

phenomenon remains uncertain, the data suggest that upregulation of glycolysis outweighs glycolytic proton inhibition by metabolic acidosis, emphasizing the complex interplay between oxygen and pH levels in modulating cellular metabolism.

The harsh conditions of the TME, characterized by low oxygen and pH levels, markedly diminish ATP production through both OXPHOS and glycolysis. Hypoxia limits oxygen availability, impairing ETC efficiency and ATP synthesis, whereas acidic pH inhibits glycolysis, further hampering ATP generation via this pathway. Consequently, the combined effects of hypoxia and metabolic acidosis pose significant challenges to MM cells, forcing them to adapt their metabolic and survival strategies. Although PRL-3 appears to augment glycolytic flux to some extent, the increased reliance on glycolysis in PRL-3-expressing cells renders them susceptible to glycolysis inhibitors, suggesting potential therapeutic avenues for MM treatment.

5.3 HIF-1α expression is significantly inhibited by mitochondrial uncouplers

Cancer cells have evolved intricate mechanisms to thrive under hypoxic conditions induced by their uncontrolled proliferation. A primary strategy employed by tumors to counteract hypoxia involves stabilizing and enhancing the transcriptional activity of the hypoxia-inducible factor 1 (HIF-1) TF. Elevated levels of HIF-1α have been correlated with increased mortality rates in patients with various cancers, including MM.[194][195] Our experiments demonstrated that CCCP and BAM15, two uncoupling agents, significantly inhibited HIF-1α expression.

The exact mechanisms underlying this reduced expression have not been fully elucidated; however, a study by Thomas et al.[196] indicated that it involves, to some extent, a decrease in HIF-1 transcriptional activity by downregulating HIF-1α protein levels. Furthermore, the study suggested that the uncoupling agents did not alter the mRNA levels of either HIF-1α or HIF-2α, nor their nuclear localization, implying post-transcriptional regulation. Additionally, the mitochondrial uncouplers were found to diminish the expression of VEGF and VEGF receptor 2, two target genes of HIF-1.

A functional ETC in mitochondria relies on O_2 for OXPHOS. Studies by Hagen et al.[197] have demonstrated that blocking this respiratory chain reduces O_2 consumption in mitochondria, leading to the redistribution of O_2 within cells. This reallocation enhances the availability of O_2 to non-respiratory enzymes, such as prolyl hydroxylase, resulting in the destabilization of HIF proteins. Mitochondrial uncouplers could potentially elevate non-respiratory oxygen levels, thereby increasing the enzymatic activity of prolyl hydroxylases. Consequently, this could destabilize HIF-1α and HIF-2α proteins, leading to their degradation. In addition to prolyl hydroxylation of HIF-1α's oxygen-dependent domain, another crucial hydroxylation occurs at an essential asparagine residue (Asn-803) within its C-terminal transactivation domain (C-TAD).[198] This oxygen-dependent hydroxylation, catalyzed by factor inhibiting HIF-1 (FIH-1), impedes the interaction between HIF-1α and the transcriptional coactivators CBP/p300, thus reducing the transcriptional activity of HIF-1α.[199] Therefore, the increase in cellular oxygen levels induced by mitochondrial uncouplers could potentially enhance FIH-1 activity, leading to increased hydroxylation of Asn-803 in the C-TAD of HIF-1α. Given the important role of HIF-1α in upregulating glycolysis under hypoxic conditions,[200] a pertinent question arises regarding whether a similar increase in the rate of glycolysis would be observed in normoxia. In particular, our findings, as illustrated in Figure 4.1B, showed a significantly higher ECAR in PRL-3-expressing cells compared to Mock cells under normoxic conditions. This observation suggests that PRL-3 acts as a major regulator of glycolysis, independent of HIF-1α.

These results are consistent with a study by Abdollahi et al.,[83] which suggests that HIF-1α and PRL-3 modulate glycolysis through distinct mechanisms. The substantial decrease in HIF-1α levels following the administration of uncoupling agents could have significant implications for MM cells. Processes such as angiogenesis, glycolysis, cell survival, and metastasis are partially regulated by HIF-1α, and a reduction in HIF-1α expression under hypoxic conditions could compromise the adaptive capabilities of cancer cells.

5.4 Cells expressing PRL-3 possess lower levels of p-AMPK and glycolytic proteins compared to Mock cells under energy depletion

AMPK serves as a critical cellular energy sensor, playing a central role in maintaining energy homeostasis by inhibiting anabolic activities and stimulating catabolic processes to replenish ATP levels, thus regulating glycolysis.[201] Its activity is modulated by various factors, including the intracellular AMP:ATP ratio, which increases during energy stress conditions such as nutrient deprivation or hypoxia.[202] In our study (Figure 4.6), we observed a significant downregulation of p-AMPK in PRL-3-expressing cells upon simultaneous blockade of OXPHOS and glycolysis, while Mock cells exhibited an upregulation of p-AMPK compared to control cells. This observation may seem counterintuitive at first, as AMPK is typically activated under conditions of low ATP levels. However, Faubert et al.[203] indicated that AMPK acts as a negative regulator of aerobic glycolysis, and demonstrated that inactivating or downregulating AMPK signaling could increase the Warburg effect by enhancing ECAR rates.

Interestingly, these findings appear to contradict those of Abdollahi et al.,[83] who showed that AMPK knockdown in INA-6 MM cells led to decreased glycolytic activity, as was also reported by Holmes et al.[204] and Yang et al.[205] Nevertheless, upon comparing the ECAR levels (Figure 4.1B) with p-AMPK expression (Figure 4.6) in our experiments, PRL-3-expressing cells exhibited a greater increase in glycolysis concomitant with reduced expression of p-AMPK compared to Mock cells, which displayed lower ECAR rates alongside higher expression of p-AMPK. This pattern was consistent across normoxic and hypoxic conditions, indicating that HIF-1α likely did not play a significant role in this regulation, although AMPK has been shown to be regulated by hypoxia.[206] Notably, the expression of p-AMPK was upregulated in control cells at pH 6.5 compared to pH 7.4 for both Mock and PRL-3 cells, suggesting that metabolic acidosis itself possibly induces energy stress by inhibiting glycolysis.

For cells expressing PRL-3, we observed stable levels (at pH 7.4) or a a decline (at pH 6.5) in p-AMPK expression after coadministration of uncoupling agents and 2-DG, while Mock cells exhibited an increase in p-AMPK expression at pH 7.4, and stable or decreasing levels at pH 6.5. Although the exact mechanism underlying the downregulation of AMPK by PRL-3 remains unclear, it is likely associated with the increased energy demand in MM cells experiencing metabolic stress, often due to low oxygen levels in the tumor microenvironment and the subsequent shift toward glycolysis.[207] Studies have linked AMPK downregulation to the upregulation of oncogenic factors such as β-catenin and COX-2, which contribute to cancer development.[208] Furthermore, AMPK downregulation has been implicated in promoting cancer cell proliferation and invasion in various cancer types.[209]

However, our Western blot experiments revealed intriguing findings: MM cells expressing PRL-3 did not exhibit higher expression levels of HKII or GLUT1 compared to Mock cells when treated with uncoupling agents and 2-DG. Despite the observed upregulation of glycolysis in PRL-3 cells, as confirmed by ECAR experiments, the absence of significant differences in the expression of key glycolytic enzymes such as HKII and GLUT1 raises questions about the underlying mechanisms mediated by PRL-3 that drive glycolytic alterations in these cells. Although PRL-3 cells demonstrated enhanced glycolytic activity, comparable levels of HKII and GLUT1 in PRL-3 and Mock cells suggest that the upregulation of glycolysis in PRL-3 cells may involve alternative pathways or post-translational modifications rather than changes in the expression of these enzymes. Vashistha et al.[210] discussed the enhanced expression of GLUT1, HKII, and lactate dehydrogenase A (LDHA) in response to exposure to the uncoupling agent 2,4-dinitrophenol, suggesting a potential link between the upregulation of these glycolytic enzymes and OXPHOS inhibition.

On the contrary, our results revealed that GLUT1 was upregulated to a greater extent in Mock cells compared to PRL-3-expressing cells across various conditions, including normoxia, hypoxia, pH 7.4, and pH 6.5, while HKII levels remained comparable in all conditions. Although the study by Vashistha and colleagues utilized an uncoupling agent sans 2-DG treatment, it is noteworthy that 2-DG has been reported to increase GLUT1 expression in breast cancer cells.[211] Abdollahi et al.[83] also investigated the expression of HKII and GLUT1 in MM cells and found significant upregulation of both proteins compared to Mock cells, although their study did not involve drug treatment. Additionally, the study suggested that PRL-3 induced aerobic glycolysis through increased glucose import via GLUT1, enabling cells to utilize exogenous nutrients. Furthermore, a study by Xu et al.[212] demon-

strated that PRL-3 increased colorectal glucose consumption, lactate production, and expression of HKII, GLUT1, PKM2, and LDHA. Xie et al.,[64] however, published a study that assessed the transport of glucose into cells under normal and lactic acidosis conditions. They showed that lactic acidosis markedly reduced the transport of [3H]-2-DG into cells, yet did not affect GLUT1 expression. Conversely, the study observed that glucose levels inside cells exposed to lactic acidosis were considerably elevated compared to those in control cells, indicating a more substantial impairment of glycolysis than of glucose transport. Since large changes in HKII and GLUT1 expression were not observed in our study, with the transition from pH 7.4 to pH 6.5, metabolic acidosis is unlikely to account for the discrepancy between PRL-3-expressing cells increased rate of glycolysis, yet relatively mild expression of HKII and GLUT. Moreover, considering that both uncoupling agents and 2-DG have been shown to increase, rather than decrease, the expression of these proteins, the observed results present a complex interplay between PRL-3 expression and glycolytic regulation that warrants further investigation.

A study by Wang et al.[213] demonstrated that glycolysis inhibition by 2-DG in rat hepatocarcinogenesis decreased glycolysis, citric acid cycle activity, fatty acid and cholesterol synthesis, and ATP production. Interestingly, administration of 2-DG resulted in compensatory upregulation of HKII, but a reduction in mRNA expression of PFK2, PKM2, and LDHA. Consistent with our findings, we observed a modest increase in HKII protein levels in both Mock and PRL-3 cells following treatment with 2 µM uncoupler and 500 µM 2-DG, particularly at physiological pH 7.4. However, increasing the dose of the uncoupler to 4 µM while maintaining constant 2-DG levels resulted in reduced HKII expression.

5.5 Proteins involved in pH regulation and lactate transport

As observed in our study, PRL-3 expression has been linked to an elevation in glycolysis, as evidenced by increased ECAR, although the precise underlying mechanism remains elusive. The shift toward aerobic glycolysis results in an accumulation of lactate, particularly evident in PRL-3-expressing cells due to the heightened glycolytic flux of pyruvate. This lactate buildup poses a risk of intracellular acidification if not effectively removed. Perturbations in intracellular pH balance within cancer cells can lead to cell death due to uncontrolled acidification.[214] Cancer cells employ various mechanisms to regulate pH, among which upregulation of MCT4 serves as a protective strategy by exporting intracellular protons to maintain a stable intracellular pH.[215] Another critical pH regulator in cancer cells is NHE1, which facilitates proton export in exchange for sodium ions to uphold an optimal intracellular pH.

Funato et al.[118] demonstrated that MDCK cells expressing PRL-3 exhibited a preference for an extracellular pH of 6.5, in contrast to the pH of 7.4 favored by control cells, suggesting a phenotype favoring metabolic acidosis in PRL-3-expressing cells. Our data revealed elevated levels of NHE1 for PRL-3-expressing cells in general under normoxia, both at pH 7.4 and pH 6.5, most likely from increased lactate production due to upregulated glycolysis. The results under hypoxia and low pH point toward the tendency that the expression of NHE1 is lower for PRL-3-expressing cells, and mechanistically, downregulation of NHE1 at pH 6.5 aligns with the inhibitory effect of metabolic acidosis on glycolysis, however, without further data and repeated experiments, it proves difficult to come to a logical conclusion.

Our experimental findings indicated that MCT4 expression was comparable between Mock and PRL-3-expressing cells at pH 7.4 under normoxia, whereas PRL-3 had moderately higher expression at pH 6.5. Interestingly, the expression of MCT4 in PRL-3-expressing cells remained comparable to untreated controls, regardless of the concentration of uncoupler or 2-DG administered. However, there was a modest increase in MCT4 expression observed in both Mock and PRL-3 cells when exposed to an acidic environment compared to pH 7.4, with PRL-3-expressing cells exhibiting a somewhat larger upregulation. Without additional studies, it is difficult to determine why we observe such a small change in expression of MCT4 upon treatment with CCCP and 2-DG.

Prior research has demonstrated that compounds such as CCCP and FCCP, which are structurally similar, can depolarize the plasma membrane and induce intracellular acidification by facilitating the influx of protons into cells.[216] For instance, Park et al.[217] investigated the impact of FCCP on plasma membrane potential in bovine aortic endothelial cells and observed alterations in ionic currents and depolarization, potentially involving

the activation of both H^+ and Na^+ currents across the plasma membrane. Similarly, Kaila et al.[216] conducted experiments using CCCP on crayfish muscle fibers and found that CCCP induced a plasmalemma H^+ conductance, resulting in intracellular acidification and membrane depolarization. Based on these findings, we postulated that the addition of CCCP to MM cells could possibly lead to upregulation of both MCT4 and NHE1 due to the uncouplers' ability to reacidify the cytosol. However, it is challenging to determine if CCCP's ability to target the plasma membrane had a noticeable impact on the expression levels of the two proteins with the methods employed in this study, as MCT4 expression remained largely unchanged with CCCP treatment, while there was an increase in NHE1 expression. In retrospect, measuring intracellular pH after the administration of CCCP could possibly have aided in elucidating this question.

5.6 PRL-3 maintains balance in the expression of glycolytic proteins when facing hypoxic conditions

Hypoxia typically triggers the upregulation of glycolytic molecules, leading to an increased reliance on glycolysis, primarily orchestrated by HIF-1α.[218] However, our investigations revealed a significant reduction in HIF-1α expression following treatment with uncoupling agents, indicating an alternative source of upregulation for these proteins. Interestingly, the expression levels of key metabolic molecules, including p-AMPK, GLUT1 and HKII, were attenuated by the addition of uncoupling agents and 2-DG in PRL-3-expressing cells compared to Mock cells, a trend consistently observed under normoxic conditions. This suggests that PRL-3 cells, upon disruption of OXPHOS and glycolysis through chemical intervention, tend to maintain a delicate balance or equilibrium, avoiding excessive down- or upregulation of any specific protein from the established baseline. The underlying mechanism governing this regulatory response remains elusive, particularly considering that the viability of Mock and PRL-3 cells appears to be comparable under many experimental conditions. Abdollahi et al. proposed that PRL-3-induced downregulation of p-AMPK could stem from more favorable energy conditions facilitated by PRL-3; however, the precise mechanism driving this adaptation remains unresolved in our study.

5.7 PRL-3 increases the susceptibility of cancer cells to mitochondrial membrane depolarization

Depolarization of the mitochondrial membrane potential can have substantial implications for cancer cells in terms of cell function, apoptosis, and ATP production. The decline in ATP production primarily stems from depolarization-induced disruption of OXPHOS, a pivotal process reliant on the proton gradient across the inner mitochondrial membrane for the synthesis of ATP.[219]

Our findings revealed a comparable basal mitochondrial potential between cells expressing Mock and PRL-3. However, upon administration of 2 µM or 4 µM of BAM15, we observed a reduction in TMRM signaling, signifying membrane depolarization, with PRL-3-expressing cells exhibiting greater depolarization compared to Mock cells. The disparity in membrane potential between cells escalated at 8 µM and 16 µM, with the most significant difference observed at 16 µM, indicating a higher sensitivity of PRL-3-expressing cells to uncouplers in terms of depolarization.

These observations corroborate the rewiring induced by the Warburg effect, as mitochondrial membrane potential correlates solely with ATP production through OXPHOS and not glycolysis.[30] Given that PRL-3-expressing cells exhibited higher ATP levels than Mock cells despite an equivalent basal membrane potential, and a more substantial reduction in mitochondrial membrane potential post-uncoupler treatment, the discrepancy in ATP production must arise independently of OXPHOS. Nonetheless, Yang et al.[220] demonstrated the involvement of PRL-3 in regulating mitochondrial membrane potential. Their findings indicated that PRL-3 knockdown in human colorectal cancer cell lines significantly hyperpolarized the mitochondrial membrane potential. Since elevated membrane potentials inhibit OXPHOS,[221] PRL-3 supposedly plays a part in mitochondrial membrane potential regulation. However, these findings did not reflect our own observations, wherein Mock cells exhibited a mem-

brane potential similar to that of PRL-3-expressing cells in the control group. Notably, two caveats exist: **i)** the precise mechanism by which PRL-3 depolarizes the mitochondrial membrane remains elusive, and **ii)**, the aforementioned study employed colorectal cancer cells (CRC) rather than MM cells.

As shown in Figure 1.11, the rate of ATP efflux correlates linearly with the mitochondrial membrane potential. Given our demonstration that PRL-3-expressing cells are more susceptible to uncoupling agents, experiencing greater depolarization, there would also be a more pronounced reduction in ATP efflux. Consequently, less ATP is transported out of the mitochondrial matrix to the cytosol, where it can be utilized as energy.

5.8 Elevated levels of superoxide in PRL-3, a double-edged sword

Research indicates that alterations in redox balance and ROS-mediated signaling play pivotal roles in governing cancer cell survival, proliferation, and invasion.[222] In addition, the inherent high levels of oxidative stress in cancer cells, coupled with their dependence on ROS signaling for growth and survival, represent a vulnerability that can be exploited by redox-focused chemotherapeutic agents.[223][224] Additionally, interventions targeting mitochondria, which affect their structure and function, hold promise for redox-based cancer cell destruction.[225] Hence, small molecule agents capable of increasing oxidative stress, such as uncoupling agents, could possibly be considered promising experimental drugs targeting cancer cells that express PRL-3. However, the effects of PRL-3 inhibitors, on their ability to form ROS as a potential inhibitory mechanism in PRL-3 have been explored . The study did not see an increase in ROS, demonstrating that PRL-3 was selectively inhibited without the mechanism of ROS.[103]

Our data revealed that the doses of uncoupling agents utilized in our study did not significantly alter the generation of superoxide in Mock or PRL-3 cells, which required a dose eight-fold higher to observe any changes. However, we did observe slightly higher basal superoxide formation in cells expressing PRL-3 compared to Mock cells.

Cancer cells exhibiting elevated ROS levels often display heightened sensitivity to ROS-inducing agents, potentially leading to potent induction of cell death.[226] Furthermore, dysregulated mitochondrial superoxide levels in cancer cells have been associated with promotion of tumor progression, resistance to cell death mechanisms, and increased metastatic potential.[227] Hence, the presence of high levels of superoxide in cancer cells can have both advantageous and detrimental effects, contributing to a complex balance. Yang et al.[220] reported that PRL-3 downregulates superoxide, as its knockdown resulted in increased superoxide production. However, our findings contradict this, showing higher superoxide production in PRL-3-expressing cells. Furthermore, the study also suggested that PRL-3 knockdown elevated mitochondrial membrane potential, again conflicting with our results, highlighting the intricate regulatory nature of PRL-3. The Warburg effect has also been linked to superoxide concentration in cancer cells. Despite forcing cancer cells to rely on glycolysis over OXPHOS, a metabolic shift that decreases OCR and consequently ROS production, still leads to elevated oxidative stress in cancer cells. While pyruvate serves as a potent antioxidant in normal cells,[228] being further metabolized to acetyl-CoA and participating in the citric acid cycle to produce antioxidant intermediates along with reducing equivalents, cancer cells metabolize glucose into lactate, depriving themselves of antioxidants. This discrepancy between our study and that of Yang et al. may stem from differences in the glycolytic phenotype between MM cells and colorectal cancer cells (CRC).

5.9 Warburg effect makes PRL-3-expressing cells more vulnerable to glycolysis inhibition

OXPHOS and glycolysis represent the primary pathways for ATP production in cells. Given the metabolic alterations in cancer cells, we investigated the effects of mitochondrial uncoupling agents and a glycolysis inhibitor on MM cells with and without PRL-3 expression.

Our viability studies using the CTG assay (Section 4.6) revealed a consistent trend: PRL-3-expressing cells exhibited higher RLU and viability compared to Mock cells when treated solely with uncoupling agents. This observation is consistent with previous findings that indicate that PRL-3-expressing cells possess substantially

higher rates of glycolysis than Mock cells, allowing for a more significant compensatory response to OXPHOS uncoupling.[229] However, it is important to note that aerobic glycolysis cannot fully substitute for OXPHOS in ATP generation,[230] and suppression of glycolysis triggers a metabolic shift back to OXPHOS, indicating a dynamic interplay between the two energy pathways in cancer cells.[231] Upon administering 2-DG, we observed a decrease in viability of PRL-3 cells below that of Mock cells under normoxic and hypoxic conditions. This suggests that the increased reliance on glycolysis, a hallmark of the Warburg effect in cancer cells, becomes a critical vulnerability when glycolysis is inhibited.[230] Despite the inherently higher OCR and ECAR in PRL-3-expressing cells, simultaneous blockade of OXPHOS and glycolysis proves detrimental to PRL-3 cells when ATP supply is compromised.

Our investigation into the cytotoxic effects of dual OXPHOS and glycolysis inhibition involved Annexin V/PI dual staining to assess cell status after a 24 h treatment period. Interestingly, we observed a larger difference in viability between Mock and PRL-3 cells compared to the results of the CTG assay. While it is not uncommon for widely different techniques to yield conflicting results, the discrepancy warrants attention. In our flow cytometry experiments, particularly with Annexin V, irregularities were revealed, especially with PRL-3 cells. The boundaries between live (Q4) and apoptotic (Q3) populations occasionally blurred, particularly evident under acidic conditions (Figure 6.10) and (Figure 6.11), possibly due to PRL-3's distinct physical properties, as PRL-3 cells tend to be larger than Mock cells.[83] Additionally, the composition of the RPMI medium may influence the efficacy of uncoupling agents, impacting cellular responses.[232]

5.10 Acidic TME renders uncoupling agents a triple threat to cancer cells

The Warburg effect, a prominent characteristic of many cancer cells, is influenced by environmental factors such as low pH. Cancer cells typically exhibit glycolytic metabolism under standard culture conditions, but in the presence of metabolic acidosis, they adopt a non-glycolytic phenotype characterized by an elevated ratio of OCR to ECAR, minimal lactate production, and efficient utilization of glucose carbons.[64]

Our experiments revealed a significant negative impact of metabolic acidosis on the viability of both Mock and PRL-3 cells. Viability was nearly reduced by 50% compared to cells cultured at pH 7.4, with PRL-3 cells showing greater sensitivity, particularly when treated with uncouplers in combination with 2-DG. This marked difference in viability between physiological and acidic conditions can possibly be explained by three factors:

i:) Our findings indicate that the combination of metabolic acidosis and hypoxia significantly affected OCR and ECAR, especially in PRL-3 expressing cells. These cells exhibited a 50% decrease in basal OCR and close to a 40% reduction in ECAR. Presuming that all OCR and ECAR contribute to ATP production, this implies a total efficiency decrease of approximately 68%. Although hypothetical and based on major assumptions, a study by Sorensen et al.[233] demonstrated a 50% reduction in total ATP turnover in cancer cells exposed to hypoxia and metabolic acidosis. Consequently, given that the TME already diminishes ATP production, further inhibition by uncouplers and 2-DG results in critically low ATP concentrations.

ii:) Chinopolous et al. investigated the role of pH on the ATP/ADP exchange rate by the Adenine nucleotide translocator (ANT). They observed a direct correlation between the rate of ATP efflux and mitochondrial membrane potential, where depolarization resulted in less ATP efflux from the mitochondrial matrix, regardless of matrix pH. Seeing as our results pointed toward that PRL-3-expressing cells had a larger mitochondrial membrane depolarization, the cells would also have a greater reduction in ATP efflux and a subsequent reduction in the free energy between ANT and ATP.[169]

iii) A smaller quantity of uncoupler is needed to induce depolarization when the pH is $<$ the pKa of the uncoupler, compared to when the pH exceeds the pKa value (the pKa of BAM15 is 7.56 ± 0.08[155]). This is because the activity of uncouplers is dependent on their protonation or deprotonation state, which is influenced by pH. With a pKa of approximately 7.56 for BAM15, an increase in pH leads to a buildup of the dissociated, deprotonated form of the uncoupler outside the mitochondria, requiring a higher concentration of uncoupler to achieve the same degree of proton flux and depolarization. Conversely, a decrease in pH enhances the protonated state of BAM15, reducing the amount needed as it more effectively accumulates inside the mitochondria. Following this,

since we treated the cells incubated at pH 7.4 or pH 6.5 with the same amount of uncoupling agents, metabolic acidosis essentially acted as an amplifier, leading to increased efficacy in terms of reducing viability. This effect was corroborated through an experimental study by Michl et al.[192] who postulated that intratumoral pH could serve as reliable markers for the potency and efficacy of uncoupling agents and other OXPHOS inhibitors, where the more acidic the pH, the greater effectiveness of these inhibitors.

Dequalinium chloride (DCQ) operates similarly by accumulating in the mitochondrial matrix and attracting uncoupling agents. Its effectiveness in reducing viability was comparable to that of metabolic acidosis. This effect was demonstrated in a study by Antonenko et al.[177] who showed that penetrating cations, such as DCQ, enhance the activity of uncoupling agents. It is possible that molecules such as DCQ could also form a positive feedback loop, as increased H^+ transport back into the mitochondrial matrix by uncouplers hyperpolarizes the mitochondrial membrane potential, leading to increased accumulation of cationic species. However, it remains unclear whether the increase in DCQ accumulation and subsequent hyperpolarization of membrane potential is offset by the depolarizing effects of acidifying the mitochondrial matrix. In our experiments, the addition of 3 µM DCQ in combination with CCCP or BAM15 yielded a reduction in viability of approximately 60%, greatly improving the potency of the uncouplers without reducing viability itself by more than 15% (Figure 6.3)

Limitations of the study

Despite the significant findings presented in this study, several limitations must be acknowledged to provide a comprehensive understanding of the results and their implications.
The experiments were exclusively conducted on the INA-6 cell line. Although this cell line provides valuable information, the findings may not be transferable to other types of cancer or even to other MM cell lines. Ideally, a broader range of cell lines with and without production of PRL-3 should have been examined, particularly IL-6 independent cell lines, alongside the use of a PRL-3 knockout model. Variations in metabolic pathways and PRL-3 expression across different cancers could lead to varied responses to metabolic interventions, as different cell lines have a wide variety in the contribution of OXPHOS and glycolysis to ATP production.

The study was conducted under controlled *in vitro* conditions, including varying pH and oxygen levels to mimic the TME. However, these conditions cannot fully replicate the complexity of the *in vivo* tumor environment. Factors such as biochemistry, interactions with stromal cells, immune responses, and vascularization are not accounted for in cell culture models, potentially influencing the metabolic behavior of the cells. Most experiments were also conducted over a time frame of 24-72 hours. By limiting incubation times, important temporal dynamics related to transient cellular and metabolic responses to prolonged adaptations are overlooked. Continuous monitoring and time-course studies could provide a more detailed understanding of how PRL-3 influences metabolic adaptation over time.

The number of repetitions for each experiment was limited by both time and resources, impacting the reproducibility and validity of the results. Increasing the number of experimental replicates could provide more reliable data and mitigate the effects of biological variability. Notably, studies related to cell viability displayed fluctuating data, as indicated by the large SEM in some of the experiments. The CTG assay, in particular, was affected by inconsistent data, likely due to the varying number of cells per well, leading to different RLU outputs. Inconsistent protein loading also affected some Western blot experiments, sowing doubt on certain observed results.

The study also had weaknesses in relation to changing two variables simultaneously, as in the Seahorse experiments, and not having adequate controls for 2-DG-only conditions in the proliferation and viability assays. Due to time and resource constraints, it was necessary to limit the number of replicates and conditions for the Seahorse assays, resulting in merged experiments for oxygen conditions and pH levels. The study could also have benefited from smaller pH intervals, as the change from pH 7.4 to pH 6.5 is logarithmic and encompasses a significant change in viability for Mock and PRL-3 cells. The doses of CCCP, BAM15, and 2-DG used were based

on preliminary data, but the exact physiological relevance of these concentrations *in vivo* remains unclear. Furthermore, potential off-target effects of these agents were not extensively investigated, which could influence the interpretation of the results.

6 Conclusion

In this thesis, we conducted a comprehensive exploration of cancer cell metabolism, focusing on the therapeutic implications of targeting mitochondrial respiration and glycolysis with the chemical uncoupling agents CCCP and BAM15 and the glycolysis inhibitor 2-DG, particularly in the context of PRL-3 expression and the acidic and hypoxic tumor microenvironment. Through a series of *in vitro* experiments encompassing cellular assays, molecular analyzes, and metabolic profiling, we gained critical insights into the metabolic vulnerabilities and adaptive responses of cancer cells, considering variations in pH and oxygen conditions.

Firstly, our findings demonstrate that PRL-3 expression confers an advantage to cancer cells in an acidic environment. We showed that PRL-3-expression led to increased ATP production and proliferation at low pH compared to the control cells, rendering cells expressing PRL-3 to thrive under the conditions of the TME.

Subsequent analyzes of oxygen consumption rate and extracellular acidification rate provided more insight into the metabolic alterations associated with PRL-3 expression, unveiling distinct metabolic phenotypes influenced by variations in pH and oxygen levels. These analyzes outlined the increase in glycolytic activity and increased dependence on glycolysis for ATP production in PRL-3-expressing cells, particularly under acidic and hypoxic conditions.

Furthermore, Western blot experiments showed the regulatory role of PRL-3 in key metabolic proteins, especially p-AMPK, GLUT1, and NHE1. PRL-3 actively suppressed the expression of p-AMPK, both under normoxia and hypoxia, and at physiological and acidic pH after inhibition of ATP production. GLUT1 expression was shown to be lower in PRL-3-expressing cells compared to Mock cells under all conditions, while NHE1 was more upregulated in PRL-3 cells under normoxia compared to Mock cells, with the opposite trend observed under hypoxia. PRL-3 was also demonstrated to affect these proteins independently of HIF-1α, and HIF-1α was not stabilized by PRL-3 under normoxic conditions.

We also examined the effects of mitochondrial uncoupling on mitochondrial membrane potential. These experiments uncovered a higher susceptibility of PRL-3-expressing cells to membrane depolarization induced by mitochondrial uncoupling agents. The greater depolarization observed in PRL-3-expressing cells contributes to a reduction in ATP efflux, directly leading to less available ATP.

Besides, our analysis of superoxide production revealed elevated basal superoxide levels in PRL-3-expressing cells but greater resistance to further superoxide elevation, highlighting the complex redox regulation in cancer cells.

Lastly, viability studies underscored the impact of metabolic interventions on cancer cell survival within the acidic TME and under varying oxygen conditions. By inhibiting glycolytic pathways and mitochondrial respiration, we observed a significant reduction in cell viability, especially in PRL-3-expressing cells possibly due to their glycolytic overreliance. Metabolic acidosis was also an important factor, essentially reducing the viability of MM cells by 50%.

In summary, this thesis advances our understanding of cancer cell bioenergetics and highlights the therapeutic potential of targeting mitochondrial function and glycolysis in PRL-3-expressing cells. By elucidating the metabolic vulnerabilities and adaptive responses associated with PRL-3 expression and variations in pH and oxygen conditions, our findings provide a foundation for the development of targeted therapeutic interventions aimed at cancer cell metabolism and improving treatment outcomes across diverse microenvironmental contexts. Further research in this field holds the promise of translating these insights into clinically viable cancer treatments.

References

[1] Niels WCJ van de Donk et al. 'T-cell redirecting bispecific and trispecific antibodies in multiple myeloma beyond BCMA'. In: *Current opinion in oncology* 35.6 (2023), pp. 601–611.

[2] Si-Wei Wang et al. 'Current applications and future perspective of CRISPR/Cas9 gene editing in cancer'. In: *Molecular cancer* 21.1 (2022), p. 57.

[3] Douglas E Joshua et al. 'Biology and therapy of multiple myeloma'. In: *Medical Journal of Australia* 210.8 (2019), pp. 375–380.

[4] Thanakorn Pungsrinont, Julia Kallenbach and Aria Baniahmad. 'Role of PI3K-AKT-mTOR pathway as a pro-survival signaling and resistance-mediating mechanism to therapy of prostate cancer'. In: *International journal of molecular sciences* 22.20 (2021), p. 11088.

[5] Klaus Podar et al. 'Targeting signalling pathways for the treatment of multiple myeloma'. In: *Expert opinion on therapeutic targets* 9.2 (2005), pp. 359–381.

[6] Facundo D Batista and Naomi E Harwood. 'The who, how and where of antigen presentation to B cells'. In: *Nature Reviews Immunology* 9.1 (2009), pp. 15–27.

[7] Federico Riccardi et al. 'Targeted therapy for multiple myeloma: an overview on CD138-based strategies'. In: *Frontiers in Oncology* 14 (2024).

[8] MH Bakkus et al. 'Evidence that multiple myeloma Ig heavy chain VDJ genes contain somatic mutations but show no intraclonal variation'. In: (1992).

[9] Ola Landgren et al. 'Monoclonal gammopathy of undetermined significance (MGUS) consistently precedes multiple myeloma: a prospective study'. In: *Blood, The Journal of the American Society of Hematology* 113.22 (2009), pp. 5412–5417.

[10] Jennifer M Bird et al. 'Guidelines for the diagnosis and management of multiple myeloma 2011'. In: *British journal of haematology* 154.1 (2011), pp. 32–75.

[11] Rafael Fonseca et al. 'Myeloma and the t (11; 14)(q13; q32); evidence for a biologically defined unique subset of patients'. In: *Blood, The Journal of the American Society of Hematology* 99.10 (2002), pp. 3735–3741.

[12] Cristina Gasparetto et al. 'Effect of t (11; 14) abnormality on outcomes of patients with newly diagnosed multiple myeloma in the connect MM registry'. In: *Clinical Lymphoma Myeloma and Leukemia* 22.3 (2022), pp. 149–157.

[13] Anna Kalff and Andrew Spencer. 'The t (4; 14) translocation and FGFR3 overexpression in multiple myeloma: prognostic implications and current clinical strategies'. In: *Blood cancer journal* 2.9 (2012), e89–e89.

[14] Hervé Avet-Loiseau et al. 'Prognostic significance of copy-number alterations in multiple myeloma'. In: *Journal of Clinical Oncology* 27.27 (2009), p. 4585.

[15] Jacques Ferlay et al. 'Estimating the global cancer incidence and mortality in 2018: GLOBOCAN sources and methods'. In: *International journal of cancer* 144.8 (2019), pp. 1941–1953.

[16] KREFTREGISTERET. 'Årsrapport for lymfoide maligniteter 2022'. In: *Nasjonalt kvalitetsregister for lymfoide maligniteter* (2022).

[17] Cecilie Hveding Blimark et al. 'Outcome and survival of myeloma patients diagnosed 2008–2015. Real-world data on 4904 patients from the Swedish Myeloma Registry'. In: (2017).

[18] National Cancer Institute Surveillance Research Program. 'Survival Rates for Multiple Myeloma'. In: (2021).

[19] Frederick L Locke et al. 'Axicabtagene ciloleucel as second-line therapy for large B-cell lymphoma'. In: *New England Journal of Medicine* 386.7 (2022), pp. 640–654.

[20] SY Kim. *Cancer energy metabolism: shutting power off cancer factory. Biomol Ther (Seoul). 2018; 26: 39–44*. 2017.

[21] Jacob Dunn and Michael H Grider. 'Physiology, adenosine triphosphate'. In: (2020).

[22] Fernando Bartolomé and Andrey Y Abramov. 'Measurement of mitochondrial NADH and FAD autofluorescence in live cells'. In: (2015), pp. 263–270.

[23] Raheel Chaudhry and Matthew Varacallo. 'Biochemistry, glycolysis'. In: (2018).

[24] David F Wilson. 'Oxidative phosphorylation: regulation and role in cellular and tissue metabolism'. In: *The Journal of physiology* 595.23 (2017), pp. 7023–7038.

[25] Riya Shrestha, Edward Johnson and Frances L Byrne. 'Exploring the therapeutic potential of mitochondrial uncouplers in cancer'. In: *Molecular Metabolism* 51 (2021), p. 101222.

[26] Peter Mitchell and Jennifer Moyle. 'Chemiosmotic hypothesis of oxidative phosphorylation'. In: *Nature* 213.5072 (1967), pp. 137–139.

[27] Ojas A Deshpande and Shamim S Mohiuddin. 'Biochemistry, Oxidative Phosphorylation'. In: (2021).

[28] Richard K Porter. 'Mitochondrial proton leak: a role for uncoupling proteins 2 and 3?' In: *Biochimica et Biophysica Acta (BBA)-Bioenergetics* 1504.1 (2001), pp. 120–127.

[29] Yuru Zhang et al. 'A comparative genomics study of carbohydrate/glucose metabolic genes: from fish to mammals'. In: *BMC genomics* 19 (2018), pp. 1–14.

[30] Erica A Melkonian and Mark P Schury. 'Biochemistry, anaerobic glycolysis'. In: (2019).

[31] I Stuart Wood and Paul Trayhurn. 'Glucose transporters (GLUT and SGLT): expanded families of sugar transport proteins'. In: *British journal of nutrition* 89.1 (2003), pp. 3–9.

[32] Ph J Randle et al. 'Regulation of pyruvate oxidation and the conservation of glucose.' In: *Biochemical Society Symposium*. 43. 1978, pp. 47–67.

[33] Barbara Muz et al. 'The role of hypoxia in cancer progression, angiogenesis, metastasis, and resistance to therapy'. In: *Hypoxia* (2015), pp. 83–92.

[34] Rodrigo Prieto-Bermejo and Angel Hernández-Hernández. 'The importance of NADPH oxidases and redox signaling in angiogenesis'. In: *Antioxidants* 6.2 (2017), p. 32.

[35] Isabella Giacomini et al. 'The pentose phosphate pathway and its involvement in cisplatin resistance'. In: *International journal of molecular sciences* 21.3 (2020), p. 937.

[36] Otto Warburg, Karl Posener and E Negelein. 'Über den stoffwechsel der carcinomzelle'. In: *Naturwissenschaften* 12.50 (1924), pp. 1131–1137.

[37] Hiromasa Yagi et al. 'Molecular mechanism of glycolytic flux control intrinsic to human phosphoglycerate kinase'. In: *Proceedings of the National Academy of Sciences* 118.50 (2021), e2112986118.

[38] Sophia Y Lunt and Matthew G Vander Heiden. 'Aerobic glycolysis: meeting the metabolic requirements of cell proliferation'. In: (2011).

[39] Preeti Ahuja et al. 'Myc controls transcriptional regulation of cardiac metabolism and mitochondrial biogenesis in response to pathological stress in mice'. In: *The Journal of clinical investigation* 120.5 (2010), pp. 1494–1505.

[40] Jihye Yun et al. 'Glucose deprivation contributes to the development of KRAS pathway mutations in tumor cells'. In: *Science* 325.5947 (2009), pp. 1555–1559.

[41] Rebecca L Elstrom et al. 'Akt stimulates aerobic glycolysis in cancer cells'. In: *Cancer research* 64.11 (2004), pp. 3892–3899.

[42] Satoaki Matoba et al. 'p53 regulates mitochondrial respiration'. In: *Science* 312.5780 (2006), pp. 1650–1653.

[43] Heather R Christofk et al. 'The M2 splice isoform of pyruvate kinase is important for cancer metabolism and tumour growth'. In: *Nature* 452.7184 (2008), pp. 230–233.

[44] Huai-Xiang Hao et al. 'SDH5, a gene required for flavination of succinate dehydrogenase, is mutated in paraganglioma'. In: *Science* 325.5944 (2009), pp. 1139–1142.

[45] Zachary J Reitman and Hai Yan. 'Isocitrate dehydrogenase 1 and 2 mutations in cancer: alterations at a crossroads of cellular metabolism'. In: *Journal of the National Cancer Institute* 102.13 (2010), pp. 932–941.

[46] Allyson E Vaughn and Mohanish Deshmukh. 'Glucose metabolism inhibits apoptosis in neurons and cancer cells by redox inactivation of cytochrome c'. In: *Nature cell biology* 10.12 (2008), pp. 1477–1483.

[47] Isaac Marin-Valencia et al. 'Analysis of tumor metabolism reveals mitochondrial glucose oxidation in genetically diverse human glioblastomas in the mouse brain in vivo'. In: *Cell metabolism* 15.6 (2012), pp. 827–837.

[48] Xin Lin Zu and Michael Guppy. 'Cancer metabolism: facts, fantasy, and fiction'. In: *Biochemical and biophysical research communications* 313.3 (2004), pp. 459–465.

[49] Jie Hu et al. 'Heterogeneity of tumor-induced gene expression changes in the human metabolic network'. In: *Nature biotechnology* 31.6 (2013), pp. 522–529.

[50] Brandon Faubert et al. 'Lactate metabolism in human lung tumors'. In: *Cell* 171.2 (2017), pp. 358–371.

[51] George A Brooks. 'Cell–cell and intracellular lactate shuttles'. In: *The Journal of physiology* 587.23 (2009), pp. 5591–5600.

[52] Pierre Sonveaux et al. 'Targeting lactate-fueled respiration selectively kills hypoxic tumor cells in mice'. In: *The Journal of clinical investigation* 118.12 (2008), pp. 3930–3942.

[53] Tiago C Leite et al. 'Lactate downregulates the glycolytic enzymes hexokinase and phosphofructokinase in diverse tissues from mice'. In: *FEBS letters* 585.1 (2011), pp. 92–98.

[54] Archana M Navale and Archana N Paranjape. 'Glucose transporters: physiological and pathological roles'. In: *Biophysical reviews* 8.1 (2016), pp. 5–9.

[55] B Pajak et al. '2-Deoxy-d-glucose and its analogs: from diagnostic to therapeutic agents'. In: *International journal of molecular sciences* 21.1 (2019), p. 234.

[56] Alberto Sols and Robert K Crane. 'Substrate specificity of brain hexokinase'. In: *Journal of Biological Chemistry* 210.2 (1954), pp. 581–595.

[57] LINDA F BIsSON and Dan G Fraenkel. 'Involvement of kinases in glucose and fructose uptake by Saccharomyces cerevisiae.' In: *Proceedings of the National Academy of Sciences* 80.6 (1983), pp. 1730–1734.

[58] Tao Jin et al. 'Glucose metabolism-weighted imaging with chemical exchange-sensitive MRI of 2-deoxyglucose (2DG) in brain: Sensitivity and biological sources'. In: *Neuroimage* 143 (2016), pp. 82–90.

[59] Anne Catherine Sprynski et al. 'The role of IGF-1 as a major growth factor for myeloma cell lines and the prognostic relevance of the expression of its receptor'. In: *Blood, The Journal of the American Society of Hematology* 113.19 (2009), pp. 4614–4626.

[60] Yi Xiao and Dihua Yu. 'Tumor microenvironment as a therapeutic target in cancer'. In: *Pharmacology & therapeutics* 221 (2021), p. 107753.

[61] Enrico Pierluigi Spugnini et al. 'Proton channels and exchangers in cancer'. In: *Biochimica et Biophysica Acta (BBA)-Biomembranes* 1848.10 (2015), pp. 2715–2726.

[62] Robert A Gatenby and Robert J Gillies. 'Why do cancers have high aerobic glycolysis?' In: *Nature reviews cancer* 4.11 (2004), pp. 891–899.

[63] Rosa A Cardone, Valeria Casavola and Stephan J Reshkin. 'The role of disturbed pH dynamics and the Na+/H+ exchanger in metastasis'. In: *Nature reviews cancer* 5.10 (2005), pp. 786–795.

[64] Jiansheng Xie et al. 'Beyond Warburg effect–dual metabolic nature of cancer cells'. In: *Scientific reports* 4.1 (2014), p. 4927.

[65] Feifei Sun et al. 'Biochemical issues in estimation of cytosolic free NAD/NADH ratio'. In: *PloS one* 7.5 (2012), e34525.

[66] Olivier Trédan et al. 'Drug resistance and the solid tumor microenvironment'. In: *Journal of the National Cancer Institute* 99.19 (2007), pp. 1441–1454.

[67] Peter Vaupel and Gabriele Multhoff. 'Revisiting the Warburg effect: Historical dogma versus current understanding'. In: *The Journal of physiology* 599.6 (2021), pp. 1745–1757.

[68] Robert J Gillies. 'Cancer heterogeneity and metastasis: Life at the edge'. In: *Clinical & Experimental Metastasis* 39.1 (2022), pp. 15–19.

[69] Noopur Raje and G David Roodman. 'Advances in the biology and treatment of bone disease in multiple myeloma'. In: *Clinical Cancer Research* 17.6 (2011), pp. 1278–1286.

[70] Masahiro Abe. 'Targeting the interplay between myeloma cells and the bone marrow microenvironment in myeloma'. In: *International journal of hematology* 94 (2011), pp. 334–343.

[71] Yasumasa Kato et al. 'Acidic extracellular microenvironment and cancer'. In: *Cancer cell international* 13 (2013), pp. 1–8.

[72] Ryota Amachi et al. 'A vicious cycle between acid sensing and survival signaling in myeloma cells: Acid-induced epigenetic alteration'. In: *Oncotarget* 7.43 (2016), p. 70447.

[73] Dai Fukumura et al. 'Hypoxia and acidosis independently up-regulate vascular endothelial growth factor transcription in brain tumors in vivo'. In: *Cancer research* 61.16 (2001), pp. 6020–6024.

[74] Gregg L Semenza. 'Targeting HIF-1 for cancer therapy'. In: *Nature reviews cancer* 3.10 (2003), pp. 721–732.

[75] Joel A Spencer et al. 'Direct measurement of local oxygen concentration in the bone marrow of live animals'. In: *Nature* 508.7495 (2014), pp. 269–273.

[76] J Martin Brown and William R Wilson. 'Exploiting tumour hypoxia in cancer treatment'. In: *Nature Reviews Cancer* 4.6 (2004), pp. 437–447.

[77] Keiyo Takubo et al. 'Regulation of the HIF-1α level is essential for hematopoietic stem cells'. In: *Cell stem cell* 7.3 (2010), pp. 391–402.

[78] Ji-Won Lee et al. 'Hypoxia-inducible factor (HIF-1) α: its protein stability and biological functions'. In: *Experimental & molecular medicine* 36.1 (2004), pp. 1–12.

[79] B Muz et al. 'The role of hypoxia in cancer progression, angiogenesis, metastasis, and resistance to therapy. Hypoxia (Auckl). 2015; 3: 83–92'. In: ().

[80] Joon Hee Kang et al. 'Aldehyde dehydrogenase is used by cancer cells for energy metabolism'. In: *Experimental & molecular medicine* 48.11 (2016), e272–e272.

[81] Jung-whan Kim et al. 'HIF-1-mediated expression of pyruvate dehydrogenase kinase: a metabolic switch required for cellular adaptation to hypoxia'. In: *Cell metabolism* 3.3 (2006), pp. 177–185.

[82] Mohammed S Ullah, Andrew J Davies and Andrew P Halestrap. 'The plasma membrane lactate transporter MCT4, but not MCT1, is up-regulated by hypoxia through a HIF-1α-dependent mechanism'. In: *Journal of Biological Chemistry* 281.14 (2006), pp. 9030–9037.

[83] Pegah Abdollahi et al. 'Phosphatase of regenerating liver-3 regulates cancer cell metabolism in multiple myeloma'. In: *The FASEB Journal* 35.3 (2021), e21344.

[84] Victoria McParland et al. 'The metastasis-promoting phosphatase PRL-3 shows activity toward phosphoinositides'. In: *Biochemistry* 50.35 (2011), pp. 7579–7590.

[85] Qi Zeng, Wanjin Hong and YH Tan. 'Mouse PRL-2 and PRL-3, two potentially prenylated protein tyrosine phosphatases homologous to PRL-1'. In: *Biochemical and biophysical research communications* 244.2 (1998), pp. 421–427.

[86] Carolyn A Cates et al. 'Prenylation of oncogenic human PTPCAAX protein tyrosine phosphatases'. In: *Cancer letters* 110.1-2 (1996), pp. 49–55.

[87] Saurabh Saha et al. 'A phosphatase associated with metastasis of colorectal cancer'. In: *Science* 294.5545 (2001), pp. 1343–1346.

[88] Jianbiao Zhou et al. 'Phosphatase of regenerating liver-3 is regulated by signal transducer and activator of transcription 3 in acute myeloid leukemia'. In: *Experimental hematology* 42.12 (2014), pp. 1041–1052.

[89] Shashwati Basak et al. 'The metastasis-associated gene Prl-3 is a p53 target involved in cell-cycle regulation'. In: *Molecular cell* 30.3 (2008), pp. 303–314.

[90] Claudia Haferlach et al. 'Mutations of the TP53 gene in acute myeloid leukemia are strongly associated with a complex aberrant karyotype'. In: *Leukemia* 22.8 (2008), pp. 1539–1541.

[91] Yanjun Jiang et al. 'Phosphatase PRL-3 is a direct regulatory target of TGFβ in colon cancer metastasis'. In: *Cancer research* 71.1 (2011), pp. 234–244.

[92] Ping Zheng et al. 'Snail as a key regulator of PRL-3 gene in colorectal cancer'. In: *Cancer biology & therapy* 12.8 (2011), pp. 742–749.

[93] Jianliang Xu et al. 'VEGF promotes the transcription of the human PRL-3 gene in HUVEC through transcription factor MEF2C'. In: *PloS one* 6.11 (2011), e27165.

[94] John S Lazo et al. 'Disruption of Ovarian Cancer STAT3 and p38 Signaling with a Small-Molecule Inhibitor of PTP4A3 Phosphatase'. In: *Journal of Pharmacology and Experimental Therapeutics* 384.3 (2023), pp. 429–438.

[95] Phyllis SY Chong et al. 'IL6 promotes a STAT3-PRL3 feedforward loop via SHP2 repression in multiple myeloma'. In: *Cancer research* 79.18 (2019), pp. 4679–4688.

[96] Haihe Wang et al. 'PCBP1 suppresses the translation of metastasis-associated PRL-3 phosphatase'. In: *Cancer cell* 18.1 (2010), pp. 52–62.

[97] Wen Li et al. 'Insights into the post-translational modification and its emerging role in shaping the tumor microenvironment'. In: *Signal transduction and targeted therapy* 6.1 (2021), p. 422.

[98] T Ishii, Y Funato and H Miki. 'Thioredoxin-related protein 32 (TRP32) specifically reduces oxidized phosphatase of regenerating liver (PRL j Biol Chem. 2013; 288 (10): 7263–70'. In: *M112* 418004 ().

[99] Qi Zeng et al. 'Prenylation-dependent association of protein-tyrosine phosphatases PRL-1,-2, and-3 with the plasma membrane and the early endosome'. In: *Journal of Biological Chemistry* 275.28 (2000), pp. 21444–21452.

[100] Beatrice Dursina et al. 'Identification and specificity profiling of protein prenyltransferase inhibitors using new fluorescent phosphoisoprenoids'. In: *Journal of the American Chemical Society* 128.9 (2006), pp. 2822–2835.

[101] Myung-Suk Choi et al. 'The essential role of FKBP38 in regulating phosphatase of regenerating liver 3 (PRL-3) protein stability'. In: *Biochemical and biophysical research communications* 406.2 (2011), pp. 305–309.

[102] Yu-Han Huang et al. 'A role of autophagy in PTP4A3-driven cancer progression'. In: *Autophagy* 10.10 (2014), pp. 1787–1800.

[103] John S Lazo et al. 'Next-generation cell-active inhibitors of the undrugged oncogenic PTP4A3 phosphatase'. In: *Journal of Pharmacology and Experimental Therapeutics* 371.3 (2019), pp. 652–662.

[104] Günther H Peters, Thomas M Frimurer and Ole H Olsen. 'Electrostatic evaluation of the signature motif (H/V) CX5R (S/T) in Protein- Tyrosine Phosphatases'. In: *Biochemistry* 37.16 (1998), pp. 5383–5393.

[105] Jaeyul Kwon et al. 'Reversible oxidation and inactivation of the tumor suppressor PTEN in cells stimulated with peptide growth factors'. In: *Proceedings of the National Academy of Sciences* 101.47 (2004), pp. 16419–16424.

[106] Annette Salmeen et al. 'Redox regulation of protein tyrosine phosphatase 1B involves a sulphenyl-amide intermediate'. In: *Nature* 423.6941 (2003), pp. 769–773.

[107] Arne Holmgren. 'Antioxidant function of thioredoxin and glutaredoxin systems'. In: *Antioxidants & redox signaling* 2.4 (2000), pp. 811–820.

[108] Denis Krndija et al. 'The phosphatase of regenerating liver 3 (PRL-3) promotes cell migration through Arf-activity-dependent stimulation of integrin α5 recycling'. In: *Journal of cell science* 125.16 (2012), pp. 3883–3892.

[109] Akiyuki Nishimura and Maurine E Linder. 'Identification of a novel prenyl and palmitoyl modification at the CaaX motif of Cdc42 that regulates RhoGDI binding'. In: *Molecular and cellular biology* (2013).

[110] Cheng Xing et al. 'Ubiquitin-specific protease 4-mediated deubiquitination and stabilization of PRL-3 is required for potentiating colorectal oncogenesis'. In: *Cancer research* 76.1 (2016), pp. 83–95.

[111] Haidong Liu et al. 'Protein Tyrosine Phosphatase PRL-3: A Key Player in Cancer Signaling'. In: *Biomolecules* 14.3 (2024), p. 342.

[112] Yosuke Funato et al. 'Membrane protein CNNM4–dependent Mg 2+ efflux suppresses tumor progression'. In: *The Journal of clinical investigation* 124.12 (2014), pp. 5398–5410.

[113] Daisuke Yamazaki et al. 'Basolateral Mg2+ extrusion via CNNM4 mediates transcellular Mg2+ transport across epithelia: a mouse model'. In: *PLoS genetics* 9.12 (2013), e1003983.

[114] Guennadi Kozlov et al. 'PRL3 pseudophosphatase activity is necessary and sufficient to promote metastatic growth'. In: *Journal of Biological Chemistry* 295.33 (2020), pp. 11682–11692.

[115] Akiyoshi Hirayama et al. 'Quantitative metabolome profiling of colon and stomach cancer microenvironment by capillary electrophoresis time-of-flight mass spectrometry'. In: *Cancer research* 69.11 (2009), pp. 4918–4925.

[116] Osamu Hashizume et al. 'Excessive Mg2+ impairs intestinal homeostasis by enhanced production of adenosine triphosphate and reactive oxygen species'. In: *Antioxidants & Redox Signaling* 33.1 (2020), pp. 20–34.

[117] Unn-Merete Fagerli et al. 'Overexpression and involvement in migration by the metastasis-associated phosphatase PRL-3 in human myeloma cells'. In: *Blood, The Journal of the American Society of Hematology* 111.2 (2008), pp. 806–815.

[118] Yosuke Funato et al. 'The oncogenic PRL protein causes acid addiction of cells by stimulating lysosomal exocytosis'. In: *Developmental cell* 55.4 (2020), pp. 387–397.

[119] Yosuke Funato, Osamu Hashizume and Hiroaki Miki. 'Phosphatase-independent role of phosphatase of regenerating liver in cancer progression'. In: *Cancer Science* 114.1 (2023), pp. 25–33.

[120] Mohammad Samie et al. 'A TRP channel in the lysosome regulates large particle phagocytosis via focal exocytosis'. In: *Developmental cell* 26.5 (2013), pp. 511–524.

[121] WY Sanchez et al. 'Dichloroacetate inhibits aerobic glycolysis in multiple myeloma cells and increases sensitivity to bortezomib'. In: *British journal of cancer* 108.8 (2013), pp. 1624–1633.

[122] Patricia Maiso et al. 'Metabolic signature identifies novel targets for drug resistance in multiple myeloma'. In: *Cancer research* 75.10 (2015), pp. 2071–2082.

[123] Shiho Fujiwara et al. 'Lactate, a putative survival factor for myeloma cells, is incorporated by myeloma cells through monocarboxylate transporters 1'. In: *Experimental Hematology & Oncology* 4 (2015), pp. 1–8.

[124] Sevim Dalva-Aydemir et al. 'Targeting the metabolic plasticity of multiple myeloma with FDA-approved ritonavir and metformin'. In: *Clinical Cancer Research* 21.5 (2015), pp. 1161–1171.

[125] Chaima El Arfani et al. 'Metabolic features of multiple myeloma'. In: *International journal of molecular sciences* 19.4 (2018), p. 1200.

[126] Zhiwen Liu et al. 'Excess glucose induces hypoxia-inducible factor-1α in pancreatic cancer cells and stimulates glucose metabolism and cell migration'. In: *Cancer biology & therapy* 14.5 (2013), pp. 428–435.

[127] Pegah Abdollahi, Esten N Vandsemb and Magne Børset. 'Phosphatases of regenerating liver are key regulators of metabolism in cancer cells–role of Serine/Glycine metabolism'. In: *Current Opinion in Clinical Nutrition and Metabolic Care* 25.1 (2022), p. 50.

[128] Miguel Lopez et al. 'Hypothalamic AMPK: a canonical regulator of whole-body energy balance'. In: *Nature Reviews Endocrinology* 12.7 (2016), pp. 421–432.

[129] D Grahame Hardie. 'AMP-activated protein kinase: maintaining energy homeostasis at the cellular and whole-body levels'. In: *Annual review of nutrition* 34 (2014), pp. 31–55.

[130] D Grahame Hardie and Simon A Hawley. 'AMP-activated protein kinase: the energy charge hypothesis revisited'. In: *Bioessays* 23.12 (2001), pp. 1112–1119.

[131] Chen-Song Zhang et al. 'Fructose-1, 6-bisphosphate and aldolase mediate glucose sensing by AMPK'. In: *Nature* 548.7665 (2017), pp. 112–116.

[132] Diana Vara-Ciruelos et al. 'Genotoxic damage activates the AMPK-α1 isoform in the nucleus via Ca2+/CaMKK2 signaling to enhance tumor cell survival'. In: *Molecular Cancer Research* 16.2 (2018), pp. 345–357.

[133] Martin Jastroch et al. 'Mitochondrial proton and electron leaks'. In: *Essays in biochemistry* 47 (2010), pp. 53–67.

[134] Carin Thomas et al. 'Hydroxyl radical is produced via the Fenton reaction in submitochondrial particles under oxidative stress: implications for diseases associated with iron accumulation'. In: *Redox Report* 14.3 (2009), pp. 102–108.

[135] Aniko Somogyi et al. 'Antioxidant measurements'. In: *Physiological measurement* 28.4 (2007), R41.

[136] Julio F Turrens. 'Mitochondrial formation of reactive oxygen species'. In: *The Journal of physiology* 552.2 (2003), pp. 335–344.

[137] Ilaria Liguori et al. 'Oxidative stress, aging, and diseases'. In: *Clinical interventions in aging* 13 (2018), p. 757.

[138] F Michael Yakes and Bennett Van Houten. 'Mitochondrial DNA damage is more extensive and persists longer than nuclear DNA damage in human cells following oxidative stress'. In: *Proceedings of the National Academy of Sciences* 94.2 (1997), pp. 514–519.

[139] Ziye Rong et al. 'The mitochondrial response to DNA damage'. In: *Frontiers in Cell and Developmental Biology* 9 (2021), p. 669379.

[140] Yun Soo Bae et al. 'Epidermal growth factor (EGF)-induced generation of hydrogen peroxide: role in EGF receptor-mediated tyrosine phosphorylation'. In: *Journal of Biological Chemistry* 272.1 (1997), pp. 217–221.

[141] Lidija Milkovic et al. 'Short overview of ROS as cell function regulators and their implications in therapy concepts'. In: *Cells* 8.8 (2019), p. 793.

[142] Jennifer L Martindale and Nikki J Holbrook. 'Cellular response to oxidative stress: signaling for suicide and survival'. In: *Journal of cellular physiology* 192.1 (2002), pp. 1–15.

[143] Bruno Perillo et al. 'ROS in cancer therapy: The bright side of the moon'. In: *Experimental & molecular medicine* 52.2 (2020), pp. 192–203.

[144] Geoffrey Gloire, Sylvie Legrand-Poels and Jacques Piette. 'NF-κB activation by reactive oxygen species: fifteen years later'. In: *Biochemical pharmacology* 72.11 (2006), pp. 1493–1505.

[145] Hiroshi Terada. 'Uncouplers of oxidative phosphorylation.' In: *Environmental health perspectives* 87 (1990), pp. 213–218.

[146] Maria LR Lim, Tetsuhiro Minamikawa and Phillip Nagley. 'The protonophore CCCP induces mitochondrial permeability transition without cytochrome c release in human osteosarcoma cells'. In: *FEBS letters* 503.1 (2001), pp. 69–74.

[147] Atul A Chaudhari et al. 'Reactive oxygen species regulate Bax translocation and mitochondrial transmembrane potential, a possible mechanism for enhanced TRAIL-induced apoptosis by CCCP'. In: *Oncology reports* 18.1 (2007), pp. 71–76.

[148] Georg Linsinger et al. 'Uncouplers of oxidative phosphorylation can enhance a Fas death signal'. In: *Molecular and cellular biology* 19.5 (1999), pp. 3299–3311.

[149] Non Miyata et al. 'Pharmacologic rescue of an enzyme-trafficking defect in primary hyperoxaluria 1'. In: *Proceedings of the National Academy of Sciences* 111.40 (2014), pp. 14406–14411.

[150] Alberto Martın Guzmán-Grenfell, Mirta Araceli Bonilla-Hernández and Marco T González-Martınez. 'Glucose induces a Na+, K+-ATPase-dependent transient hyperpolarization in human sperm. I. Induction of changes in plasma membrane potential by the proton ionophore CCCP'. In: *Biochimica et Biophysica Acta (BBA)-Biomembranes* 1464.2 (2000), pp. 188–198.

[151] Kyum-Yil Kwon, Benoit Viollet and Ook Joon Yoo. 'CCCP induces autophagy in an AMPK-independent manner'. In: *Biochemical and biophysical research communications* 416.3-4 (2011), pp. 343–348.

[152] Vladimir L Gabai. 'Inhibition of uncoupled respiration in tumor cells: A possible role of mitochondrial Ca2+ efflux'. In: *FEBS letters* 329.1-2 (1993), pp. 67–71.

[153] Guoji Xiong et al. 'BAM15 as a mitochondrial uncoupler: a promising therapeutic agent for diverse diseases'. In: *Frontiers in Endocrinology* 14 (2023), p. 1252141.

[154] Sergio Rius-Pérez et al. 'PGC-1α, inflammation, and oxidative stress: an integrative view in metabolism'. In: *Oxidative medicine and cellular longevity* 2020 (2020).

[155] Brandon M Kenwood et al. 'Identification of a novel mitochondrial uncoupler that does not depolarize the plasma membrane'. In: *Molecular metabolism* 3.2 (2014), pp. 114–123.

[156] Trenton L Place and Frederick E Domann. 'Prolyl-hydroxylase 3: evolving roles for an ancient signaling protein'. In: *Hypoxia* (2013), pp. 13–27.

[157] Guido Kroemer and John C Reed. 'Mitochondrial control of cell death'. In: *Nature medicine* 6.5 (2000), pp. 513–519.

[158] JB Hoek, DG Nicholls and JR Williamson. 'Determination of the mitochondrial protonmotive force in isolated hepatocytes.' In: *Journal of Biological Chemistry* 255.4 (1980), pp. 1458–1464.

[159] David G Nicholls and Samantha L Budd. 'Mitochondria and neuronal survival'. In: *Physiological reviews* 80.1 (2000), pp. 315–360.

[160] Naoufal Zamzami and Guido Kroemer. 'The mitochondrion in apoptosis: how Pandora's box opens'. In: *Nature reviews Molecular cell biology* 2.1 (2001), pp. 67–71.

[161] Josephine S Modica-Napolitano and June R Aprille. 'Delocalized lipophilic cations selectively target the mitochondria of carcinoma cells'. In: *Advanced drug delivery reviews* 49.1-2 (2001), pp. 63–70.

[162] Meredith F Ross et al. 'Accumulation of lipophilic dications by mitochondria and cells'. In: *Biochemical journal* 400.1 (2006), pp. 199–208.

[163] Sébastien Bonnet et al. 'A mitochondria-K+ channel axis is suppressed in cancer and its normalization promotes apoptosis and inhibits cancer growth'. In: *Cancer cell* 11.1 (2007), pp. 37–51.

[164] Barbara G Heerdt, Michele A Houston and Leonard H Augenlicht. 'Growth properties of colonic tumor cells are a function of the intrinsic mitochondrial membrane potential'. In: *Cancer research* 66.3 (2006), pp. 1591–1596.

[165] Anna Maria Porcelli et al. 'pH difference across the outer mitochondrial membrane measured with a green fluorescent protein mutant'. In: *Biochemical and biophysical research communications* 326.4 (2005), pp. 799–804.

[166] Joseph R Casey, Sergio Grinstein and John Orlowski. 'Sensors and regulators of intracellular pH'. In: *Nature reviews Molecular cell biology* 11.1 (2010), pp. 50–61.

[167] Ming Yang and William J Brackenbury. 'Membrane potential and cancer progression'. In: *Frontiers in physiology* 4 (2013), p. 56081.

[168] Mehdi Damaghi, Jonathan W Wojtkowiak and Robert J Gillies. 'pH sensing and regulation in cancer'. In: *Frontiers in physiology* 4 (2013), p. 70349.

[169] Christos Chinopoulos et al. 'A novel kinetic assay of mitochondrial ATP-ADP exchange rate mediated by the ANT'. In: *Biophysical journal* 96.6 (2009), pp. 2490–2504.

[170] WB Hugo and M Frier. 'Mode of action of the antibacterial compound dequalinium acetate'. In: *Applied microbiology* 17.1 (1969), pp. 118–127.

[171] John J Merianos. 'Quarternary ammonium antimicrobial compounds'. In: *Disinfection, sterilization and preservation* (1991), pp. 225–255.

[172] Seung R Paik and Chung Soon Chang Do Hyung Kim. 'Stimulation of an esterase activity of thrombin by dequalinium and its relationship with blood coagulation'. In: *BMB Reports* 29.3 (1996), pp. 225–229.

[173] Shaoqiu Zhuo et al. 'Photoinactivation of the bovine heart mitochondrial F1-ATPase by [14C] dequalinium crosslinks phenylalanine-403 or phenylalanine-406 of an. alpha. subunit to a site or sites contained within residues 440-459 of a. beta. subunit'. In: *Biochemistry* 32.9 (1993), pp. 2219–2227.

[174] Christian Bailly. 'Medicinal applications and molecular targets of dequalinium chloride'. In: *Biochemical Pharmacology* 186 (2021), p. 114467.

[175] William L Bodden, Sanjeewani T Palayoor and William N Hai. 'Selective antimitochondrial agents inhibit calmodulin'. In: *Biochemical and biophysical research communications* 135.2 (1986), pp. 574–582.

[176] Shaoqui Zhuo and Williams S Allison. 'Inhibition and photoinactivation of the bovine heart mitochondrial F1-ATPase by the cytotoxic agent, dequalinium'. In: *Biochemical and biophysical research communications* 152.3 (1988), pp. 968–972.

[177] Yuri N Antonenko et al. 'Penetrating cations enhance uncoupling activity of anionic protonophores in mitochondria'. In: *PloS one* 8.4 (2013), e61902.

[178] Ana I García-Pérez et al. 'Dequalinium induces human leukemia cell death by affecting the redox balance'. In: *Leukemia research* 35.10 (2011), pp. 1395–1401.

[179] Pilar Sancho et al. 'Raf/MEK/ERK signaling inhibition enhances the ability of dequalinium to induce apoptosis in the human leukemic cell line K562'. In: *Experimental biology and medicine* 237.8 (2012), pp. 933–942.

[180] *TECHNICAL MANUAL CellTiter-Glo® 2.0 Assay, https://www.promega.com/resources/protocols/technical-manuals/101/celltiterglo-2-0-assay-protocol/?cs=y*.

[181] Aja M Rieger et al. 'Modified annexin V/propidium iodide apoptosis assay for accurate assessment of cell death'. In: *JoVE (Journal of Visualized Experiments)* 50 (2011), e2597.

[182] Nicholas J Kruger. 'The Bradford method for protein quantitation'. In: *The protein protocols handbook* (2009), pp. 17–24.

[183] Tahrin Mahmood and Ping-Chang Yang. 'Western blot: technique, theory, and trouble shooting'. In: *North American journal of medical sciences* 4.9 (2012), p. 429.

[184] Megan E Kauffman et al. 'MitoSOX-based flow cytometry for detecting mitochondrial ROS'. In: *Reactive oxygen species (Apex, NC)* 2.5 (2016), p. 361.

[185] AK Bhuyan, A Varshney and MK Mathew. 'Resting membrane potential as a marker of apoptosis: studies on Xenopus oocytes microinjected with cytochrome c'. In: *Cell Death & Differentiation* 8.1 (2001), pp. 63–69.

[186] Tobias S Slørdahl et al. 'The phosphatase of regenerating liver-3 (PRL-3) is important for IL-6-mediated survival of myeloma cells'. In: *Oncotarget* 7.19 (2016), p. 27295.

[187] Caroline N Smith and Jessica S Blackburn. 'PRL-3 promotes a positive feedback loop between STAT1/2-induced gene expression and glycolysis in multiple myeloma'. In: *The FEBS journal* 288.23 (2021), pp. 6674–6676.

[188] Qinghua Wu et al. 'Hypoxia-inducible factors: master regulators of hypoxic tumor immune escape'. In: *Journal of hematology & oncology* 15.1 (2022), p. 77.

[189] John P Fruehauf and Frank L Meyskens Jr. 'Reactive oxygen species: a breath of life or death?' In: *Clinical Cancer Research* 13.3 (2007), pp. 789–794.

[190] Shaojie Wu et al. 'Metabolic reprogramming induces immune cell dysfunction in the tumor microenvironment of multiple myeloma'. In: *Frontiers in oncology* 10 (2021), p. 591342.

[191] Melis Karabulutoglu et al. 'Oxidative stress and x-ray exposure levels-dependent survival and metabolic changes in murine HSPCs'. In: *Antioxidants* 11.1 (2021), p. 11.

[192] Johanna Michl et al. 'CRISPR-Cas9 screen identifies oxidative phosphorylation as essential for cancer cell survival at low extracellular pH'. In: *Cell Reports* 38.10 (2022).

[193] Cyril Corbet and Olivier Feron. 'Tumour acidosis: from the passenger to the driver's seat'. In: *Nature Reviews Cancer* 17.10 (2017), pp. 577–593.

[194] Archana Bhaskar and Bhupendra Nath Tiwary. 'Hypoxia inducible factor-1 alpha and multiple myeloma'. In: *International journal of advanced research* 4.1 (2016), p. 706.

[195] Paola Storti et al. 'Hypoxia-inducible factor (HIF)-1α suppression in myeloma cells blocks tumoral growth in vivo inhibiting angiogenesis and bone destruction'. In: *Leukemia* 27.8 (2013), pp. 1697–1706.

[196] Rusha Thomas and Myoung H Kim. 'Targeting the hypoxia inducible factor pathway with mitochondrial uncouplers'. In: *Molecular and cellular biochemistry* 296 (2007), pp. 35–44.

[197] Thilo Hagen et al. 'Redistribution of intracellular oxygen in hypoxia by nitric oxide: effect on HIF1α'. In: *Science* 302.5652 (2003), pp. 1975–1978.

[198] David Lando et al. 'Asparagine hydroxylation of the HIF transactivation domain: a hypoxic switch'. In: *Science* 295.5556 (2002), pp. 858–861.

[199] David Lando et al. 'FIH-1 is an asparaginyl hydroxylase enzyme that regulates the transcriptional activity of hypoxia-inducible factor'. In: *Genes & development* 16.12 (2002), pp. 1466–1471.

[200] Rupert Courtnay et al. 'Cancer metabolism and the Warburg effect: the role of HIF-1 and PI3K'. In: *Molecular biology reports* 42 (2015), pp. 841–851.

[201] Sébastien Herzig and Reuben J Shaw. 'AMPK: guardian of metabolism and mitochondrial homeostasis'. In: *Nature reviews Molecular cell biology* 19.2 (2018), pp. 121–135.

[202] Chen-chen Cai et al. 'Glycine protects against hypoxic-ischemic brain injury by regulating mitochondria-mediated autophagy via the AMPK pathway'. In: *Oxidative medicine and cellular longevity* 2019 (2019).

[203] Brandon Faubert et al. 'AMPK is a negative regulator of the Warburg effect and suppresses tumor growth in vivo'. In: *Cell metabolism* 17.1 (2013), pp. 113–124.

[204] Burton Fielding Holmes, EJ Kurth-Kraczek and WW Winder. 'Chronic activation of 5-AMP-activated protein kinase increases GLUT-4, hexokinase, and glycogen in muscle'. In: *Journal of applied physiology* 87.5 (1999), pp. 1990–1995.

[205] Qiuhua Yang et al. 'PRKAA1/AMPKα1-driven glycolysis in endothelial cells exposed to disturbed flow protects against atherosclerosis'. In: *Nature communications* 9.1 (2018), p. 4667.

[206] Franziska Dengler. 'Activation of AMPK under hypoxia: many roads leading to Rome'. In: *International journal of molecular sciences* 21.7 (2020), p. 2428.

[207] Ram Hari Pokhrel et al. 'AMPK promotes antitumor immunity by downregulating PD-1 in regulatory T cells via the HMGCR/p38 signaling pathway'. In: *Molecular cancer* 20 (2021), pp. 1–15.

[208] Sha-Sha Meng et al. 'Gradual deterioration of fatty liver disease to liver cancer via inhibition of AMPK signaling pathways involved in energy-dependent disorders, cellular aging, and chronic inflammation'. In: *Frontiers in Oncology* 13 (2023), p. 1099624.

[209] Zhiming Xiao et al. 'SDHB downregulation facilitates the proliferation and invasion of colorectal cancer through AMPK functions excluding those involved in the modulation of aerobic glycolysis'. In: *Experimental and therapeutic medicine* 15.1 (2018), pp. 864–872.

[210] Mohit Vashishta et al. 'Enhanced glycolysis confers resistance against photon but not carbon ion irradiation in human glioma cell lines'. In: *Cancer Management and Research* (2023), pp. 1–16.

[211] Rebecca L Aft, FW Zhang and D Gius. 'Evaluation of 2-deoxy-D-glucose as a chemotherapeutic agent: mechanism of cell death'. In: *British journal of cancer* 87.7 (2002), pp. 805–812.

[212] Heyang Xu et al. 'PRL-3 improves colorectal cancer cell proliferation and invasion through IL-8 mediated glycolysis metabolism'. In: *International Journal of Oncology* 51.4 (2017), pp. 1271–1279.

[213] Zhaofa Wang et al. 'Glycolysis inhibitor 2-deoxy-D-glucose suppresses carcinogen-induced rat hepatocarcinogenesis by restricting cancer cell metabolism'. In: *Molecular medicine reports* 11.3 (2015), pp. 1917–1924.

[214] Z-W Lee et al. 'Utilizing hydrogen sulfide as a novel anti-cancer agent by targeting cancer glycolysis and p H imbalance'. In: *British journal of pharmacology* 171.18 (2014), pp. 4322–4336.

[215] Anna Maria Reuβ. 'MCT4 promotes tumor malignancy in F98 glioma cells'. PhD thesis. Friedrich-Alexander-Universität Erlangen-Nürnberg (FAU), 2022.

[216] K Kaila, K Mattsson and J Voipio. 'Fall in intracellular pH and increase in resting tension induced by a mitochondrial uncoupling agent in crayfish muscle.' In: *The Journal of Physiology* 408.1 (1989), pp. 271–293.

[217] Kyu-Sang Park et al. 'FCCP depolarizes plasma membrane potential by activating proton and Na+ currents in bovine aortic endothelial cells'. In: *Pflügers Archiv* 443 (2002), pp. 344–352.

[218] Nicole Nowak, Anna Kulma and Jan Gutowicz. 'Up-regulation of key glycolysis proteins in cancer development'. In: *Open life sciences* 13.1 (2018), pp. 569–581.

[219] Hao Chen et al. 'Caspase inhibition rescues F1Fo ATP synthase dysfunction-mediated dendritic spine elimination'. In: *Scientific reports* 10.1 (2020), p. 17589.

[220] Yongyong Yang et al. 'Knockdown of PRL-3 increases mitochondrial superoxide anion production through transcriptional regulation of RAP1'. In: *Cancer Management and Research* (2018), pp. 5071–5081.

[221] Icksoo Lee, Elisabeth Bender and Bernhard Kadenbach. 'Control of mitochondrial membrane potential and ROS formation by reversible phosphorylation of cytochrome c oxidase'. In: *Molecular and cellular biochemistry* 234 (2002), pp. 63–70.

[222] Dunyaporn Trachootham, Jerome Alexandre and Peng Huang. 'Targeting cancer cells by ROS-mediated mechanisms: a radical therapeutic approach?' In: *Nature reviews Drug discovery* 8.7 (2009), pp. 579–591.

[223] Georg T Wondrak. 'Redox-directed cancer therapeutics: molecular mechanisms and opportunities'. In: *Antioxidants & redox signaling* 11.12 (2009), pp. 3013–3069.

[224] Christopher M Cabello, Warner B Bair 3rd and Georg T Wondrak. 'Experimental therapeutics: targeting the redox Achilles heel of cancer.' In: *Current opinion in investigational drugs (London, England: 2000)* 8.12 (2007), pp. 1022–1037.

[225] Valeria R Fantin et al. 'A novel mitochondriotoxic small molecule that selectively inhibits tumor cell growth'. In: *Cancer cell* 2.1 (2002), pp. 29–42.

[226] Hyang Yeon Lee et al. 'Reactive oxygen species synergize to potently and selectively induce cancer cell death'. In: *ACS chemical biology* 12.5 (2017), pp. 1416–1424.

[227] S Kamarajugadda et al. 'Manganese superoxide dismutase promotes anoikis resistance and tumor metastasis'. In: *Cell death & disease* 4.2 (2013), e504–e504.

[228] Xiaofei Wang et al. 'Pyruvate protects mitochondria from oxidative stress in human neuroblastoma SK-N-SH cells'. In: *Brain research* 1132 (2007), pp. 1–9.

[229] Thomas M Ashton et al. 'Oxidative phosphorylation as an emerging target in cancer therapy'. In: *Clinical Cancer Research* 24.11 (2018), pp. 2482–2490.

[230] Caroline Jose, Nadège Bellance and Rodrigue Rossignol. 'Choosing between glycolysis and oxidative phosphorylation: a tumor's dilemma?' In: *Biochimica et Biophysica Acta (BBA)-Bioenergetics* 1807.6 (2011), pp. 552–561.

[231] Reika Shiratori et al. 'Glycolytic suppression dramatically changes the intracellular metabolic profile of multiple cancer cell lines in a mitochondrial metabolism-dependent manner'. In: *Scientific reports* 9.1 (2019), p. 18699.

[232] Marc PM Soutar et al. 'FBS/BSA media concentration determines CCCP's ability to depolarize mitochondria and activate PINK1-PRKN mitophagy'. In: *Autophagy* 15.11 (2019), pp. 2002–2011.

[233] Brita Singers Sørensen et al. 'Simultaneous hypoxia and low extracellular pH suppress overall metabolic rate and protein synthesis in vitro'. In: *PloS one* 10.8 (2015), e0134955.

Appendix

Preliminary titration experiments with CCCP, BAM15 , dequalinium chloride and 2-DG

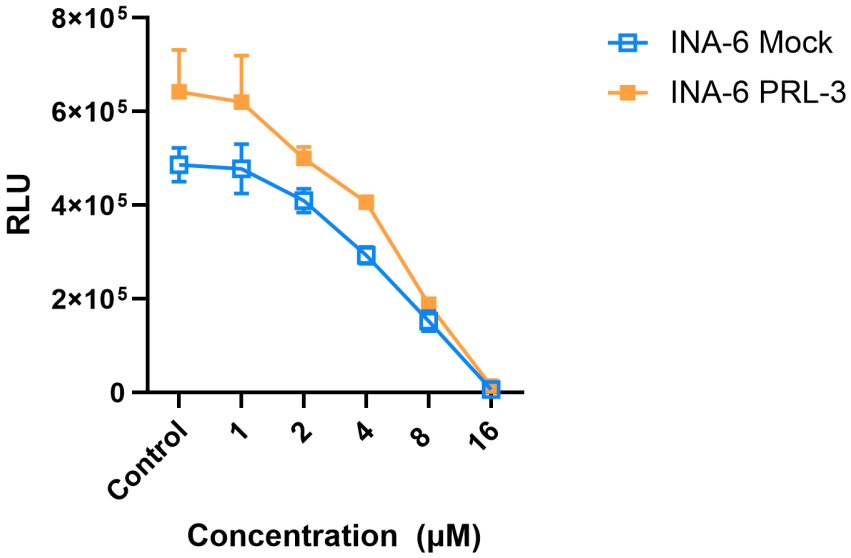

Supplementary 6.1: Titration curve for CCCP: INA-6 Mock and INA-6 PRL-3 cells were treated with the indicated concentrations of CCCP, then incubated for 24 h in normoxic conditions at pH 7.4. ATP content was measured by the CTG assay. The data is given as mean ± 2×SEM.

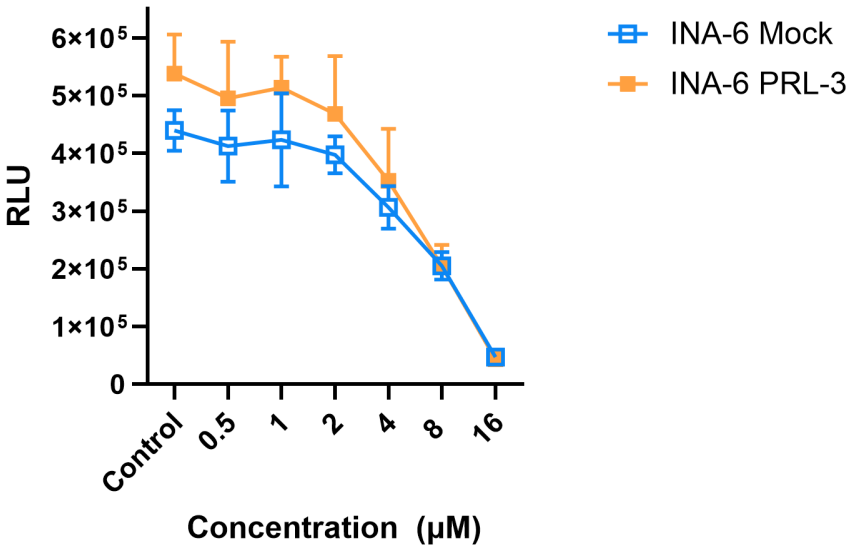

Supplementary 6.2: Titration curve for BAM15: INA-6 Mock and INA-6 PRL-3 cells were treated with the indicated concentrations of BAM15, then incubated for 24 h in normoxic conditions at pH 7.4. ATP content was measured by the CTG assay. The data is given as mean ± 2×SEM.

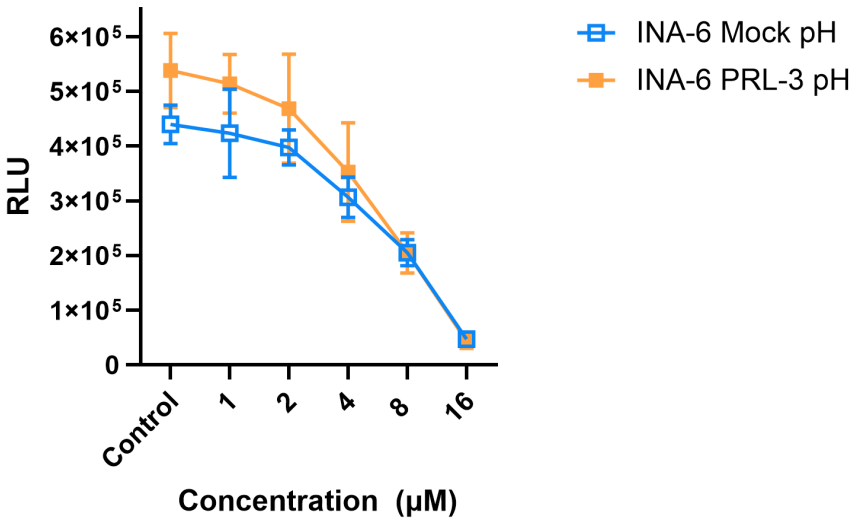

Supplementary 6.3: Titration curve for dequalinium chloride: INA-6 Mock and INA-6 PRL-3 cells were treated with the indicated concentrations of dequalinium chloride, then incubated for 24 h in normoxic conditions at pH 7.4. ATP content was measured by the CTG assay. The data is given as mean ± 2×SEM.

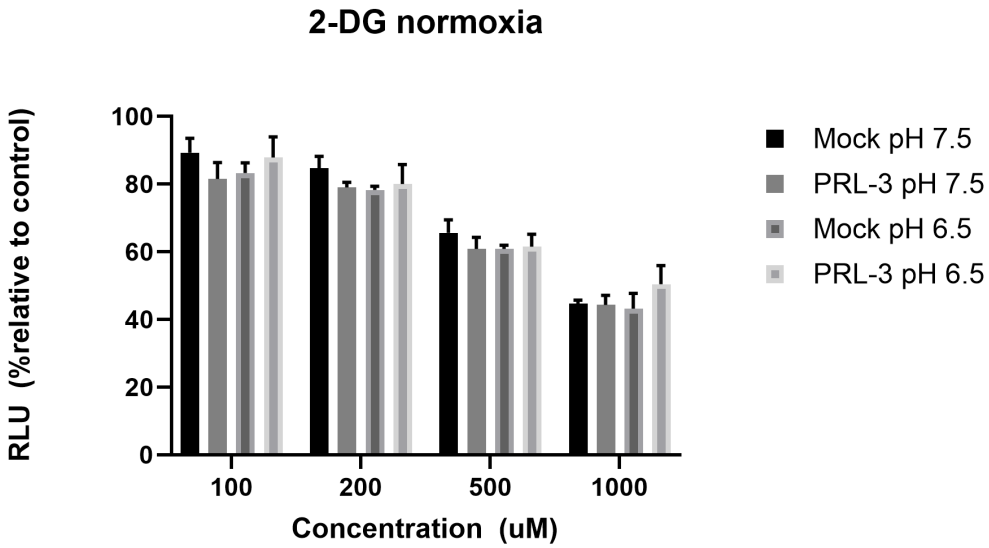

Supplementary 6.4: Titration curve for 2-DG under normoxia: INA-6 Mock and INA-6 PRL-3 cells were treated with the indicated concentrations of 2-DG, then incubated for 24 h in normoxic conditions at pH 7.4 or pH 6.5. ATP content was measured by the CTG assay. The data is given as mean ± 2×SEM.

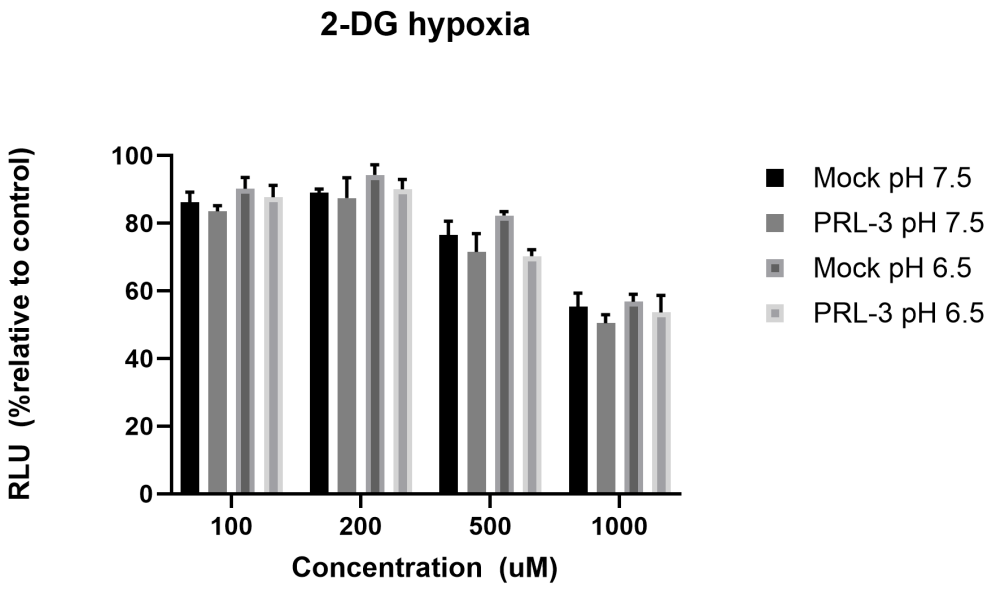

Supplementary 6.5: Titration curve for 2-DG under hypoxia: INA-6 Mock and INA-6 PRL-3 cells were treated with the indicated concentrations of 2-DG, then incubated for 24 h in hypoxic conditions at pH 7.4 or pH 6.5. ATP content was measured by the CTG assay. The data is given as mean ± 2×SEM.

Flow cytometry gating

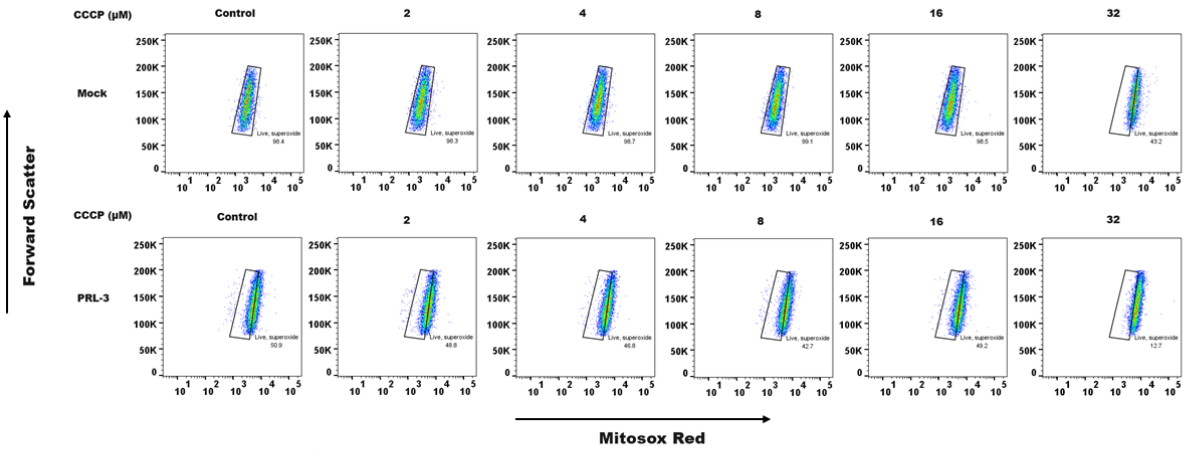

Supplementary 6.6: MitoSox Red Superoxide Indicator gating: The figure shows live cells, gated by Forward-Scatter, and the MitoSox Red signal. The gate was set for the Mock control cell and applied to all other conditions. This was performed in FlowJo.

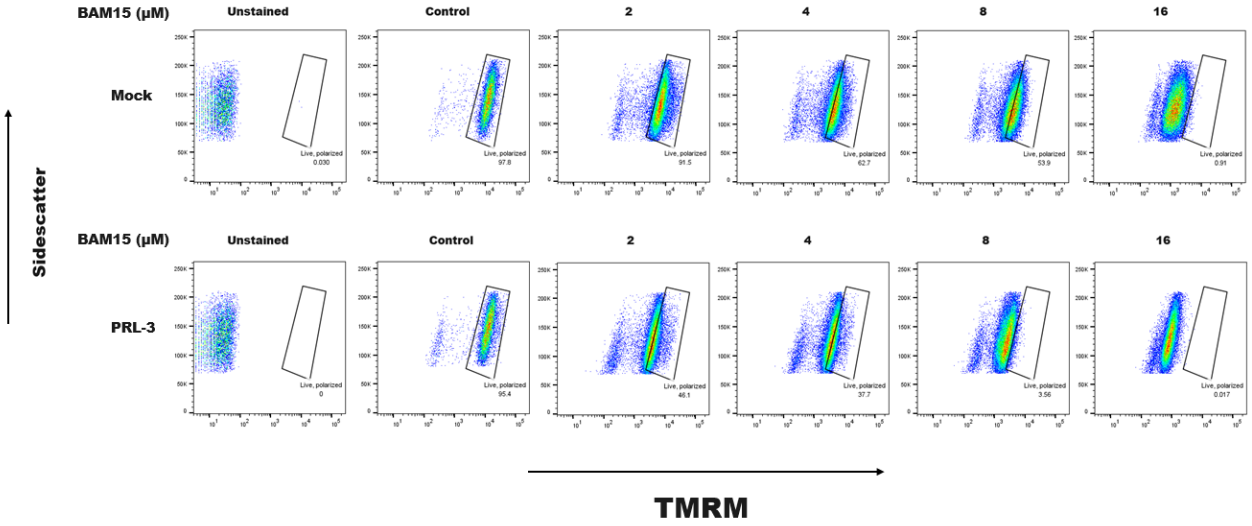

Supplementary 6.7: TMRM gating: The figure shows live cells, gated first by GFP, then Side-scatter, and the TMRM signal. The gate was set for the Mock control cell and applied to all other conditions. This was performed in FlowJo.

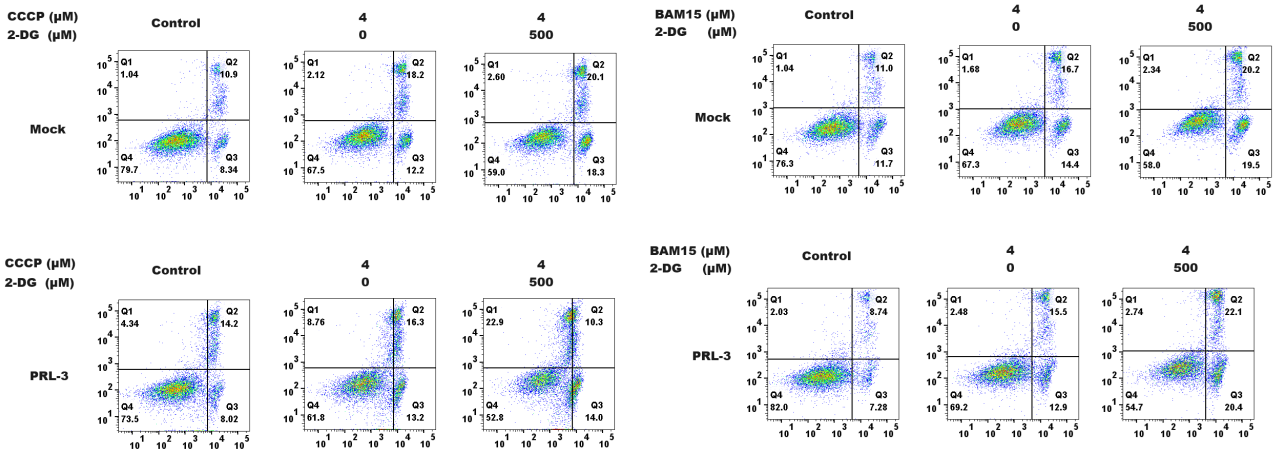

Supplementary 6.8: Annexin V / PI gating for Flow cytometry viability at pH 7.4 and normoxia: Figures show concentration of uncouplers and 2-DG, and the accompanying Annexin V / PI quadrants and their respective cell populations. This was performed in FlowJo.

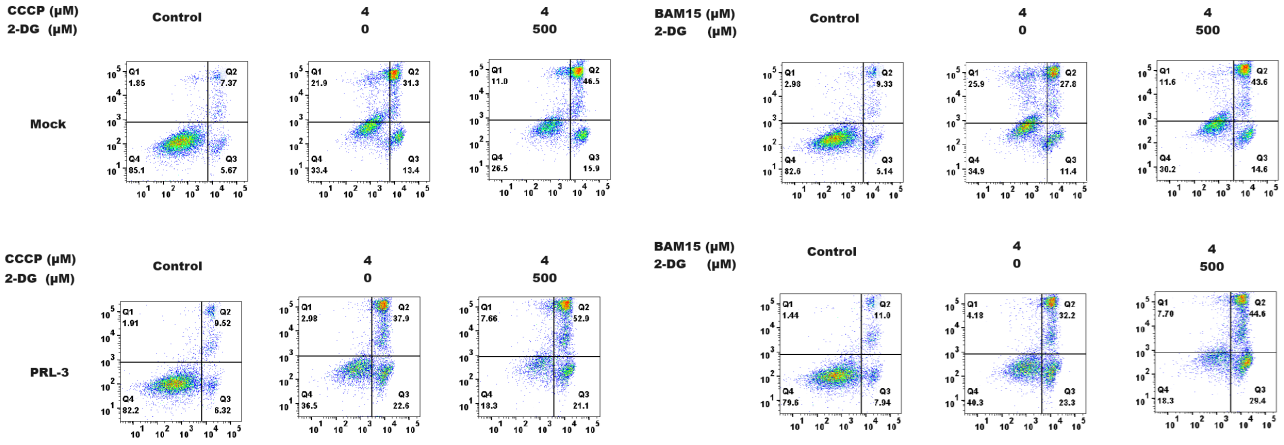

Supplementary 6.9: Annexin V / PI gating for Flow cytometry viability at pH 7.4 and hypoxia: Figures show concentration of uncouplers and 2-DG, and the accompanying Annexin V / PI quadrants and their respective cell populations. This was performed in FlowJo.

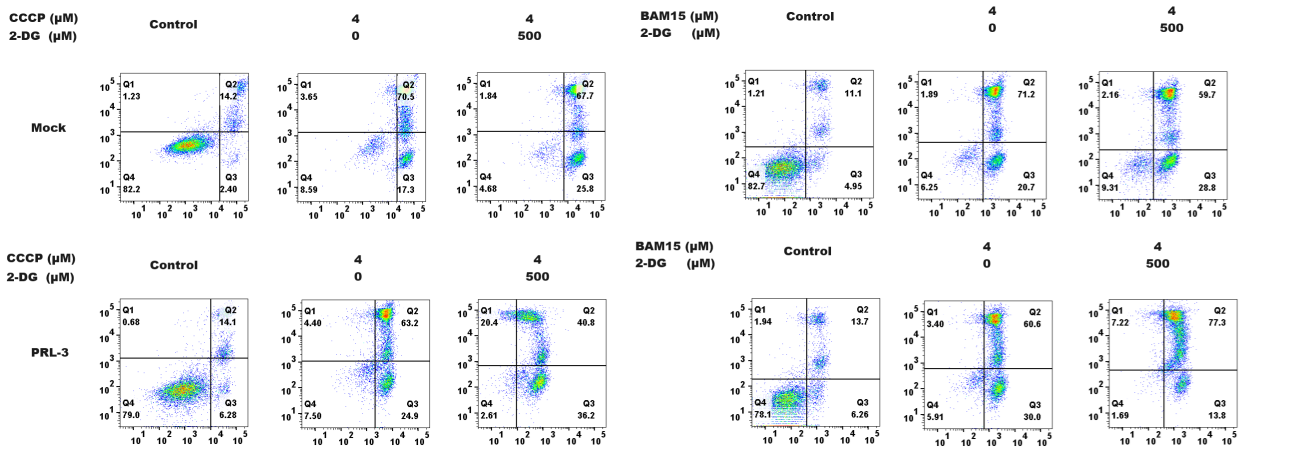

Supplementary 6.10: Annexin V / PI gating for Flow cytometry viability at pH 6.5 and normoxia: Figures show concentration of uncouplers and 2-DG, and the accompanying Annexin V / PI quadrants and their respective cell populations. This was performed in FlowJo.

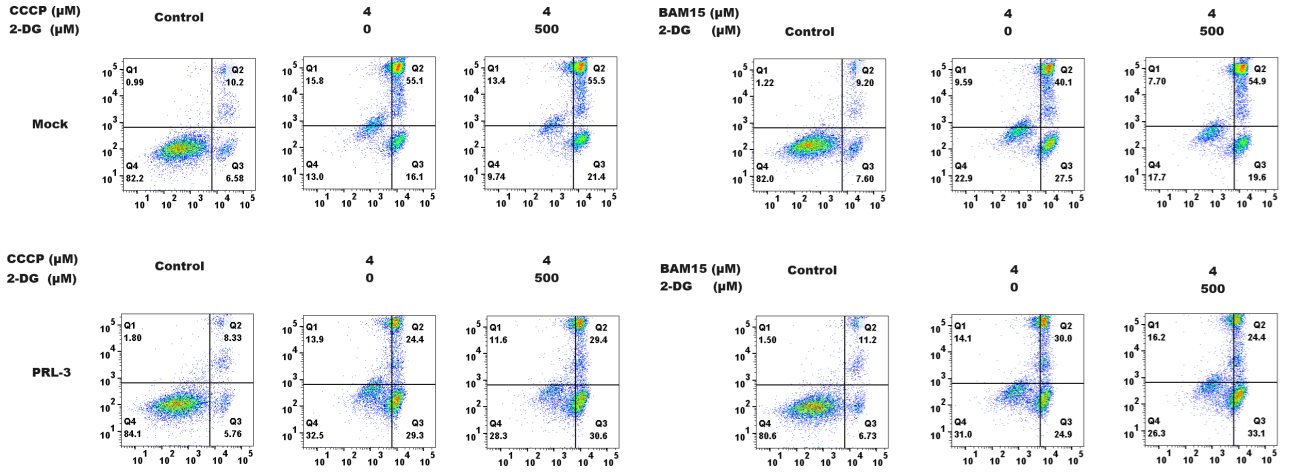

Supplementary 6.11: Annexin V / PI gating for Flow cytometry viability at pH 6.5 and hypoxia: Figures show concentration of uncouplers and 2-DG, and the accompanying Annexin V / PI quadrants and their respective cell populations. This was performed in FlowJo.

Resources

Reagent or Resource	Source	Identifier
INA-6	CLPUB00090	RRID:CVCL_5209
Fetal Calf Serum	Invitrogen, Carlsbad, CA, USA	#10082147
RPMI 1640	Sigma Aldrich, St.Louis, MO, USA	#R8758
D-(+)-Glucose	Merck	#G8270
Sodium Pyruvate	Sigma Aldrich, St.Louis, MO, USA	#P5280
L-Glutamine	Sigma Aldrich, St.Louis, MO, USA	#G7513
GLUT1	Cell Signaling Technology (BioNordika AS, Oslo, Norway	#12939
Hexokinase II	Cell Signaling Technology (BioNordika AS, Oslo, Norway	#2867
p-AMPK	Cell Signaling Technology, BioNordika AS, Oslo, Norway	#2535
PRL-3	Santa Cruz Biotechnology, Dallas, TX, USA	#sc-130355
NHE-1	Santa Cruz Biotechnology, Dallas, TX, USA	#sc-136239
HIF-1α	R&D systems, Minneapolis, MN, USA	#AF1935
MCT4	Santa Cruz Biotechnology, Dallas, TX, USA	#sc-376140
Dequalinium Chloride	Sigma Aldrich, St.Louis, MO, USA	#PHR1300
2-Deoxy-D-glucose	Sigma Aldrich, St.Louis, MO, USA	#D8375
Carbonyl cyanide m-chlorophenyl hydrazone (CCCP)	Sigma Aldrich, St.Louis, MO, USA	#C2759
2-fluorophenyl) {6-[(2-fluorophenyl) amino] (1,2,5-oxadiazolo [3,4-e] pyrazin-5-yl (BAM15)	Sigma Aldrich, St.Louis, MO, USA	#SML1760
Albumin Standard (BSA)	Thermo Fisher Scientific Waltham, MA, USA	#23209
NuPAGE® LDS Sample Buffer (4X)	Invitrogen, Carlsbad, CA, USA	#NP0007
NuPAGE™ 4 to 12%, Bis-Tris, 1.0 mm x 20 well	Invitrogen, Carlsbad, CA, USA	# WG1402A
1 M DTT solution	PanReach AppliChem, Darmstadt, Germany	#A3668-0050
Nonidet P40 (NP40)	ThermoFisher Scientific, Waltham, MA, USA	#FNN0021
Sodium orthovanadate (Na_3VO_4)	Sigma Aldrich, St.Louis, MO, USA	#450243
HCl-Tris	Sigma Aldrich, St.Louis, MO, USA	#T5941
SeeBlue® Plus2 Pre-stained Protein Standard	Invitrogen, Carlsbad, CA, USA	#LC5925
MagicMark™ XP Western Protein Standard	Invitrogen, Carlsbad, CA, USA	#LC5602
Mini, EDTA-free Protease Inhibitor Cocktail	Sigma Aldrich, St.Louis, MO, USA	#11836170001
Polyclonal rabbit anti-goat Immunoglobulins /HRP)	Daco, Glostrup, Denmark	#P0449
Polyclonal goat anti-mouse antibody/HRP	ThermoFisher Scientific, Waltham, MA, USA	#31430
Super Signal® West Femto	ThermoFisher Scientific, Waltham, MA, USA	#34095
iBlot® 2NC Regular Stacks	Invitrogen, Carlsbad, CA, USA	#IB23002
Tween 20	Sigma Aldrich, St.Louis, MO, USA	#P1379
Bradford Reagent	Sigma Aldrich, St.Louis, MO, USA	#B6916
Tetramethylrhodamine, methyl ester (TMRM)	ThermoFisher Scientific, Waltham, MA, USA	#T668
MitoSOX ™ Red Mitochondrial Superoxide Indicator	ThermoFisher Scientific, Waltham, MA, USA	#M36008
Oligomycin from Streptomyces diastatochromogenes	Merck	#O4876
Seahorse XF Pro FluxPak and Seahorse XF base medium	Agilent	# 103792-100 # 102353-100
CellTiter-Glo® 2.0 Luminescent Cell Viability Assay	Promega, Madison, Wisconsin, USA	#G9242
FlowJo v10.2.1	FlowJo	RRID: SCR_008520
GraphPad Prism software	GraphPad	RRID: SCR_002798

Supplementary 6.12: Resource table for reagents and resources used in this study: Image shows reagent or resources, source, and identifiers for cell line, antibodies, reagents, compounds, and programs employed in this thesis.

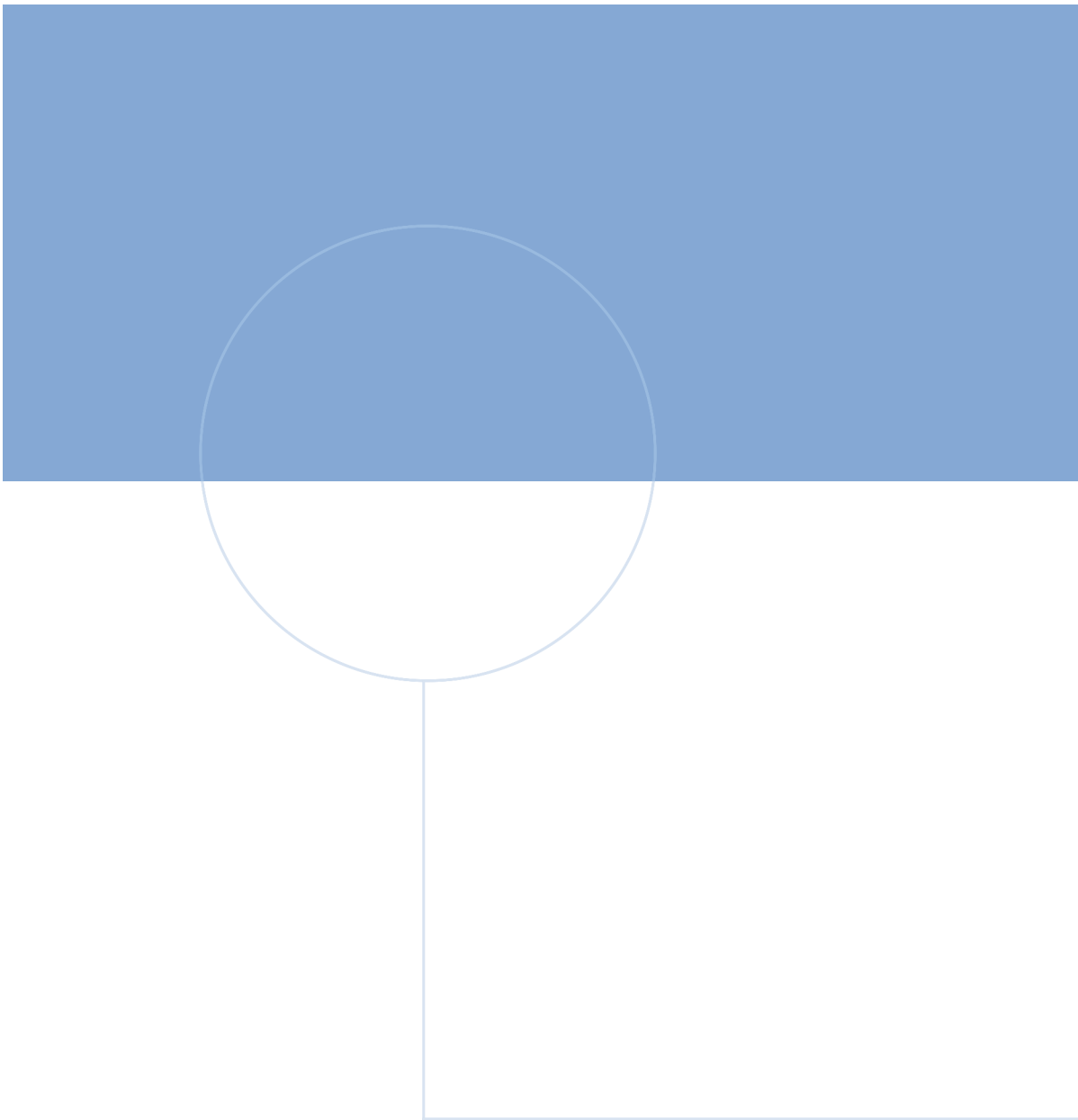

NTNU

Norwegian University of
Science and Technology